UNIVERSITÉ DU QUÉBEC

THÈSE PRÉSENTÉE À
L'UNIVERSITÉ DU QUÉBEC À TROIS-RIVIÈRES

COMME EXIGENCE PARTIELLE
DU DOCTORAT EN BIOPHYSIQUE

PAR

GLENN WEAGLE

THE ASSESSMENT OF PHEOPHORBIDE *a* ETHANOLAMIDE AS A POTENTIAL DUAL ACTION ANTI CANCER PHOTOSENSITIZER

(ÉVALUATION DE l'ÉTHANOLAMIDE DU PHÉOPHORBIDE *a* COMME PHOTOSENSIBILISATEUR ANTI-CANCÉRIGÈNE À DOUBLE ACTION)

AOÛT 1995

Résumé

Quelques grammes du phéophorbide *a* ethanolamide (PEA), un nouveau médicament potentiellement anti-cancereux à double action, présentant des propriétés chimio- et photochimiothérapeutique, a été synthétisée en trois étapes à partir de la chlorophylle *a*. La structure du PEA a été confirmée par spectroscopie électronique, infrarouge et résonance magnétique nucléaire. Sa pureté fut vérifiée par chromatographie liquide à haute pression.

La dose létale pour tuer 50% des sujets sous observations (DL_{50}) du PEA est plus grande que 500 mg/kg. Ceci indique une faible toxicité et un indice thérapeutique élevé. En l'absence de lumière excitatrice le PEA montre une activité chimiothérapeutique chez des souris porteuses de tumeurs. Le PEA, présent en concentration dix fois supérieure à la dose d'adriamycine, produit, *in vitro*, un effet cytotoxique comparable sur les tissus humains cancéreux.

Le traitement chimiothérapeutique avec le PEA sur des souris $B6D2F_1$ porteuses du carcinôme pulmonaire de Lewis a accru le délai avant la mort par un facteur de 2,5 par rapport à des souris témoins. L'activité chimiothérapeutique peut être due à l'action d'alkylation du groupe ethanolamide dont la structure chimique est similaire à la partie active des agents moutardes azotés. Alors que les doses utilisées dans cette étude étaient insuffisantes pour éradiquer les cancers, le PEA semblait réduire les possibilités d'apparition de métastases chez des animaux porteurs du carcinôme pulmonaire de Lewis.

La fluorescence du PEA a été utilisée pour suivre la pharmacocinétique du médicament. Lorsque les injections de PEA étaient intrapéritonéales ou intraveineuses dans la souris porteuse d'une tumeur (l'adénocarcinôme pulmonaire M4898 chez des souris Balb c), le temps de fluorescence maximum dans la tumeur était de 3 heures après l'injection, et le rapport de la fluo-rescence provenant de la tumeur et du muscle était de 6,7, montrant que le PEA présente une bonne sélectivité pour les tissus néoplastiques. Le temps de disparition du PEA dans la peau est de 24 h, ce qui implique que la photosensibilité de la peau est réduite à un minimum, contrairement à plusieurs médicaments PTD.

La photohémolyse est une méthode qui peut être utilisée pour évaluer l'activité photosensibilisatrice de nouveaux photosensibilisateurs potentiels. Le PEA a montré des effets photohémolytiques probants en présentant un accroissement d'activité de 200 % en comparaison de la polyhématoporphyrine (pHP), un agent PTD disponible couramment, à des concentrations physiologiquement appropriées.

Le PEA peut donc être considéré comme un nouvel agent anti-tumeur à double action, présentant une activité à la fois chimio- et photochimiothérapeutique.

Abstract

Pheophorbide *a* ethanolamide, a new potential dual action anti-cancer drug exhibiting chemo- and photochemotherapeutic properties, was synthesized in gram quantities in three steps from chlorophyll *a*. The structure of pheophorbide *a* ethanolamide was confirmed by electronic, Fourier transform infrared and nuclear magnetic resonance spectroscopy, and its purity was confirmed by high performance liquid chromatography.

The lethal dose 50% for pheophrobide *a* ethanolamide was greater than 500 mg kg^{-1} indicating low toxicity and high therapeutic index. Pheophorbide *a* ethanolamide showed chemotherapeutic activity in tumour-bearing mice in the absence of activating light. At about 10 times the concentration of adriamycin, pheophorbide *a* ethanolamide exhibited a comparable cytotoxic effect on human cancer cell lines *in vitro*. Chemotherapeutic treatment with pheophorbide *a* ethanolamide on $B6D2F_1$ mice with Lewis lung carcinoma increased the time to death by a factor of 2.5. The chemotherapeutic activity may be due to the alkylating action of the ethanolamide moiety, which is similar in chemical structure to the active component of nitrogen mustards. While the low doses used in this study were insufficient to eradicate the cancers, pheophorbide *a* ethanolamide appeared to reduce the likelihood of metastasis in Lewis lung cancer-bearing animals.

The fluorescence of pheophorbide *a* ethanolamide was used to monitor the drug's pharmacokinetics. When pheophorbide *a* ethanolamide was injected intraperitoneally or intravenously into tumour bearing mice (M4898 Lung adenocarcinoma in Balb c mice), the time of maximum fluorescence in the tumour was at 3 hours post injection, and the tumour to muscle fluorescence ratio was 6.7, showing that pheophorbide *a* ethanolamide exhibited good selectivity for neoplastic tissue. The observed skin clearance time of 24 hours for pheophorbide *a* ethanolamide implies that skin photosensitivity would be minimal unlike many photodynamic therapy drugs.

Photohemolysis is a method that can be used to evaluate the photosensitizing activity of new potential photodynamic photosensitizers. pheophorbide *a* ethanolamide demonstrated efficient photohemolytic effects when irradiated with light, with a 200% increase in activity compared to polyhematoporphyrin, a currently available photodyamic therapy agent, at physiologically relevant concentrations.

Pheophorbide *a* ethanolamide can thus be considered a new dual action antitumour agent, exhibiting both chemo- and photochemotherapeutic activity.

Acknowledgements

First of all I would like to thank the Département de Chimie-biologie de l'Université du Québec à Trois Rivières and the Department of Chemistry and Chemical Engineering at the Royal Military College of Canada, Kingston; whose cooperation enabled this research project to proceed.

I would like to thank Dr Michel Ringuet and Dr Camille Chapados for their guidance in this project as it evolved.

I would also like to thank Dr Roy Pottier for his direction and guidance in the research for this project.

I am grateful to the members of Dr. Pottier's laboratory, namely Dr. Eva Dickson, and Dr. Pierre Nadeau who were always available to help and discuss issues involved in the research.

I appreciated the guidance and direction from Dr James Kennedy in the animal and cell studies involved in this research

Last but not least I want to thank Karen and Pam who had to cope with myself as I proceeded through this project.

I would like to acknowledge and thank the Natural Sciences and Engineering Research Council of Canada and DUSA Pharmaceuticals Inc. for the their financial assistance that made this project possible.

Table of Contents

List of Tables

List of Figures

List of Abbreviations

ALA	Aminolevulinic acid
$AlPcS_n$	Aluminum phthalocyanine n-sulfonated
AlSPc	Sulfonated aluminum phthalocyanine
Al S_2Pc	Aluminum di-sulfonated phthalocyanine
b-	Bacterio
Bchlorin *a*	Bacteriochlorin *a*
BPD-MA	Benzoporphyrin derivative monoacid ring A
C8KC	7,12-Dioctyl-3,7,13,17-tetramethyl-8-porphinone-2,18-dipropionic acid
CA-6E	Bacteriochlorin derivative
bChl	Bacteriochlorophyll
Chl	Chlorophyll
Chl *a*	Chlorophyll *a*
Chloro Al SPc	Chloro aluminum sulfonated phthalocyanine
CPS	Cationic dyes
CRM	Cremophor EL formulation (derivative of castor oil and ethylene oxide)
DMSO	Dimethyl sulphoxide
EDA	Chlorin e_6 ethylenediamide
ET2	Etiopurpurin
FTIR	Fourier transformed infrared spectrophotometer
GaPc	Ga phthalocyanine
H_2TNP	Free base tetranaphthaloporphyrin
HDL	High density lipoprotein
HEDP	Pheophorbides
HP	Hematoporphyrin
HPIX	Hematoporphyrin IX
HpD	Hematoporphyrin derivative

HPLC	High pressure liquid chromatography
HPPEEA	Hematoporphyrin propyl ether ethanolamide
HPPH	2-[1-Hexyloxyethyl]-2-devinylpyropheophorbide *a*
HSA	Human serum albumin
Hz	Hertz
IC_{50}	Inhibitory concentration 50%
ID	Intradermal
IP	Intraperitoneal
IR	Infrared
isoBosinc	Bis(di-isobutyloctadecylsiloxy)siliconnaphthalocyanine
IT	Intratumoural
IV	Intravenous
LD_{50}	Lethal dose 50%
LDL	Low density lipoprotein
MPH	Methylpheophorbide *a* -hexyl-ether
mPheo	Methylpheophorbide *a*
MTBP	Metallo-tetrabenzoporphyrins
MTT	3-[4,5-Dimethylthiazol-2-yl]-2,5-diphenyl-tetrazolium bromide
NMR	Nucleur magnetic resonance
NPc	Naphthalocyanine
NPe6	Mono-L-aspartyl chlorin e_6
O_2^-	Superoxide
$^1O_2$	Singlet oxygen
Pc	Phthalocyanine
PDT	Photodynamic therapy
PEA	Pheophorbide *a* ethanolamide
PFII	Photofrin II®
pHP	Polyhematoporphyrin
Pheo *a*	Pheophorbide *a*

PO_2	Partial pressure of oxygen (measured in Torr)
S_1	Singlet excited state
SPc	Sulfonated phthalocyanine
S_2Pc	Disulfonated phthalocyanine
Si NPc	Si(IV)-Naphthalocyanine
Si(IV) NPc	Si(IV)-Naphthalocyanine
SiNc	Si(IV)-Naphthalocyanine
SnET2	Tin etiopurpurin
T_1	Triplet excited state
TBS	Tris buffered saline
TD	Time to death
THF	Tetrahydrofuran
TLC	Thin layer chromatography
T/M	Tumour to muscle drug concentration ratio
T/N	Tumour to normal tissue drug concentration ratio
TNP	Tetranaphthaloporphyrin
T/S	Tumour to skin drug concentration ratio
TPP	Tetraphenylporphyrin
Tris	Tris(hydroxymethyl)aminomethane HCl
TW80	Tween 80 formulation (polyoxyethylene (20) sorbitan monooleate)
UV	Ultraviolet
ZnPc	Zn Phthalocyanine
$ZnPc(OH)_4$	Zn Phthalocyanine tetrahydroxyl
Zn NPc	Zn Naphthalocyanine
Zn TNP	Zn Tetranaphthaloporphyrin
Φ_T	Quantum yield of the triplet state
Φ_Δ	Quantum yield of singlet oxygen

Chapter 1 General introduction

1.1 Cyclic tetrapyrroles

Cyclic tetrapyrroles have been extensively studied for their potential medical use. The cyclic tetrapyrroles are based on an eighteen (18) membered ring, where four (4) pyrrole subunits are joined together with methine bridges into a ring system (Fig. 1.1). Their molecular structure can be described as a rather flat molecular tablet that is approximately 49Å squared with a large central hole which can be occupied by a metal ligand. This unique structure has a conjugated double bond resonance system, leading to a high absorption ($\varepsilon > 10^5$ M^{-1} cm^{-1}), and fluorescence in the visible region of the compounds.

The chromophoric region of the cyclic tetrapyrroles is based on the porphin ring (Fig. 1.1). The light absorption properties of the tetrapyrrole can be modified by metal ligands attached to the central region of the molecule and by side groups attached to the outside of the ring. Four medically relevant classes of tetrapyrroles which absorb in the far red region of the visible spectrum are: the porphyrins; the chlorins; the bacteriochlorins; and the phthalocyanines (Fig. 1.2). The chlorins can be defined as dihydroporphyrins due to the saturation of a pyrrole. The phthalocyanines are also referred to as azaporphyrins. The rich colours of the cyclic tetrapyrroles also have led to their commercial application as pigments and dyes in paints for example.

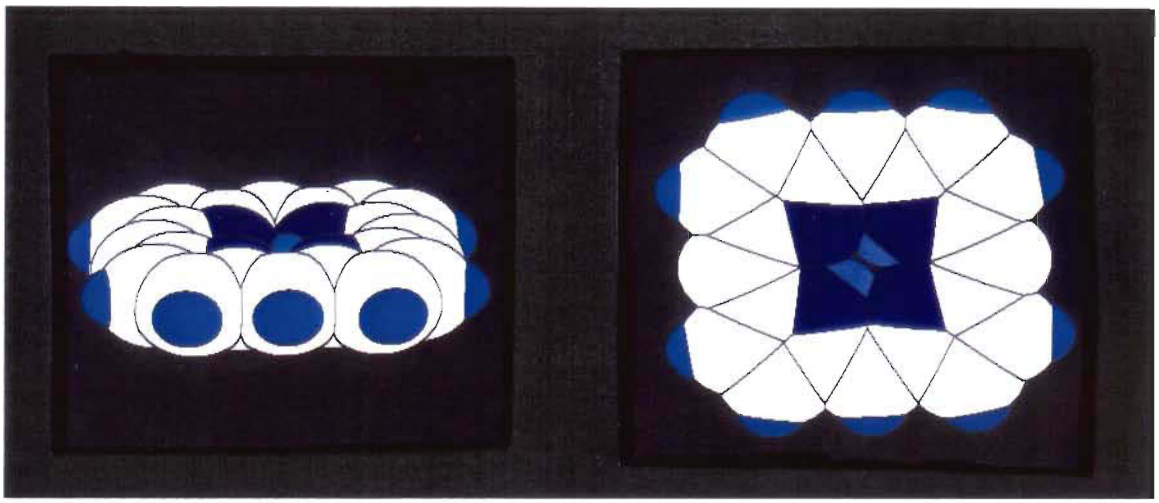

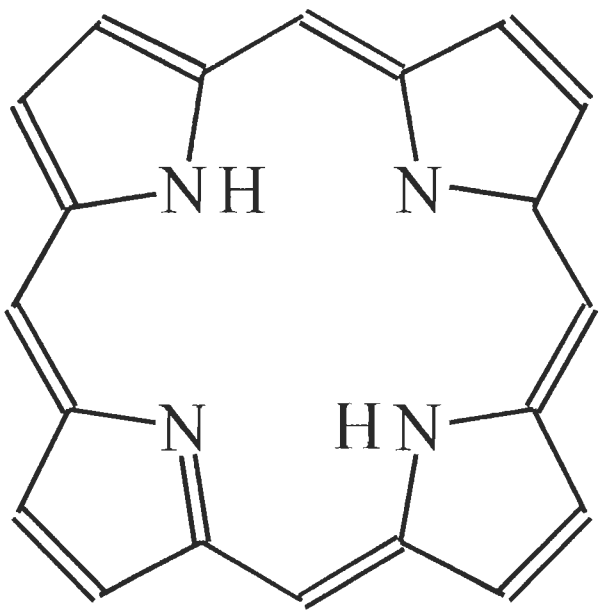

Figure 1.1. The space filled molecular model of the porphin ring viewed from two different orientations, and the chemical structure showing the planar shape of tetrapyrroles (d= 7.3 Å; surface= 49 $Å^2$).

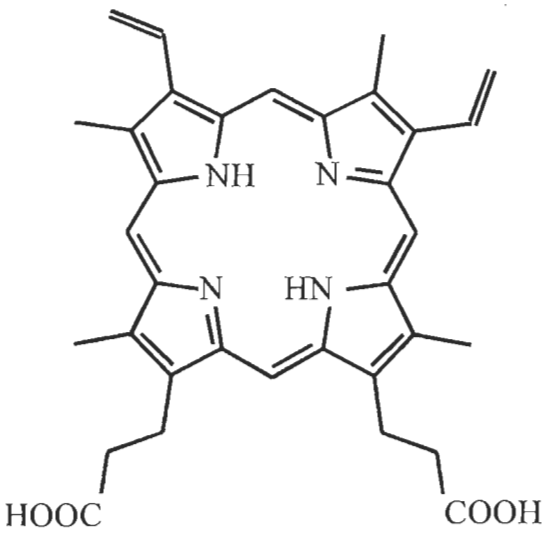

Protoporphyrin IX

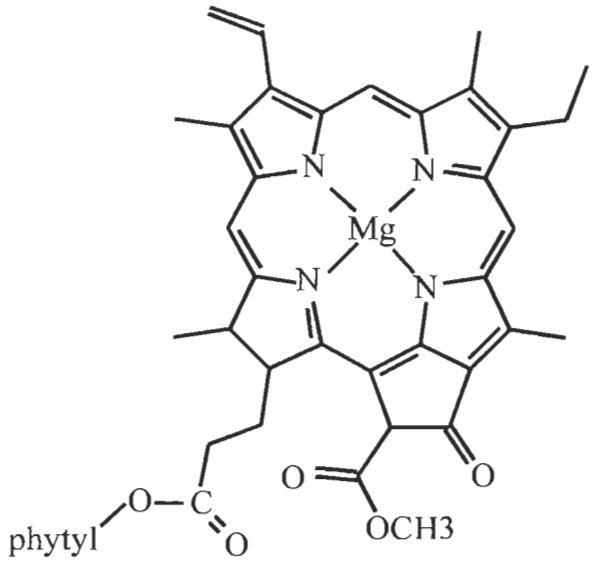

Chlorophyll *a*

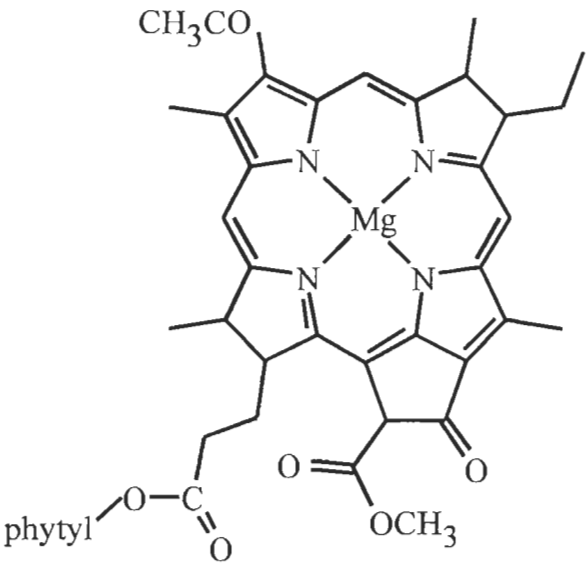

Bacteriochlorophyll *a*

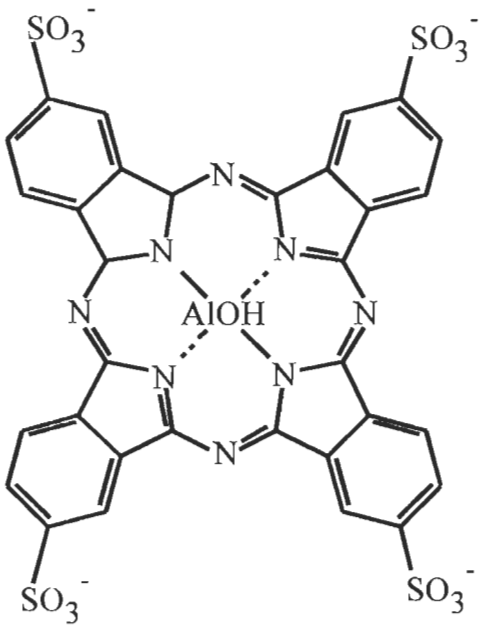

Tetrasulfonated
Al phthalocyanine

Figure 1.2. Representative molecules from four of the tetrapyrrole classes which have potential medical applications: Protoporphyrin = porphyrin; chlorophyll *a* = chlorin; bacteriochlorophyll *a* = bacteriochlorin; tetrasulfonated aluminum phthalocyanine = phthalocyanine.

A photon, once absorbed by a tetrapyrrole, can have several fates. The large conjugated double bond ring structure of these molecules permits an absorbed photon to be either emitted at a longer wavelength as fluorescence, or passed to another molecule as energy, resulting in photosensitization. The surroundings of the tetrapyrrole molecule can affect the choice of fates of an absorbed photon. For example, if an acceptor molecule such as oxygen is in proximity to the tetrapyrrole, then the photon energy could be passed to the oxygen; however if there is no acceptor molecule in proximity, then the photon energy may be re-emitted from the tetrapyrrole as fluorescence.

The cyclic tetrapyrroles have a diverse collection of roles in nature. Some notable examples of such functions are: i) chlorophyll, a chlorin or dihydroporphyrin which is responsible for the photosynthesis in plants; ii) heme, an iron metalloporphyrin which is involved in oxygen transport of blood; iii) cytochrome, another iron metalloporphyrin which is involved in several energy transfer functions of the respiratory electron transport pathway; and iv) the corrin ring of the vitamin B_{12}, a cobalt metalloporphyrin which acts as a coenzyme in several enzymatic processes. The molecular structures of the tetrapyrroles involved in these examples are illustrated in Figure 1.3. Some cyclic tetrapyrroles also have a potential use in medical applications such as disease diagnostics and cell killing due to their fluorescence and photosensitization properties.

1.2 Use of cyclic tetrapyrroles in medicine

The application of light in either the diagnosis or treatment of disease is called photomedicine. Modern photomedicine can be separated into two fields, i) phototherapy and ii) photochemotherapy. In phototherapy, light alone is applied, which is absorbed by endogenous chromophore molecules, resulting in a photochemical response. In photochemotherapy, exogenous chromophore molecules such as the cyclic tetrapyrroles are administered prior to the illumination. The administered exogenous molecules will absorb light leading to the photochemical response through photosensitization. In some photochemotherapy cases, oxygen is required as the energy acceptor. Then, the photochemical reaction is called photodynamic.

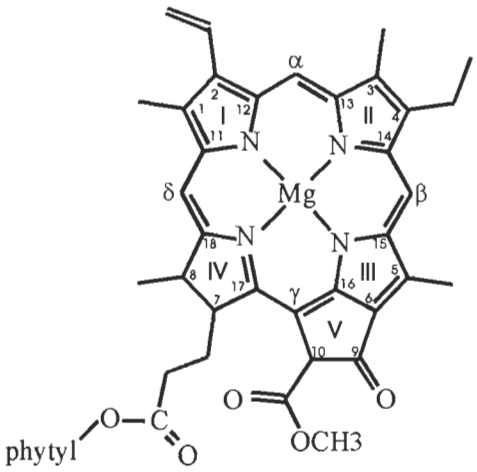

Chlorophyll *a*

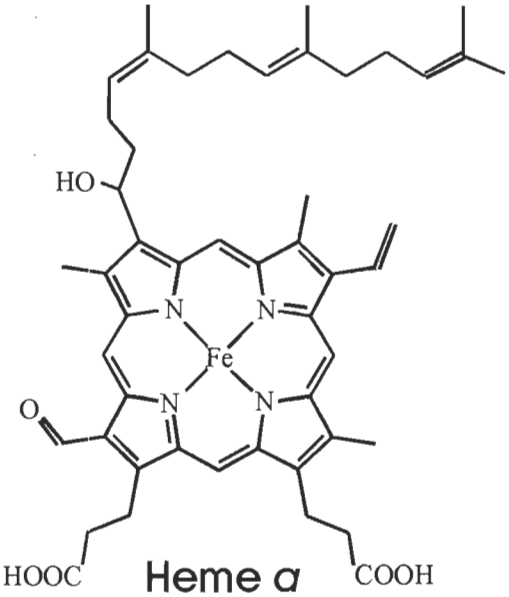

Heme *a*

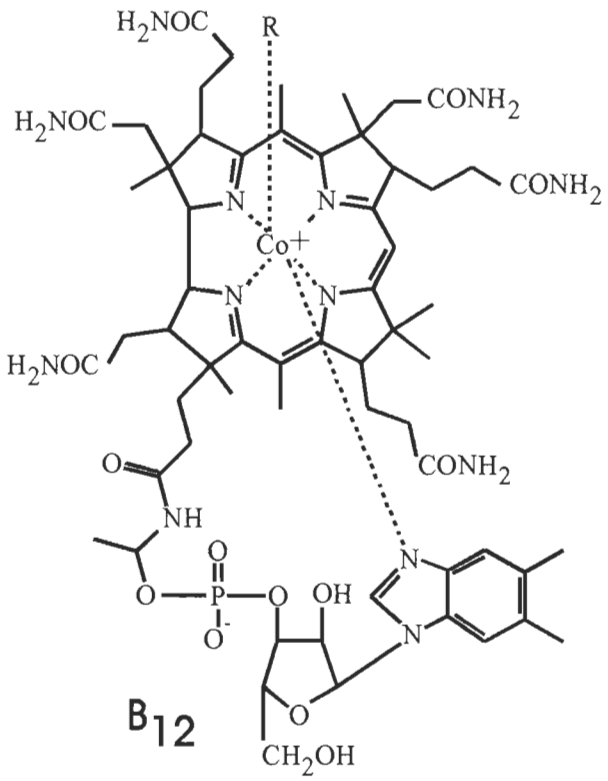

B_{12}

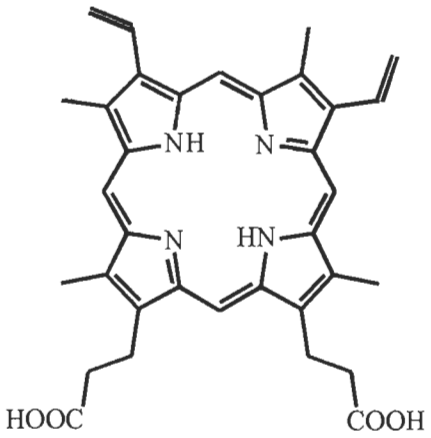

Protoporphyrin IX

Figure 1.3. Molecular structures of some common natural tetrapyrroles: chlorophyll *a*; heme *a*, the tetrapyrrole unit of the cytochromes; vitamin B_{12}, which contains the corrin ring; and protoporphyrin IX the precursor hemoglobin.

Photomedicine has been practiced in some form for over thirty centuries in India, China, and Egypt. Modern scientific investigation into photomedicine and its mechanisms began in the early 1900's. Several skin disorders such as pityriasis, versicolour, and psoriasis vulgaris were treated in the early 1900's by applying exogenous photosensitizing dyes and light (von Tappeiner and Jesionek, 1903). The selective response of diseased tissue was observed in such early photomedicine treatments; the normal tissue surrounding the diseased area was unaffected by the photosensitization reaction and the light induced photosensitization was selective to wounded and/or rapidly proliferating tissues.

The brilliant red fluorescence of cyclic tetrapyrrole dyes, coupled with their selective retention within rapidly proliferating tissues such as tumours, was shown to provide a useful diagnostic tool for cancer. Tumours in animals emitted a bright red fluorescence when irradiated with blue light after the exogenous porphyrin dye hematoporphyrin (HPIX) was administered to the animals (Rassmussen-Taxdal *et al.*, 1955). Some years later Lipson *et al.* (1961) confirmed that an exogenous porphyrin dye that had been administered to animals and/or human patients could selectively localize in tumour tissue and be used for diagnosis of the tumours due to the red fluorescence of the dye when illuminated with intense blue light.

By combining the selective retention and photosensitization characteristics of tetrapyrrole dyes it was proposed that these dyes could be used to kill cells and destroy tumour tissue. The treatment by photosensitization of lesions had been known for many years, but the application of these properties of dyes to cancer treatment was a new concept. Damage to tumour cells was observed when those cells were irradiated with visible light after prior administration of the dye HPIX (Diamond *et al.*, 1972). This treatment for cancer known as photodynamic therapy (PDT) can be described as the selective retention by tumour tissue of a photosensitizer which will generate reactive compounds by photosensitization and those reactive compounds will undergo chemical reactions with biomolecules leading to cell death (Fig. 1.4).

With the establishment of PDT, research was initiated in an attempt to improve the photosensitizer properties relevant to photodynamic therapy. As a result of these investigations many new and modified forms of photosensitizing dyes continue to be

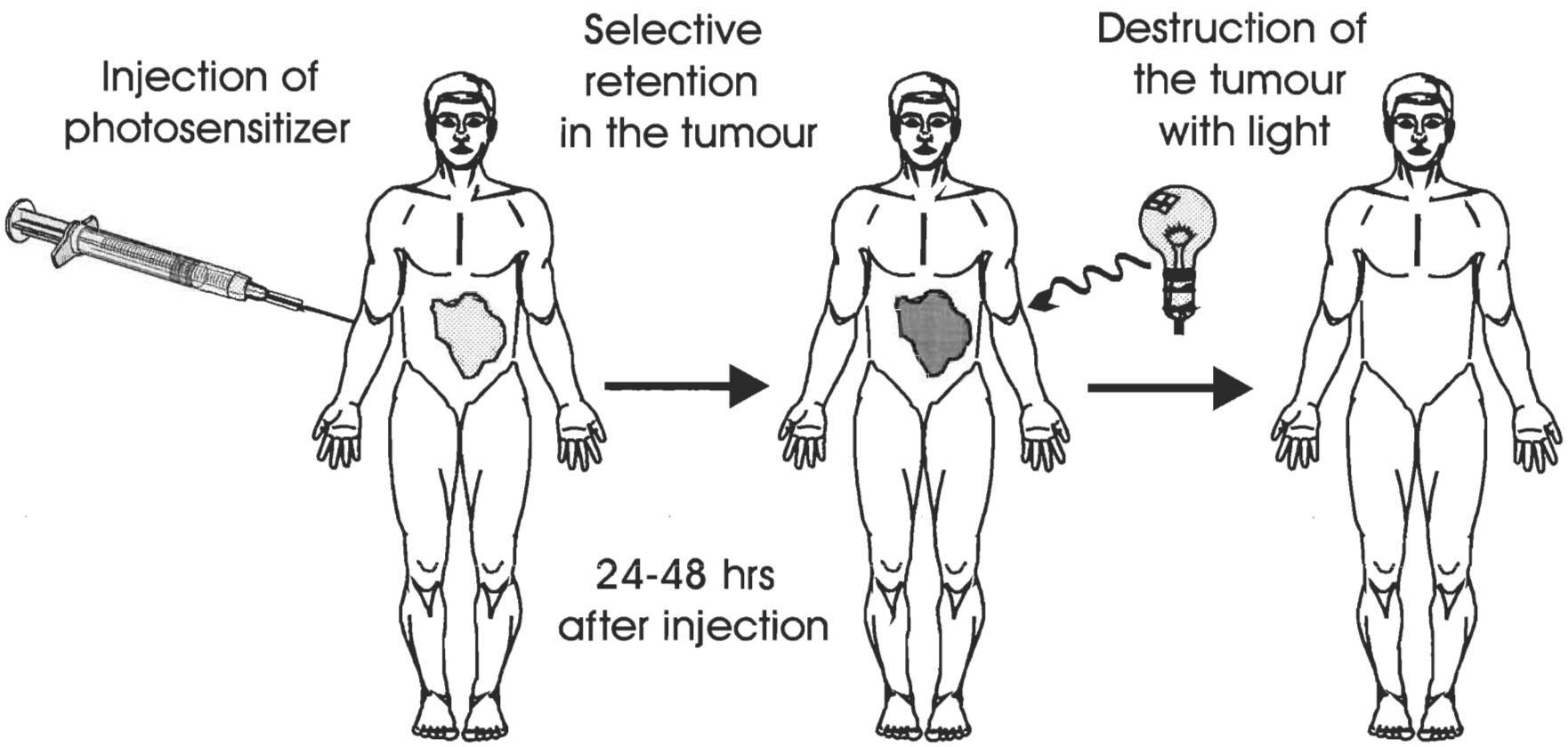

Figure 1.4 Generalized scheme of photodynamic therapy treatment using a photosensitizer injected IV.

synthesized in order to improve the PDT response of tumours. A brief survey of some tetrapyrrole photosensitizer dyes is warranted since many have a potential use as PDT agents.

The first tetrapyrrole based dye used as a light activated anti-tumour agent was hematoporphyrin derivative (HpD) (Lipson *et al.*, 1961). HpD is a water soluble formulation derived from the porphyrin hematoporphyrin (HPIX) (Lipson *et al.*, 1961). HpD has been shown to contain several different components (Bonnett and Berenbaum, 1989). The active anti-tumour components of HpD were further isolated and purified, and the purified active anti-tumour composition of HpD is now called Photofrin. Photofrin was found to contain a polymeric mixture of dihematoporphyrins and oligomers (Kessel and Cheng, 1985; van Lier, 1988). A commercial preparation of the original Photofrin is called Photofrin porfimer sodium® or Photofrin II® (PFII) (Quadra Logic Technology Inc., Vancouver, B.C., Canada). Photofrin II® has improved light activated anti-tumour properties as compared to the original Photofrin. Other research groups have also synthesized a variety of tetrapyrrole based dyes in an attempt to find compounds with improved anti-tumour properties as compared to PFII. The primary aims when synthesizing the new dyes, were to improve the dye properties of tumour selectivity (for example via increased hydrophobicity) and to increase the far red absorbance in order to take advantage of the high tissue transmission of far red light. These new far red absorbing dyes have been categorized as "second generation photosensitizers". Some of these, which have a potential use for PDT, are summarized in Table 1.1.

Table 1.1: Summary of some of the more promising second generation PDT photosensitizers.

Photosensitizer	Hydrophobicity	λ_{max} (nm) [a]
NPe6	hydrophilic	660
AlSPc	hydrophilic	670
BPD-MA	hydrophobic	690
SnET2	hydrophobic	650
Pheophorbides (HEDP)	hydrophobic	660
ALA	hydrophilic	640 [b]
Cationic dyes (CPS)	hydrophilic	600-900 [c]

(a) The approximate location of the longest absorption wavelength relevant to PDT; (b) ALA is converted to protoporphyrin IX within tissues; (c) Many different CPS dyes have been suggested for PDT with absorption ranging from 600-900 nm. Abbreviations: NPe6= Mono-L-aspartyl chlorin e_6, AlSPc = Sulfonated aluminum phthalocyanine, BPD-MA= Benzoporphyrin derivative monoacid ring A, SnET2= Tin etiopurpurin, ALA.= Aminolevulinic acid (from Grossweiner, 1994).

Of the many potential exogenous tetrapyrrole photosensitizers currently under investigation for use in PDT, PFII, mono-L-aspartyl chlorin e_6 (NPe6), benzoporphyrin derivative monoacid ring A (BPD-MA), and tin etiopurpurin, are currently in various stages of clinical trials (Spikes and Bommer, 1993; Dougherty, 1993). The PDT photosensitizer formulation PFII has been approved for clinical use in bladder malignancies (Marcus, 1992; Dougherty, 1993). As other potential PDT photosensitizers undergo clinical trials, it can be expected that more of these will be approved for clinical use.

Chapter 2 Background

2.1 Modes of action in PDT

From an operational viewpoint, PDT can be subdivided into four phases: i) drug administration, ii) distribution into tissues, iii) photosensitization, and iv) biochemical reactions. These phases are discussed individually in the following subsections.

2.1.1 Drug administration

There are three major factors that need to be optimized for successful drug administration: i) the administration route by which the dye is introduced into the body; ii) the solvent mixture (solvent formulation) used to dissolve the photosensitizer dye; and iii) the blood component (blood fraction) which transports the dye to the various tissue sites.

The six possible administration routes for PDT photosensitizing dyes are: i) intravenous (IV); ii) intraperitoneal (IP); iii) intradermal (ID); iv) intratumoural (IT); v) oral; and vi) topical. The first two (intravenous and intraperitoneal) are the most frequently used of all these possible administration routes. The four other possible routes are of limited use mainly due to the poor membrane transport of large molecules such as the tetrapyrroles and the potential leakage of the dye from the administered site into other normal tissues. When the dye is injected IV or IP, the photosensitizer must enter the circulatory system in order to travel to specific tissues. Two routes of administration whereby the drug may not need to pass through the circulatory system are intratumoural and topical (Kostron *et al.*, 1985; Hebeda *et al.*, 1995). Other administration methods for PDT dyes, such as intratumoural injection (IT), may in some cases provide better dye selectivity for the tumour tissue, as suggested by Hebeda *et al.* (1995) who used the IT injection into brain neoplasia. The IT injection of a PDT drug directly into the brain bypasses the transport inhibition across the brain's blood barrier. Leakage of the dye from the intratumoural injection site into other normal brain tissues was a major difficulty

encountered with that application method (Hebeda *et al.*, 1995). The second exception to using the blood for transporting a compound to the tumour is the topical administration of 5-aminolevulinic acid (ALA) to the tumour site (Kennedy and Pottier, 1992). ALA can penetrate the skin and diffuse directly into the tumour due to its small size and water solubility. Once ALA is assimilated by tumour cells it is metabolized into the endogenous photosensitizer protoporphyrin IX.

The dye can bind to different blood fractions depending on the solvent formulation and its hydrophobicity. For example, the dye ketochlorin (C8KC) binds to the low density lipoprotein (LDL), instead of the albumin blood fraction, when the more hydrophobic Cremophor EL (CRM) rather than the less hydrophobic Tween 80 (TX80) is used as the solvent formulation (Woodburn *et al.*, 1994). The hydrophobicity of the solvent formulation carrying the dye can also modify the dye's concentration in tissues as well as its tissue distribution (Reddi *et al.*, 1990; Gurinovich *et al.*, 1992; Henderson and Dougherty, 1992; Jori, 1992; Kessel and Morgan, 1993; Obochi *et al.*, 1993; Rosenberger and Margalit, 1993; and Woodburn *et al.*, 1994). For example the concentration of the dye ketochlorin (C8KC) increased in all tissues when Cremophor EL solvent formulation was used instead of the solvent formulation Tween 80 (Woodburn *et al.*, 1994). Also, the ratio of dye concentration in tumour to muscle increased from 3.3 to 5.5 for the photosensitizer ZnPc when LDL instead of liposomes was used as a solvent formulation (Reddi *et al.*, 1990).

For PDT the importance of photosensitizer binding to the LDL is associated with the large number of LDL receptor sites on neoplastic cells. Those LDL receptor sites permit the LDL-bound dye to be incorporated into neoplastic cells by endocytosis. Hence the PDT dye is often transported more efficiently to the tumour when the dye solvent formulation contains blood proteins. The dye selectivity for tumour tissues and the dye concentration in tumour tissue will often increase when LDL is part of the solvent formulation or when the solvent formulation enhances the photosensitizer binding to LDL present in the blood (Jori, 1992). For example the photosensitizer (HpD) concentration increased in cells when LDL rather than high density lipoprotein (HDL) or human serum

albumin (HSA) was included in the drug-solvent formulation (Rosenberger and Margalit, 1993). The degree of hydrophobicity of a photosensitizer affects its binding to the LDL protein fraction (Moan and Berg, 1992). For example the water soluble dye chlorin e_6 binds to the LDL when that dye is rendered more hydrophobic by the addition of an amide to that dye (Gurinovich *et al.*, 1992). Thus, the degree of hydrophobicity of a dye or the solvent formulation containing a dye can increase the dye's binding to LDL and increase the tumour selectivity of the dye.

2.1.2 Kinetics of tissue distribution (pharmacokinetics) of photosensitizers

The pharmacokinetic properties of an anti-tumour photosensitizer can be examined in three parts: i) the clearance of the dye from a tissue; ii) the selective distribution of the dye in different tissues; and iii) the distribution of the dye within subcellular organelles of a cell.

The clearance curve of a drug is derived from the drug's concentration while the drug moves through the body to be eventually metabolized or cleared. A triexponential equation mathematically describes the clearance curves of most tetrapyrrole photosensitizers from several tissues (Henderson and Bellnier, 1989). For example, radiolabeled Photofrin II® (PFII) has three elimination half lives at 4 h, 9 days, and 36 days as it is cleared from the serum of DBA mice (Henderson and Bellnier, 1989). PDT treatment can be coordinated with photosensitizer peak concentration in the body by knowing the clearance curves of the dye in the relevant tissues. The time at which the peak concentration of different photosensitizers is observed can be quite different (2 to 60 min for NPe6, 3h for BPD-MA, and 5 to 10 h for PFII) (Grossweiner, 1994).

The selective retention of an anti-tumour dye by tissues can be determined from its clearance rate from those tissues relative to others (Fig. 2.1). The tissue distribution of a dye may not remain constant while the dye passes through the body, due to different clearance rates from different tissues. Thus, the tissue distribution is time dependent. For example, at 1h post injection, the NPe6 concentrations in the tumour and muscle were respectively 3.81 $\mu g\ g^{-1}$ and 0.86 $\mu g\ g^{-1}$, but after 10 h these corresponding values were

1.49 μg g^{-1} and 0.11 μg g^{-1} (Gomer and Ferrario, 1990). Thus, while the absolute drug concentration in the tumour only diminished by half, the tumour to muscle ratio actually increase threefold. The clearance curve and the peak concentration of a dye in the tumour are two crucial points used by clinicians to determine the best treatment time for PDT.

The optimum PDT treatment time normally occurs when the dye concentration is highest in malignant tissue and lowest in the surrounding normal tissues. The ratio of the dye concentration in the malignant tissue to the surrounding normal tissue as a function of time is used to estimate the treatment time. This concentration ratio is often referred to as "the tumour to normal muscle" (T/M) ratio, since the surrounding tissue of a tumour is frequently muscle. A photosensitizer is considered to have a high tumour selectivity when its T/M ratio is large. Two examples of dyes that have high tumour selectivity and a high T/M ratio are BPD-MA (T/M ratio=19.2) (Richter *et al.*, 1993), and AlS_2Pc (T/M ratio=9.8) (Peng *et al.*, 1993). The pharmacokinetics, tissue distribution, and T/M ratios of some second generation photosensitizers are summarized in Table 2.1.

The pharmacokinetics and tissue distribution of tetrapyrrole photosensitizers can vary between different animal breeds or different tumour types within the same animal. For example, the chlorin e_6 peak concentration varied from 2.5 to 9.5 μg g^{-1} in different tumour types within the same animals (wistar rats) (Kostenich *et al.*, 1993). The T/M ratio for chlorin e_6 also peaked at different values and times in different tumours within the same animals (Kostenich *et al.*, 1994). For example, the T/M ratio peaked at 18 h at a value of 8.8 in the M1 tumours and at 12 h at a value of 6.0 in the tumour type 45 (Table 2.1). Thus, the pharmacokinetics and tissue distribution of a dye from one animal model or tumour type may not be applicable to another animal or tumour type, and the optimum PDT treatment time can also vary between tumour or animal type, since the pharmacokinetics and tissue distribution of the dye within the body are used to estimate the PDT treatment time. It is thus obvious that pharmacokinetics data obtained from animal models may not readily conform to human pharmacokinetics data.

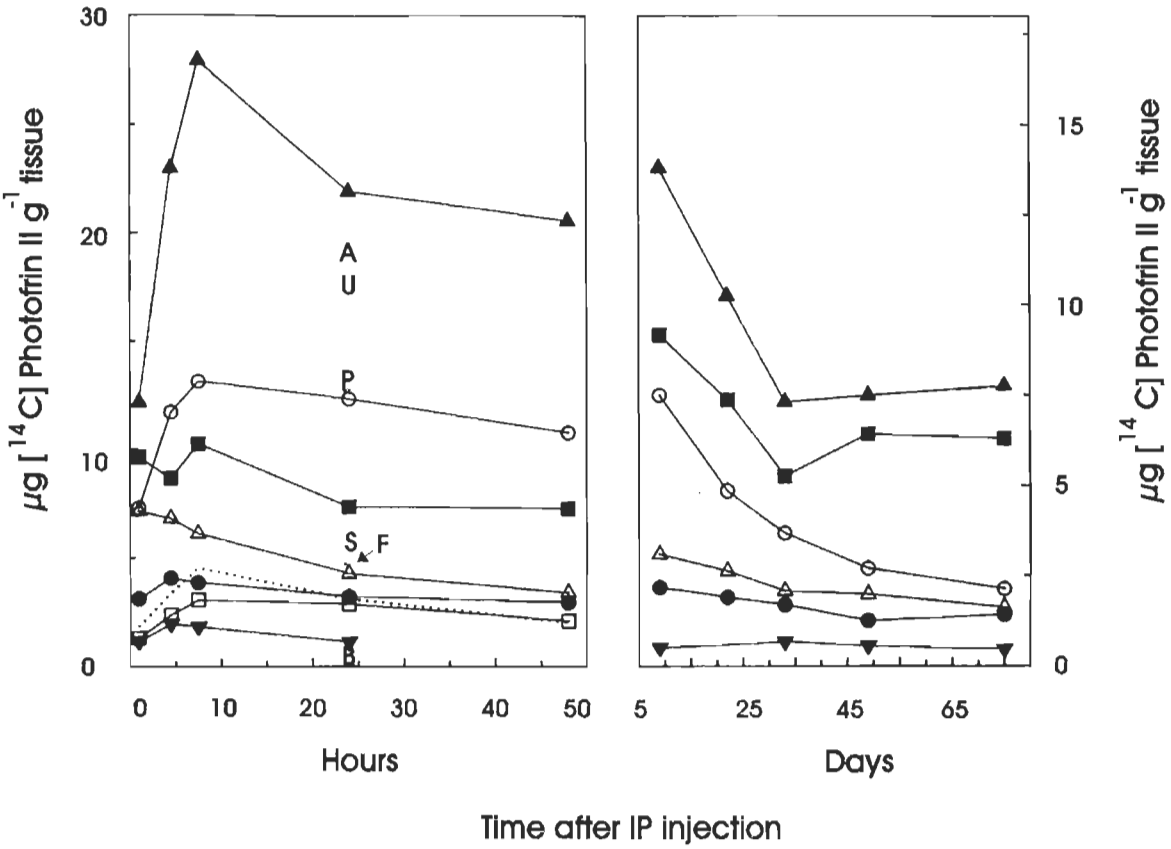

Figure 2.1. Clearance curves for radiolabeled Photofrin II in DBA/2 Ha mice for various tissues. Animals received 5 mg kg^{-1} of ^{14}C Photofrin II IP and were killed at the indicated intervals. Each point is the average of values from 3 to 6 animals, which differed by less than 30%. Concentrations in the liver (▲), kidney (⬭), spleen (■), lung (△), heart (●), skin contralateral to the tumour (□), muscle (▼), and SMT-F tumour (.....) were calculated as if all radioactivity was accounted for by ^{14}C Photofrin II. The letters indicate 24 h points for the following organs: A, adrenal glands; P, pancreas; S, stomach; F, femur; U, urinary bladder; B, brain. (from Henderson and Bellnier, 1989).

Table 2.1: Summary of recent pharmacokinetics data for of some second generation photosensitizers administered by IV or IP.

Sensitizer	Dose ($mg\ kg^{-1}$)	Tissue	Tissue conc ($\mu g\ g^{-1}$)	Time (h)	T/M Ratio	T/S Ratio	Reference
SnET2	1.5	Tumour Skin Liver Plasma	0.2 0.2 0.8 0.7	24		1.0	Kessel and Morgan, 1993
Bchlorin CA-6E	5	Tumour Skin Plasma	0.94 0.21 0.4	4		4.5	Kessel *et al.*, 1993
Ketochlorin C8KC (CRM formulation)	5	Tumour Skin Muscle Liver Plasma	6.69±1.25 2.27±0.12 1.69±0.16 22.45±2.5 9.97±2.14	24	4.0	2.9	Woodburn *et al.*, 1994
Ketochlorin C8KC (TW80 formulation)	5	Tumour Skin Muscle Liver Plasma	3.5±0.43 1.46±0.18 0.84±0.05 24.77±0.4 4.72±0.60	24	4.2	2.4	Woodburn *et al.*, 1994
Chlorin e_6	10	Tumour (M1) Muscle Liver Blood	4.4±0.4 0.5±0.1 2.0±0.3 12.0±0.6	18	8.8		Kostenich *et al.*, 1994
Chlorin e_6	10	Tumour (45) Muscle Liver Blood	3.6±0.3 0.6±0.2 2.6±0.2 14.2±0.7	12	6.0		Kostenich *et al.*, 1994
Bchlorin *a*	10			0.5-24	2.4		Schuitmaker *et al.*, 1993
MPH	5.8	Tumour Liver Blood	20.4 25.7 14.8	1			Mayhew *et al.*, 1993

Sensitizer	Dose ($mg\ kg^{-1}$)	Tissue	Tissue conc ($\mu g\ g^{-1}$)	Time (h)	T/M Ratio	T/S Ratio	Reference
Chlorin e_6	10	Tumour(SM-1)	4.4±0.4	24			Kostenich *et al.*, 1993
		Tumour(S45)	2.5±0.6	24			
		Tumour(PC-1)	7.4±0.1	24			
		Tumour(PLS)	3.7±0.1	24			
		Blood	9.5±0.7	24			
		Tumour(SM-1)	7.6±0.1	0.25			
		Tumour(S45)	6.7±0.9	0.25			
		Tumour(PC-1)	9.1±0.2	0.25			
		Tumour(PLS)	10.8±0.8	0.25			
		Blood	35±1.7	0.25			
mPheo a	10	Tumour	6.3±0.7	1			Kessel and Smith, 1989
mPheo b		Tumour	5.7±0.6				
Chloro Al SPc	10	Fibrosarcoma		24-48		2	Chan *et al.*, 1988
		M5076 Sarcoma				4	
		Colon 26				7	
Si NPc	1	Tumour	0.58±0.13	48		1.16	Biolo *et al.*, 1994
		Skin	0.50±0.08				
		Liver	9.78±1.25				
		Serum	0.21±0.11				
Zn NPc	.25	Tumour	1.5±0.70	20		2.5	Shopova *et al.*, 1994
		Skin	0.60±0.20				
		Liver	1.20±0.50				
PF II	0.2				1	1	Jori, 1992
NPe6	5	Tumour	3.81±1.64	1	4.43	1.04	Gomer and Ferrario, 1990
		Skin	3.67±0.66				
		Muscle	0.86±0.28				
		Liver	16.92±4.9				
		Plasma	12.91±3.0				
BPD-MA	4	Tumour	1.7±0.30	3		5.9	Richter *et al.*, 1993
			0.8±0.20	24	19.2		
Ammonium Salts of PP	20	Tumour	100%		10	3.0	Kawabe *et al.*, 1991
		Skin	33%				
		Muscle	10%				
		Liver	23.3%				
Al S_2Pc	10	Tumour	7	48	9.8	2.3	Peng *et al.*, 1993
		Skin	3.5				
		Muscle	1				
		Liver	40				

Sensitizer	Dose (mg kg^{-1})	Tissue	Tissue conc ($\mu g\ g^{-1}$)	Time (h)	T/M Ratio	T/S Ratio	Reference
isoBosinc	0.25	Tumour Skin Muscle Serum	0.61±0.06 0.42±0.13 0.07±0.01 1.17±0.08	24	8.7	1.5	Zuk *et al.*, 1994
Al SPc	20	Tumour Skin Muscle	14 4.7 3.2	36	4.4	3.0	Chen *et al.*, 1993
HPPH	1	Tumour Skin Plasma	3 0.5 9	12		6.0	Bellnier *et al.*, 1993
Zn NPc	0.3	Tumour Muscle Liver	0.7 0.50 0.65	24	1.4		Wohrle *et al.*, 1993
Al SPc	5	Colon Pancreas Brain	48 24-48 24		2 (T/N) 3 (T/N) 28 (T/N)		Tralau *et al.*, 1987
Chlorin e_6	10	Tumour Muscle Liver	16 5 20	6	3.2		Gurinovich *et al.*, 1992
EDA	10	Tumour Muscle Liver	40 3 10	18	13.3		
Zn Pc	0.5	Tumour Muscle Liver	0.75 0.1 .5	24	7.5		Reddi *et al.*, 1987
Zn Pc (liposomes)	0.12	Tumour Muscle Liver	0.3 0.1 0.3	24	3		Reddi *et al.*, 1990
Zn Pc (LDL)	0.12	Tumour Muscle Liver	0.55 0.1 0.3	24	5.5		

Abbreviations: T/M= Drug concentration ratio of the tumour to muscle; T/N= Drug concentration ratio of tumour to normal tissue; T/S= Drug concentration ratio of tumour to skin; ET2= Etiopurpurin; Bchlorin= Bacteriochlorin; CRM= Cremophor EL formulation; TW80= Tween 80 formulation; MPH= Methyl pheophorbide *a*-hexyl-ether; mPheo= Methylpheophorbide *a*; Chloro Al SPc= Chloro aluminum sulfonated phthalocyanine; NPc= Naphthalocyanine; PF II= Photofrin II®; NPe6= Mono-L-aspartyl chlorin e_6; BPD-MA= Benzoporphyrin derivative monoacid ring A; S_2Pc= Disulfonated phthalocyanine; isoBosinc= Bis(di-isobutyloctadecylsiloxy)silicon naphthalocyanine; SPc= Sulfonated phthalocyanine; HPPH= 2-[1-Hexyloxyethyl]-2-devinyl pyropheophorbide *a*; LDL= Low density lipoprotein; EDA= Chlorin e_6 ethylenediamide.

Skin photosensitivity is a concern in PDT treatment of human patients, due to the fact that the photosensitizer may linger in the skin for some time after treatment. Thus, a higher selectivity for tumours, less selectivity for skin, and faster skin clearance would be desirable characteristics for improved PDT photosensitizers. The skin photosensitivity can occur for quite a long time after PDT treatment. For example, 2 months after administration PFII was still detected (Henderson and Dougherty, 1992). The duration of skin photosensitivity is decreased when using some of the new photosensitizers developed for PDT. For example, skin photosensitivity was reduced to 2 weeks when using the dye $AlPcS_n$ (Tralau *et al.*, 1989), 5 days for bacterial chlorophyll *a* (bChl *a*) (Henderson *et al.*, 1991), and 24 h for the new photosensitizer NPe6 (Roberts *et al.*, 1989). Some of these new dyes can be easily photodegraded, and this assists in clearing them from the skin (Henderson and Dougherty, 1992). The photodegradation of the sensitizer by normal ambient light may partly explain the short duration of skin photosensitivity observed with some of these new photosensitizers (Henderson and Dougherty, 1992).

Dye selective retention can occur within regions of a given tissue as well as between tissues. The vascular regions of a tumour will often selectively retain photosensitizer dyes (Henderson and Dougherty, 1992). When the photosensitizer concentration in proximity to the vascular network of the tumour is high relative to the other tumour regions, vascular damage is also apparent during PDT treatment (Henderson and Dougherty, 1992; Korbelik and Krosl, 1994). Damage to the vascular system of the tumour interrupts the blood supply to the tumour, thereby starving it of nutrients and oxygen. This mechanism has been proposed for tumour killing by PDT (Marcus, 1992).

Tetrapyrrole dyes can selectively localize into various organelles within cells. Most of the hydrophobic dyes bind to membrane-rich organelles such as the mitochondria (Ricchelli *et al.*, 1993), the lysosomes (Gèze *et al.*, 1993), and the golgi apparatus (Moser *et al.*, 1992), whereas the hydrophilic dyes bind to aqueous non-membrane cytoplasmic sites, such as proteins (Kessel and Smith, 1989). Thus the sub-cellular localization of a tetrapyrrole photosensitizer can be affected by its hydrophobicity or lipophilicity, which may affect the location of sub-cellular damage.

2.1.3 Light penetration into tissue

The spectral properties of the activating light must be matched to the absorption of the photosensitizing dye, and must be able to penetrate into the tissue for it to interact with the photosensitizer that is located in that tissue. It is desirable during PDT that the photosensitization process occur only in the tumour tissue, but in some cases the activating light may also have to penetrate through other tissues in order to reach the tumour. The absorption of all the tissues in the light path can change the light intensity and spectral properties, which may thus not correspond to those of the irradiation source. Light scattering and absorption by endogenous chromophores are the principal properties of tissues which are responsible for modifying light penetration. The typical light transmission curve that results from these tissue properties is shown in Fig. 2.2. The light transmission through typical tissues slowly increases with increasing wavelength to level off at about 700 nm. Thus the preferred wavelengths of light for PDT activation are these higher wavelengths (650-900 nm), due to the higher light transmission. This requires a PDT dye to have an absorption band in this region for the best photosensitization.

Quantification of the amount of photoactivating light present at the treatment site would provide the most precise method of determining actual light dosimetry. Frequently this is not possible or practical. Tissue model systems permit the light properties within the tissues to be estimated (Wan *et al.*, 1981; Grossweiner, 1987, 1994; and Patterson *et al.*, 1991a, 1991b). The light measured at the illumination source can be corrected using these model systems in order to estimate the light properties within the tissues. Alternately, light monitoring devices that permit simultaneous *in situ* measurements during PDT treatment are in continual development (Stamp and Williams, 1991; Sroka *et al.*, 1993; and Grossweiner, 1994).

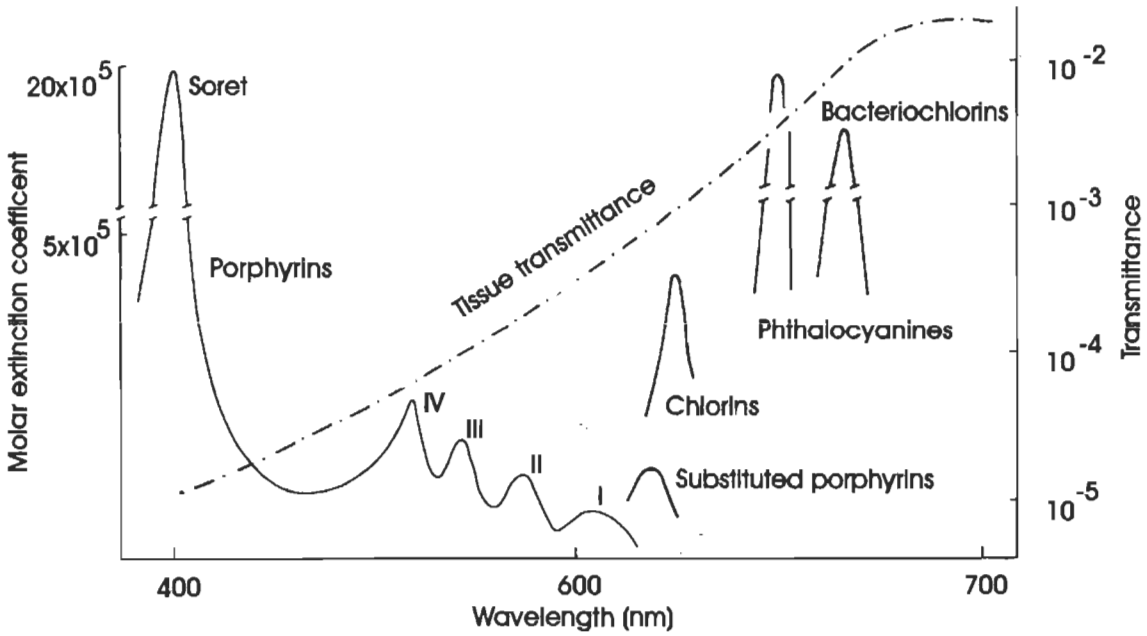

Figure 2.2. A generalized light transmittance curve through tissues (note the log scale). The absorption peak of the common classes of PDT drug is overlaid on the tissue light transmission curve. (from Bonnett and Berenbaum, 1989).

Strongly absorbing photosensitizers in the upper tissue layers can shade or screen the light penetration into the underlying deeper tissues. A significant percentage of the photons from a light source can be absorbed by photosensitizers early in the light path such that the underlying tissue layers are effectively shaded. This screening, or optical shading of deep-lying tissues, has been observed with some of the far red PDT photosensitizers with high molar extinction coefficient, such as the phthalocyanines (Henderson, 1989). For example, the transmittance of 680 nm light was reduced by 50% through tissue containing the dye Ga phthalocyanine (GaPc) compared to that same tissue without GaPc (Henderson, 1989), while the transmittance of 630 nm light (which is not absorbed by GaPc) in that same tissue was not reduced, confirming that the light attenuation resulted from the GaPc absorption. The shading of underlying tissues by strongly absorbing dyes can limit the available light needed for PDT photosensitization

in deep-lying tissues, resulting in decreased PDT activity in those deeper tissues (Dougherty and Potter, 1990). Such optical shading could partly explain why only a threefold increase in PDT effectiveness was observed with phthalocyanines compared to HpD, even though phthalocyanines absorb 20 times more than HpD (Jori *et al.*, 1984). A proposed solution to overcome optical shading is to maintain the photosensitizer concentration in tissues at a level where the effect of shading is minimized (Dougherty and Potter, 1990).

Light penetration can also be reduced by endogenous melanin pigments present in tissues in a manner similar to the optical shading by strongly absorbing dyes. Melanin is a yellowish brown or black pigment normally found in the skin. Melanin formation is light stimulated such that increased light exposure accelerates the formation of melanin and its migration into the upper skin layers. The main purpose of melanin in the upper skin layers is to absorb harmful electromagnetic radiation, thus preventing the radiation from penetrating into the skin. In other words, melanin acts as an endogenous sun screen absorbing excessive UV light from sun light. The melanin absorption is particularly high for UV light and gradually decreases to near zero by 900 nm (Epstein, 1989). Under some conditions and in some skin types the amount of melanin pigments in the skin can be considerably higher than normal for caucasian type skin, which results in a larger attenuation of light penetration through the skin. PDT using any visible light absorbing dye may be affected significantly due to the melanin absorption at visible wavelengths typically used for photosensitization.

One type of skin cancer, pigmented melanoma, contains high concentrations of melanin, which can result in significantly reduced PDT effectiveness. Treatment of pigmented melanomas by PDT may be improved by using far red absorbing dyes since those wavelengths are less affected by melanin absorption. Some of the new second generation photosensitizers meet the necessary requirement of high molar extinction coefficient in the far red region of the visible spectrum (780-800 nm). A preclinical PDT treatment study of a pigmented melanoma (B16) in mice using the anti-tumour photosensitizer Si(IV)-Naphthalocyanine (SiNc) has been shown to produce partial results (Biolo *et al.*, 1994).

2.1.4 Photosensitization by tetrapyrroles used in PDT

Photodynamic photosensitization involves the transfer of excitation energy from the dye to molecular oxygen. Typically, it is the dye triplet state which transfers energy to oxygen, due to the long lifetime of the triplet, which permits it to interact with oxygen. The triplet quantum yield (Φ_T) is a measure of the probability that a light activated dye molecule will form the excited triplet state. A large Φ_T implies that more triplet dye molecules can be produced, leading to a potentially higher photosensitization efficiency.

There are two possible photochemical mechanisms by which reactive oxygen species can be generated, each involving the interaction of the triplet photosensitizer molecule with ground state O_2. These two photochemical schemes are termed type 1 (Eq 1a and 1b) and type 2 (Eq 2a and 2b). The oxygen becomes a radical ion in the type 1 reaction scheme due to electron transfer from the photosensitizer triplet. Singlet oxygen ($^1O_2$) is generated in the type 2 reaction scheme, due to the energy transfer from the triplet photosensitizer to the triplet ground state oxygen. The photosensitizer molecule returns to the ground state in the type 2 reaction scheme after the energy has been transferred to oxygen; thus, that dye molecule can absorb another photon and repeat the reaction. Conversely, a type 1 reaction may result in destruction of the photosensitizing molecule.

Type 1: $P(T_1) + Subs \rightarrow P^{\cdot +} + Subs^{\cdot -}$ (1a)

$P(T_1) + O_2 \rightarrow P^{\cdot +} + O_2^{\cdot -}$ (1b)

Type 2: $P(T_1) + {}^3O_2 \rightarrow P(S_0) + {}^1O_2^*$ (2a)

${}^1O_2^* + Subs \rightarrow$ Photo-oxidation (2b)

Reaction scheme for type 1 and type 2 photosensitization with oxygen. P= Photosensitizer; T= Triplet; Subs= Substrates; S_0= Ground state singlet.

The main reactions involved in PDT photosensitization are believed to be type 2 (van Lier and Spikes, 1989; Patterson *et al.*, 1990), but type 1 reactions cannot be completely excluded (Persad *et al.*, 1983; Hadjur *et al.*, 1995). The type 2 reaction scheme can be virtually catalytic, since the photosensitizer returns to the ground state after it has transferred the photon energy to oxygen, which implies that a single photosensitizer molecule may produce many $^1O_2$ molecules. A substantial biological effect can result from rather low photosensitizer concentration, due to this catalytic cycle of the type 2 reaction scheme.

For oxygen photosensitization by a dye, the dye triplet state must possess sufficient energy to permit excitation of the ground state oxygen triplet to the singlet excited state ($^1O_2$). A tetrapyrrole dye requires ~150 kJ mol^{-1} of excitation energy (< 800 nm light) due to a loss of 50-60 kJ mol^{-1} of that energy during singlet to triplet inter-system crossing of the dye (van Lier and Spikes, 1989; Grossweiner, 1994). Photons of longer wavelengths than 800 nm could be used to excite a given dye still permitting $^1O_2$ formation, if the dye's energy loss during the intersystem crossing between the singlet and triplet excited states could be reduced.

The quantum yield of singlet oxygen production (Φ_Δ) from photosensitization by a dye is often used to estimate PDT effectiveness of that dye (Grossweiner, 1994). The Φ_Δ for the dye is usually measured in solvent or organized lipid systems *in vitro*, rather than *in vivo*. This is due to an inability to detect $^1O_2$ *in vivo*. A single case of $^1O_2$ detection *in vivo* has been reported (Parker, 1987). This result has not been repeated in other laboratories, in spite of numerous attempts. Patterson *et al.* (1990) have determined that the lifetime of $^1O_2$ *in vivo* is less than 5 μs, which is shorter than the detection time constant of current instrumentation.

The quantum yield of $^1O_2$ and photosensitizer triplet (T_1) properties can be used in preliminary evaluation of any new potential PDT photosensitizer. The PDT activity of a dye generally increases as these quantum yields increase. A detailed review of values of Φ_Δ, ΦT_1, and other physical properties of many potential photosensitizers has been given by McGarvey and Truscott (1990). Table 2.2 documents some recent data on

Table 2.2: Summary of recent photophysical values from some potential PDT photosensitizers.

Sensitizer	Singlet Lifetime (ns)	Triplet Lifetime (μs)	Triplet Φ_T	$^1O_2$ Φ_Δ	Solvent	Reference
CA-6E	3.75				ethanol	Kessel *et al.*, 1993
bChl c		200-250		.61	acetone	Krasnovsky *et al.*, 1993
Chl a				.63		
bChl d		200.220		.55		
bPheophytin c				.77		
bPheophytin d		200-215		.75		
bPheophorbide d				.75		
TPP		350-370		.65		
Azaporphyrin				.65	toluene	Schiwon *et al.*, 1994
Chl derivatives		190	.37	.39	benzene	Fiedor *et al.*, 1993
		330	.29	.30	D_2O	
NPe6		300			H_2O	Spikes and Bommer, 1993
				.77	D_2O	
Pheo *a*			1.0	0.60	EtOH	Krasnovsky *et al.*, 1990
			0.6	0.74	di ethyl ether	
			1.1		H_20/triton	
				0.50	D_2O/triton	
Chl *a*			0.60		EtOH	Krasnovsky *et al.*, 1990
			1.60		di ethyl ether	
				0.57	CCl_4	
Pheophytin *a*			1.1	0.60	EtOH	Krasnovsky *et al.*, 1990
			0.70	0.70	di ethyl ether	
			1.0		H_2O/triton	
				0.70	D_2O/triton	
Chlorin e_6	5.3				EtOH	Adam *et al.*, 1987
Pheo *a*	6.1					
HP	12.0					Roeder and Wabnitz, 1987
bChl c	2.6				MeOH	Brune *et al.*, 1988
	6.5				CH_2Cl_2/MeOH	
	7.6				DMSO	

Sensitizer	Singlet Lifetime (ns)	Triplet Lifetime (μs)	Triplet Φ_T	$^1O_2$ Φ_Δ	Solvent	Reference
HpD PFII MTBP ZnPc(OH_4)				.215 .191 .019- .023 0.005	liposomes	Gross *et al.*, 1993
BPD-MA	5.2	25	0.68	0.78	methanol benzene	Aveline *et al.*, 1994
Chalcogenapyrylium				.0004- .12	methanol	Detty and Merkel, 1990
Perylenequinonoid				.07-.83	benzene	Diwu and Lown, 1993
PFII (mono) PFII (aggreg) bChlorin Zn Pc Zn Pc Deriv's Cu Pc Si(IV) NPc			0.60 0.20 0.54 0.67 0.46- 0.59 0.95 0.39	0.30 0.10 0.20 0.53 0.35- 0.45 0.00 0.19	organic solvent or organized systems (eg liposomes)	Jori, 1992
H_2 TNP Zn TNP				0.47 0.24 0.375 0.6 0.38 0.76	DMF ethanol pyridine DMF ethanol pyridine	Roitman *et al.*, 1994
Porphyrin c Zn Pc HpD	8.0 2.0			1.0 0.73 0.54	aqueous buffer	Ghiggino *et al.*, 1988
Zn NPc		110-330	0.20	.135- .164	DMSO	Wohrle *et al.*, 1993

Abbreviations: CA-6E= Bacteriochlorin derivative; bChl= Bacteriochlorophyll; Chl= Chlorophyll; b= Bacterio; TPP= Tetraphenylporphyrin; Pheo *a*= Pheophorbide *a*; HpD= Hematoporphyrin derivative; PFII= Photofrin II®; MTBP= Metallo-tetrabenzoporphyrins; ZnPc(OH_4)= Zn Phthalocyanine tetrahydroxyl; BPD-MA= Benzoporphyrin derivative monoacid ring A; Pc= Phthalocyanine; NPc= Naphthalocyanine; TNP= Tetranaphthaloporphyrin.

these physical properties of numerous new second generation photosensitizers in various solvents, or organized systems such as liposomes. The Φ_Δ production by photosensitizers is usually higher in organic solvents than in aqueous systems.

It is apparent from Table 2.2 and McGarvey and Truscott (1990) that most tetrapyrroles have a Φ_T of around 0.6 to 0.9 and a Φ_Δ of around 0.5 to 0.8. The photosensitization ability of tetrapyrroles can be assessed by these photophysical properties of the molecules, however these parameters are usually measured in *in vitro* conditions. It would in general, be beneficial to measure the photosensitization potential PDT photosensitizers in a biologically relevant system (McGarvey and Truscott, 1990). However, Patterson *et al.* (1990) indicated that direct $^1O_2$ measurement *in vivo* is not possible at this time, thus the *in vitro* photophysical mesurements have to be used (McGarvey and Truscott, 1990). A simple biological system that can be used to estimate oxygen mediated photosensitization *in vivo* is photohemolysis (Bjellerup, 1988). The photosensitization of tetrapyrroles can be estimated using photohemolysis of red blood cells into which a photosensitizer has been incorporated (Ben-Hur *et al.*, 1993a). The cell membrane lysis caused by activated oxygen species subsequent to irradiation is determined by the release of hemoglobin into the medium. Thus photohemolysis is a practical method to assess the PDT photosensitizing ability of any new dye, since it can be used not only to determine if photosensitization occurs in a biological system, but can also be used to study both the light dose and dye concentration on the photosensitization process.

2.1.5 O_2 concentration

Photodynamic action of PDT dyes is oxygen dependent, with the molecular acceptor usually being oxygen (Moan and Berg, 1992). This is indicated by the absence of photodynamic activity of a PDT photosensitizer without oxygen. Other anti-tumour treatments like radiation therapy are only O_2 sensitive, in that their activity decreases about 2 to 3 times in the absence of oxygen (Moan and Berg, 1992). Thus oxygen must

be present in order to have PDT action.

The oxygen concentration (measured by the partial pressure of oxygen (PO_2)) in tumours is generally lower (< 40 Torr (5.3 kPa)) than in normal tissues (>50 Torr) (Freitas, 1985). The low O_2 concentration in tumours is due to poor O_2 diffusion from the circulatory system (Moan and Berg, 1992) and high O_2 consumption by the rapidly growing neoplastic cells (Jain, 1984). Some regions within a tumour may have a PO_2 values near zero (Freitas, 1985). The consumption of O_2 by the photodynamic process can further decrease the oxygen concentration within tumour tissue. For example, O_2 concentration dropped from 21 to less than 3 Torr during PDT treatment (Reed *et al.*, 1989). With such low O_2 concentrations the photodynamic process is certain to be limited (Freitas, 1985).

The O_2 concentration within tumour tissue needs to be maintained at near normal levels if the photodynamic activity of PDT is not to be limited. The oxygen consumption rate of the photodynamic process is usually greater than the diffusion of oxygen into the tumour tissue from the blood. There have been some successful attempts to increase O_2 concentration before or during PDT treatment so that the photodynamic process would not be O_2 limited (Freitas, 1985). Oxygen enrichment techniques that have been attempted are: i) blood transfusions to maintain high hemoglobin levels; ii) allowing the patient to breathe pure oxygen during the treatment; and iii) giving the patient perfluorocarbons which are a synthetic material capable of carrying high O_2 concentrations. All of these O_2 enrichment techniques have increased the PDT effectiveness which suggests that O_2 was previously limited (Freitas, 1985).

2.1.6 Tissue damage resulting from PDT

The two main types of PDT-incurred damage are believed to be i) injury to the microvascular system of the tumour and ii) direct intracellular damage (Henderson and Dougherty, 1992). The injury to the vascular supply of the tumour results in starvation of the tumour (Marcus, 1992). The photodynamic product $^1O_2$ will react with the cellular structures leading to cell damage. The short microsecond lifetime of $^1O_2$ in biological

systems prevents it from diffusing any great distance, which suggests that the location of any chemical reaction between $^1O_2$ and biomolecules must occur in proximity to the site where the $^1O_2$ was generated. Cell death will occur from the oxidative cellular damage caused by $^1O_2$ when that damage exceeds the cellular repair capability of the cell. A distinct boundary of necrosis or cell death, rather then a gradual transition from total tissue destruction to little damage, has been observed in numerous PDT treated tumours (Bown *et al.*, 1986). The cellular repair of PDT-incurred damage could explain the observed boundary, where necrosis boundary is believed to represent the threshold between those regions of the tumour where the cells were able to repair themselves and those regions where they were not (Wilson, 1989).

The intracellular damage to sub-cellular organelles of tumour cells caused by $^1O_2$ attack can lead to cell death. The degree of sub-cellular photosensitization damage has been correlated to the lipophilicity of a photosensitizer such that the more lipophilic dyes produce greater PDT induced cellular damage (Henderson and Dougherty, 1992). This has been shown by the higher rate of cellular photoinactivation with photosensitizing dyes that have a higher hydrophobicity measured using Triton X-114/H_2O partition coefficients (Moan *et al.*, 1987). More hydrophobic second generation PDT drugs, such as the chlorins, are anticipated to have improved PDT response compared to current PDT drugs like PFII, due to this correlation between cell inactivation and hydrophobicity.

2.2 Toxicity

2.2.1 Cytotoxicity assay

A rapid method often used to evaluate chemotherapeutic activity of drugs is cellular toxicity of tissue cultured neoplastic cells. The MTT assay is a convenient assay used to evaluate cellular cytotoxicty (Cole, 1986). MTT, a tetrazolium salt is enzymatically converted into a coloured formazan complex by living cells. The presence of the coloured product of the MTT by the cell can be used as a measure of cell viability. The viability can be estimated by a simple colourimetric assay of the cell suspension. A

known cytotoxic agent can be added as a positive control. That positive control would kill the cells and thus prevent the coloured product formation. A negative control compound can also be used which would not kill the cells and thus the coloured product of the MTT can be formed.

2.2.2 *In vivo* toxicity

The acute toxicity of any compound must be evaluated before that compound can be used as a drug in clinical trials. The therapeutic index is a ratio of the drug dose which causes acute toxicity to that used for treatment. A high therapeutic index implies that the dose used for treatment is well below the drug dose that would result in acute toxicity, and thus that drug possesses a minimum toxic risk (Gilman *et al.*, 1990).

The acute toxicity is generally estimated by the LD_{50} (lethal dose for 50% of the test cases). The LD_{50} for some potential PDT photosensitizers is given in Table 2.3. The therapeutic dose for PDT is typically 1-10 mg kg^{-1}, which is approximately 10 times lower than the LD_{50} values of those photosensitizers, yielding a good therapeutic index.

Table 2.3. LD_{50} values for some potential PDT photosensitizers.

Photosensitizer	LD_{50} (mg kg^{-1})	Conditions	Reference
Chlorin e_6	189	mice	Kostenich *et al.*, 1994
Chlorin e_6	113	rats	Kostenich *et al.*, 1994
AlSPc	>100	IV in rats[a]	Tralau *et al.*, 1990
HpD	275	IP in mice[a]	Tralau *et al.*, 1990
PII	130	IP in mice[a]	Tralau *et al.*, 1990

(a) It should be noted that when investigating acute toxicity using photosensitizers it is necessary to keep the animals in the dark such that there is no contribution to the results from photosensitization.

2.3 Possibility of dual action anti-tumour drugs.

2.3.1 First observation of anti-tumour activity by a porphyrin derivative

It was incidentally observed during a recent study on a new series of water soluble porphyrin derivatives, that one of these derivatives, namely hematoporphyrin propyl ether ethanolamide (HPPEEA), showed anti-tumour activity in the absence of light (Girard, 1992). Tumour regression was observed in the absence of light when HPPEEA (10 mg kg^{-1} body weight) was administered to SKH-HR1 mice carrying transitional bladder carcinoma (FCB).

It was concluded that the ethanolamide moiety of HPPEEA must be involved in the anti-tumour activity since no porphyrin derivative until that time had ever shown chemotherapeutic activity in the absence of light. It was realized upon closer examination of the chemical structure of the ethanolamide moiety that there was some correlation to the structure of the nitrogen mustards, which are a class of alkylating chemotherapeutic drugs.

2.3.2 Nitrogen mustards

The nitrogen mustards are a diverse class of compounds which share a common structural moiety. This structural moiety consists of a nitrogen attached to one or more ethyl halide(s) (Fig. 2.3). The ethyl halide can undergo a rearrangement to form a metastable intermediate called an aziridinium ion, with the concomitant removal of the halide (Calabresi and Chabner, 1990). The metastable aziridinium ion intermediate is a three membered ring consisting of the nitrogen and the two carbons of the ethyl group (Fig. 2.3). The aziridinium ion intermediate can form spontaneously when a nitrogen mustard is introduced into an aqueous environment. This aziridinium ion intermediate is a very reactive electrophile, which can undergo alkylating reactions with other nucleophilic molecules.

The principal anti-tumour reactivity of nitrogen mustards involves their interaction

with a DNA molecule (Calabresi and Chabner, 1990; Calsou and Salles, 1993). An S_N2 type nucleophilic attack by the N-7 of the guanine base of DNA on the aziridinium ion intermediate leads to the alkylation of DNA (Kohn, 1981; Calabresi and Chabner, 1990) (Fig. 2.4). The result of the nitrogen mustard binding to the guanine is a defect in the DNA strand. A cross-link between two guanine bases on adjacent DNA strands can also occur if the nitrogen mustard contains two alkylating moieties. Rapidly proliferating cells, such as those in neoplastic tissues, are the most sensitive to these DNA cross-links, thus a selective tumour toxicity can be achieved.

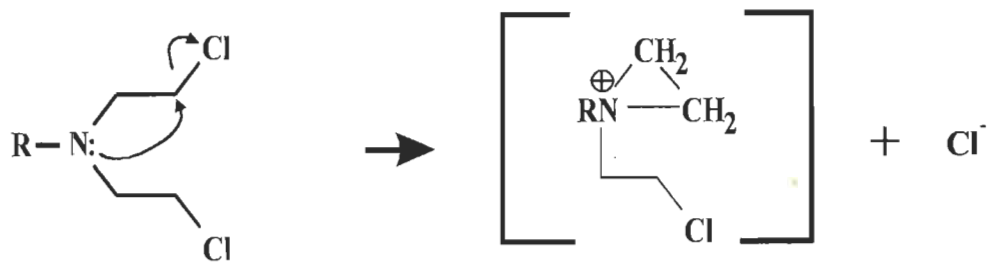

Nitrogen mustard

meta-stable aziridinium ion

Figure 2.3. The nitrogen mustard rearrangement into the meta-stable aziridinium ion intermediate.

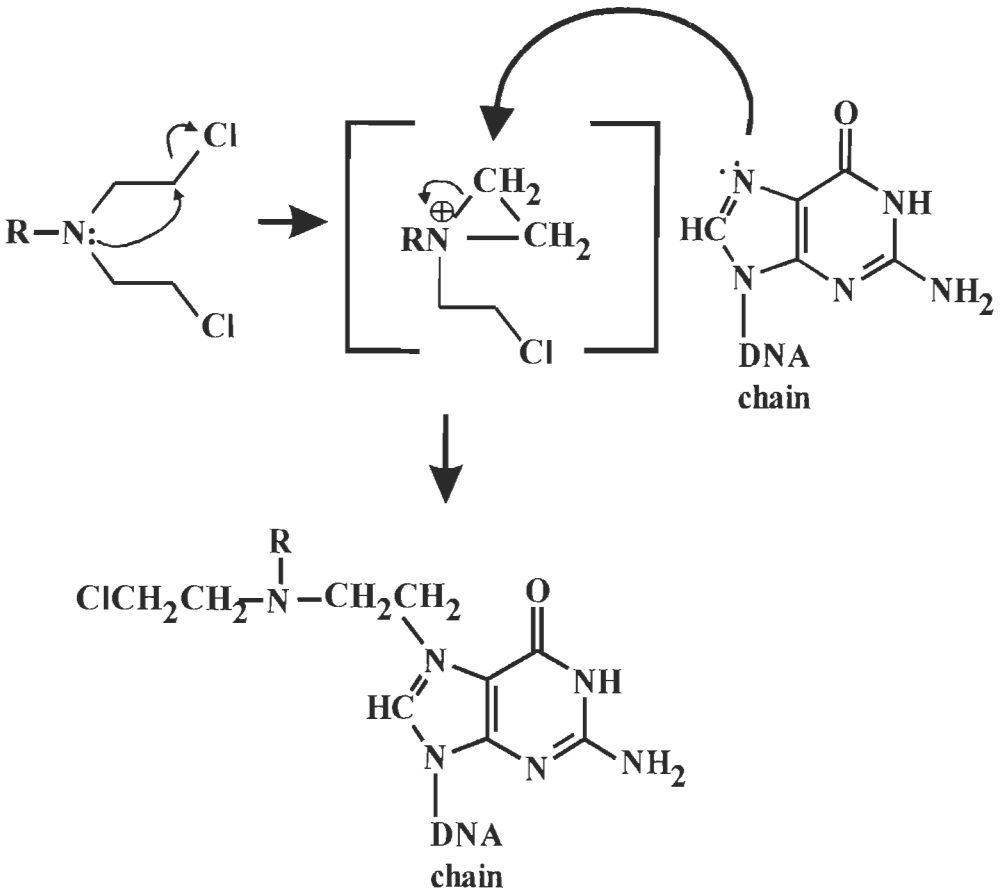

Figure 2.4. DNA-nitrogen mustard reaction scheme. The nitrogen mustard reacts with the N-7 nitrogen of guanine bases of DNA. A second similar reaction with the adjacent DNA strand leads to a cross-link.

The S_N2 nucleophilic attack on the aziridinium ion intermediate is not exclusive to reaction with DNA. The aziridinium ion moiety can also react with other substrate molecules, such as H_2O. The reaction of H_2O with aziridinium ion, which is significant in biological tissues, leads to the formation of an ethanolamide (Wilman and Connors, 1983). The reaction of an aziridinium ion with H_2O to form an ethanolamide occurs when the Cl of the ethyl halide is exchanged by an OH from the H_2O (Fig. 2.5a). The ethanolamide is likely to have lower alkylating reactivity than the nitrogen mustards, due to slower formation of the aziridinium ion intermediate, as ^-OH is a poorer leaving group than Cl^-. However, the conversion of an ethanolamide into an aziridinium ion

intermediate might become more favourable, under certain biological conditions. One such situation can be found in the blood, where the high Cl^- concentration favours the exchange between OH and Cl thereby converting the ethanolamide into a nitrogen mustard via an aziridinium ion (Wilman and Connors, 1983). Another plausible condition occurs in acidic medium, in which the higher hydronium ion concentration could induce the formation of an aziridinium ion via the formation of an oxonium ion, the latter being a good leaving group (Fig. 2.5b). Tumour tissue is often more acidic than normal tissue (Tannock and Rotin, 1989), thus the latter situation becomes a possible explanation for the observed anti-tumour activity of the porphyrin ethanolamides.

The nitrogen mustards show selective alkylating reactivity toward neoplastic tissues, while tetrapyrroles are selectively retained by such tissues. Thus a cyclic tetrapyrrole ethanolamide could be expected to have both selective retention and anti-tumour activity, providing that the tissue environment is favourable to the formation of the aziridinium ion intermediate from the ethanolamide moiety. A tetrapyrrole ethanolamide derivative could be seen as a potential dual action chemotherapeutic photosensitizer, due in part to the photosensitization property of the tetrapyrrole unit and in part to the anti-tumour alkylating property of the ethanolamide moiety.

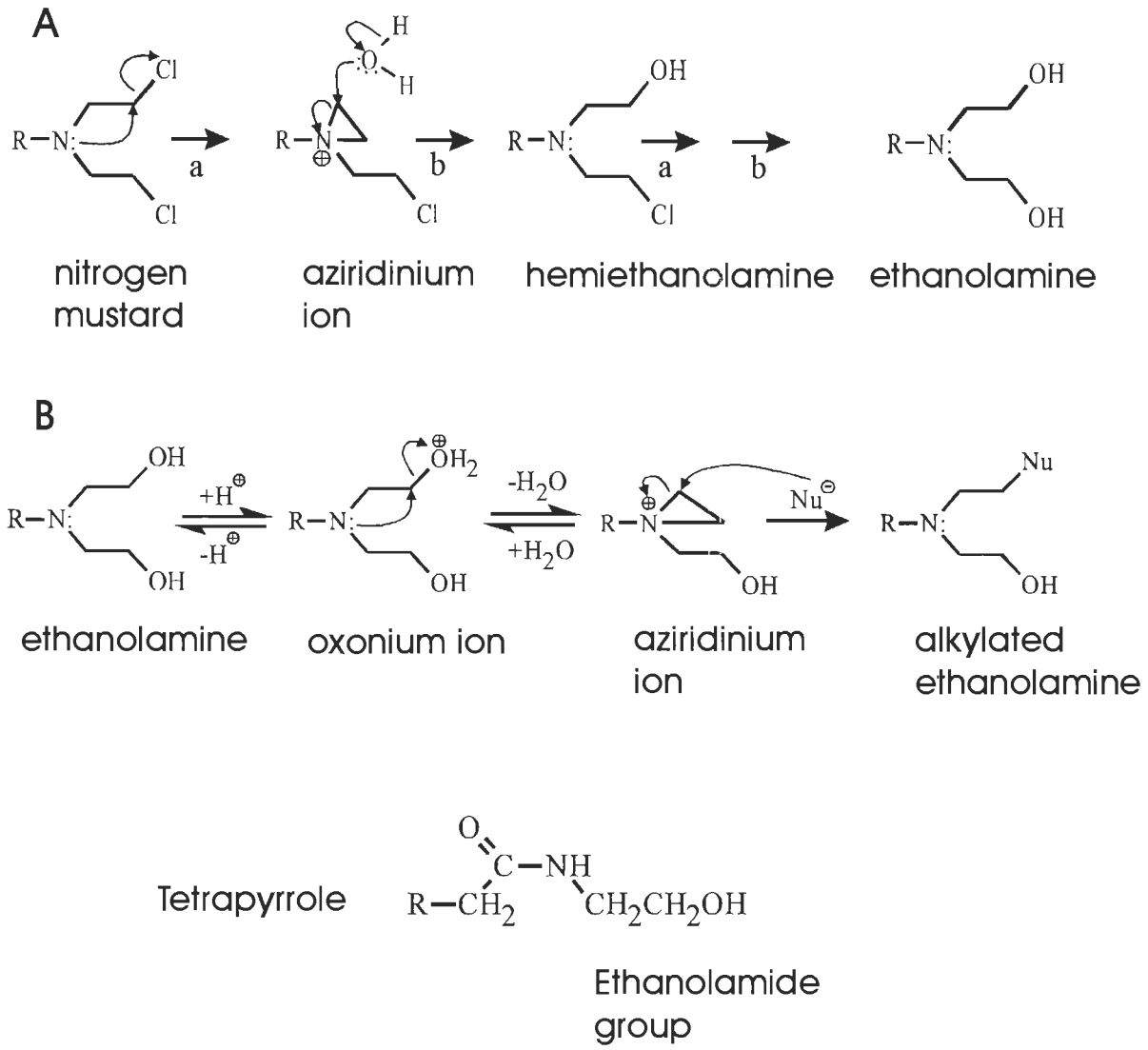

Figure 2.5. (A) The reaction scheme by which a nitrogen mustard changes to an ethanolamine due to an attack of the aziridinum ion by H_2O. (B) The reaction scheme by which an ethanolamine in an acidic environment can form an aziridimium ion which can undergo a nucleophilic attack to form an alkylated ethanolamide. The tetrapyrole ethanolamides are very similar to the ethanolamines formed by interaction between a nitrogen mustard and H_2O.

2.4 Chlorins

2.4.1 Sources of chlorins

Large quantities (gram size) are required if a potential new photosensitizer dye is to be used in clinical trials. The requirement for such large quantities has led to synthetic difficulties with many new dyes, including the chlorins. It is difficult by *de novo* synthesis to produce adequate quantities of purified chlorins due to the isomeric mixtures which frequently are produced during the synthesis and which are difficult to separate (Montforts *et al.*, 1994). Previous studies using mixed compounds or formulations (for example HpD) have led to uncertain results (Bonnet and Berenbaum, 1989). Alternately, chlorophyll and other natural cyclic tetrapyrroles can be used as starting materials for the synthesis of chlorins, so that many of the difficulties associated with *de novo* synthesis can be avoided (Montforts *et al.*, 1994). There are two necessary steps if a compound from a natural source is to be used in organic synthesis: i) isolation and purification of the compound from the natural source; and ii) modification of that molecule into the desired product. Chlorophyll *a* (Chl *a*) was used as the starting material in the synthesis discussed here.

2.4.1.1 Chlorophyll *a* isolation

Isolation and purification of Chl *a* (Fig. 1.2) from plant sources has been documented by Strain and Svec (1966), Svec (1991), and Pandey *et al.* (1991). A common Chl *a* source is the spinach plant because of its abundance and accessibility. The purification of Chl *a* from spinach is somewhat troublesome due to the presence of both Chl *a* and *b* (Strain and Svec, 1966; Svec, 1991; Rahmani *et al.*, 1993). The blue-green alga *Spirulina* which contains no Chl *b* has also been used as a source for Chl *a*, in order to simplify the extraction and purification, but the alga requires elaborate growth apparatus (Pandey *et al.*, 1991).

The first step in isolating Chl *a* from plants is to make a crude extract of the plant pigments. Purification of the Chl *a* from the crude pigment extract is usually done by liquid column chromatography (Strain and Svec, 1966; Svec, 1978; Brockmann and Risch, 1991; Pandey *et al.*, 1991). The column's stationary phase is usually one of the following: powdered sucrose, cellulose, silica gel, or alumina (Strain and Svec, 1966; Brockmann and Risch, 1990). The Chl *a* bands from the column can be tested for purity by spectroscopy and high pressure liquid chromatography (HPLC) (Roy, 1987; Shioi, 1991). The Chl *a* of sufficient purity is then ready for use in the synthesis of chlorin type PDT drugs.

2.4.1.2 Synthesis using chlorophyll *a*

Chlorins synthesized from Chl *a* for use as PDT photosensitizers have previously been reported. Chlorophyll *a* was modified by the addition of amines in the late 1960's (Pennington *et al.*, 1967) and the use of these chlorin amide derivatives for PDT was suggested by Gurinovich *et al.* (1992). Chlorin e_6 ethylenediamide was synthesized by Gurinovich *et al.* (1992) using a synthesis scheme detailed by Pennington *et al.* (1967). The synthesis of other chlorin derivatives of Chl *a* are described in detail by Pandey *et al.* (1991), and Montforts *et al.* (1994). Refer to Figure 3.2 for a detailed reaction scheme used in this research project.

2.4.2 Chlorin spectroscopy

Spectroscopy is a useful tool which can be used to identify and examine organic synthesis products, such as the chlorins. The visible light absorption of a potential PDT photosensitizer must be known, since visible light is used in PDT for excitation. The UV-visible absorbance spectrum of chlorins can be compared to that of the parent compound Chl *a*, which is well documented (Brown, 1968; Scheer and Katz, 1978; Hynninen *et al.*, 1979; Hoff and Amesz, 1991; Rahmani *et al.*, 1993; Brereton *et al.*, 1994) (Fig. 2.6 (a)).

The two major absorption bands for Chl *a* in diethyl ether are at 428.5 and 662 nm and have molar extinction coefficients of 1.358×10^5 and 1.007×10^5 M^{-1} cm^{-1}, respectively (Brown, 1968).

Reactions of the carbonyl groups of chlorins during synthesis can be monitored by IR spectroscopy (Pennington *et al.*, 1967, 1964; Scheer and Katz, 1978). The carbonyl region of the IR spectrum (between 1750-1600 cm^{-1}) (Fig. 2.6 (b)) is particularly useful in monitoring changes to carbonyl groups on chlorins (Katz *et al.*, 1966; Chapados, 1988; Lutz and Mantele, 1990; and Okada *et al.*, 1993). For example in Chl *a* the C=O esters at positions C-7 and C-10 (Fig. 1.3 for carbon numbering) are responsible for the band at 1730 cm^{-1} and the C=O ketone carbonyl at position C-9 is responsible for the band at 1700 cm^{-1}(Katz *et al.*, 1966; Chapados, 1988). The carbonyl bands in the IR spectrum can move by as much as 50 cm^{-1} depending on the solvent environment surrounding the molecule (Lutz and Mantele, 1991).

By using ^{13}C NMR the ketone carbonyl carbon (C-9) of ring V of chlorophyll type molecules can be monitored, producing a line at 189-195 ppm in the ^{13}C spectrum (Fig. 2.6 (c)) when ring V of Chl *a* is intact (Katz and Janson, 1973; Smith and Unsworth, 1975; Katz *et al.*, 1978; and Abraham and Rowan, 1990). When ring V of Chl *a* is opened during a synthesis the C-9 carbonyl carbon is reassigned to C-6a (observed at 172 ppm) and the 189 ppm line disappears (Smith and Unsworth, 1975). The new line at 172.4 ppm produced by C-6a is difficult to distinguish from that of C-7 (172.8 ppm), because both carbons are similar alkyl-type carbons.

This brief discussion of synthesis and spectroscopy of chlorins and Chl *a* is intended to provide some basic understanding of the field. The background provided here will be reexamined during the discussion of the synthesis carried out in this study.

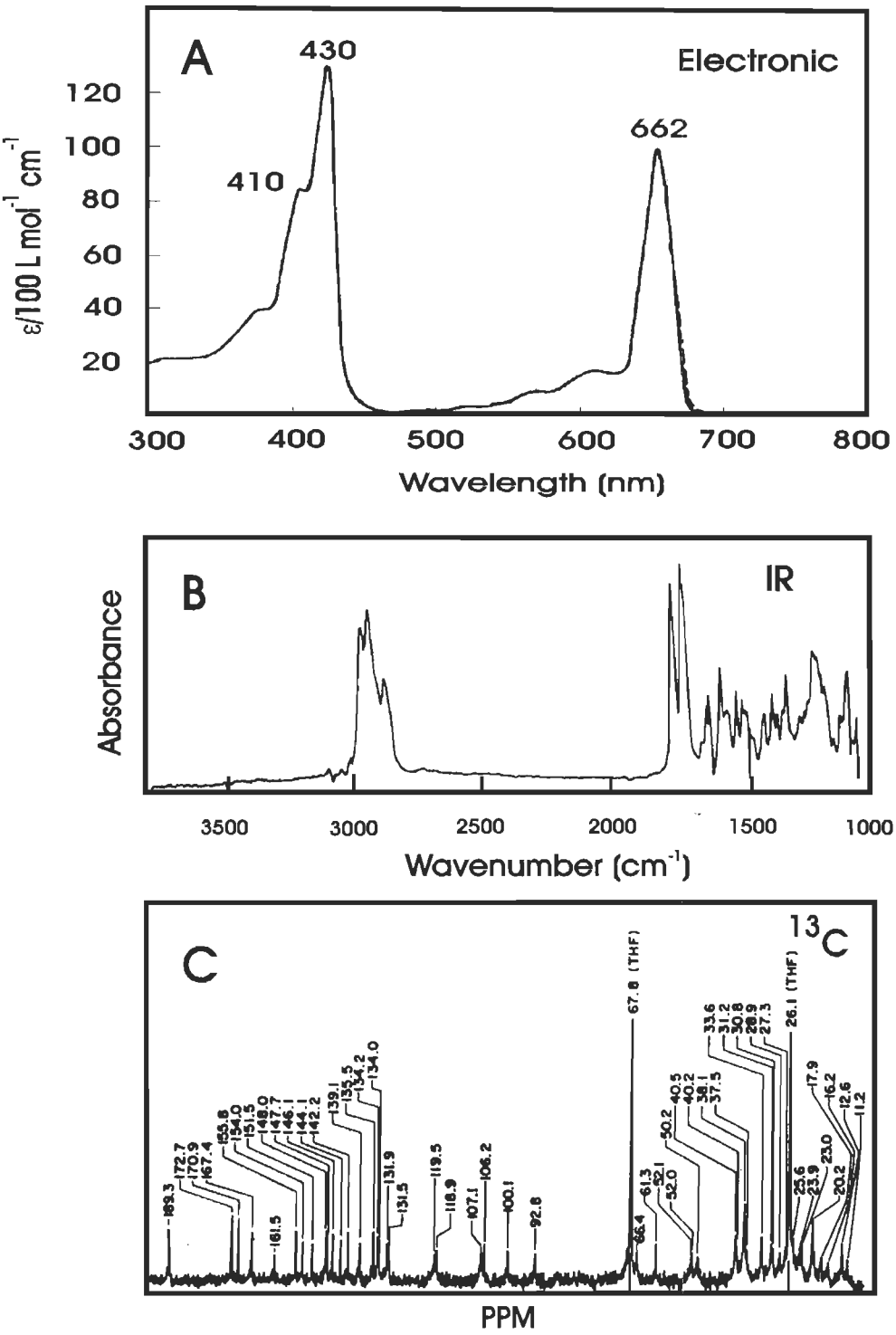

Figure 2.6. Chlorophyll *a* spectra: (a) electronic absorption in diethyl ether, (b) IR in CCL_4/pyridine, and (c) ^{13}C NMR in deuterated THF. (adapted from (a) Hoff and Amesz, 1990, (b) Katz *et al.*, 1978, and (c) Katz and Janson, 1973).

2.5 Aim of present work

The original porphyrin ethanolamide derivatives synthesized by Girard (1992) were primarily developed for spectroscopic studies. They exhibited rather poor selectivity for neoplastic tissues and somewhat limiting absorbance in the far red, yet these porphyrin ethanolamides did show both chemotherapeutic and photohemolytic activity. The aim of the work described here was to synthesize another ethanolamide derivative, using a chlorin which is known to have higher absorbance in the far red, and to examine its chemotherapeutic and photochemotherapeutic activity, in order to hopefully develop more potent dual action anti-tumour drug.

The scope of this project included: i) synthesis of pheophorbide *a* ethanolamide (PEA) starting from Chl *a*; ii) purification of PEA; and iii) evaluation of its toxicity, chemotherapeutic, pharmacokinetics, and photosensitization effects both, *in vitro* and *in vivo* where possible. The chemotherapeutic activity of PEA was evaluated by its cytotoxicity toward human cancer cell lines and its effect on animal cancer models. In order for PEA to be a potential photochemotherapeutic agent it must demonstrate both selective localization in tumours and photosensitization. The two properties used to assess the photochemotherapeutic activity of PEA were its pharmacokinetic behaviour in animal tumour models, and its photohemolytic activity. The pharmacokinetic data were used to demonstrate selective localization of PEA in tumours. The photohemolysis results were used to demonstrate the photosensitization activity of PEA. The goal of this work was thus to establish whether PEA was a potentially useful dual-action anti-tumour drug.

Chapter 3 Experimental

3.1 Chlorophyll extraction from spinach

Chl *a* was extracted from locally purchased spinach leaves by solvent extraction (Fig. 3.1). The plants leaves were deribbed and separated into 100 g (fresh weight) lots. Methanol (500 mL), 0.5 g NaH_2CO_3 and 100 g spinach were combined in a 1 liter flask. The leaf tissue was homogenated into a pulp using a tissue homogenator (Model L-04719-00 Cole Parmer). Room temperature was maintained during the grinding. The methanol was separated from the pulp by gravity filtration through fluted Whatman #1 filter paper. All methanol lots were pooled, and the extracted dye was partitioned into petroleum ether (35-60 °C grade), by adding equal parts petroleum ether (pet ether) and water. The water-methanol partition was discarded, and the pet ether fraction was further washed with a 50 mM NaCl-H_2O solution (Folch *et al.*, 1957). The resulting crude pigment extract was dried by rotary evaporation.

The pigments in the crude extract were separated by liquid column chromatography. The silica (Davisil silica 300 Å 90-130 μm Alltech Mandel Scientific) columns were 5 cm by 200 cm with a mobile phase of 5% *n* propanol in pet ether. The pigment was dissolved in a minimum volume of solvent (typically < 5 mL) and placed on the top of the column. Elution began after 10 min during which the pigments were allowed to adhere to the silica. Mobile phase solvent was continuously added until the blue-green Chl *a* band was eluted from the bottom of the column (Fig. 3.1). The silica, with the remaining pigments, was then removed for bulk cleaning and reused. The Chl *a* fraction was dried by rotary evaporation.

The silica was regenerated in bulk by washing with acetone and then with distilled water. The silica was mixed with acetone into a thick slurry and heated to 80 °C while stirring, then allowed to cool. The acetone was removed by vacuum filtration. The procedure was repeated using distilled water. The silica was dried at 100 °C for 5 days before reuse.

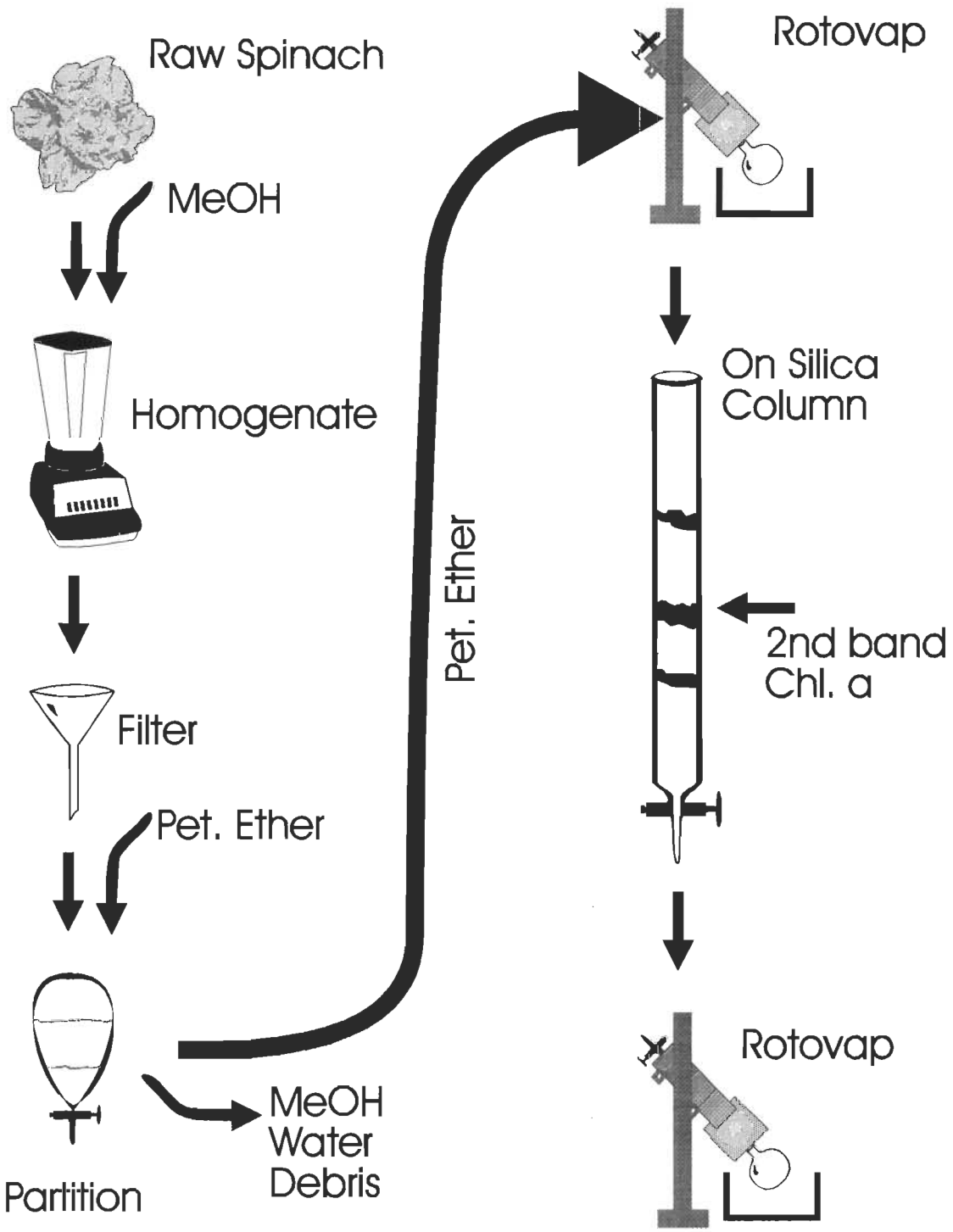

Figure 3.1. Flow diagram of chlorophyll extraction and purification procedure.

3.2 Conversion of chlorophyll *a* to methyl pheophorbide *a*

Chl *a* was immediately converted into methyl pheophorbide *a* (mPheo) by removing the phytyl chain and coordinated Mg^{+2} (see Fig. 3.2). Acidic methanol (Moser *et al.*, 1992) was prepared immediately before use by adding anhydrous H_2SO_4 to anhydrous methanol (10 mL to 90 mL) and cooling to room temperature. Chlorophyll *a* was added to the reaction mixture (1 g per 100 mL acidic methanol) and stirred, while maintaining a gaseous nitrogen environment. The progress of the reaction was monitored by testing aliquots at intervals on silica thin layer chromatography plates (TLC) using 5% methanol in dichloromethane as a mobile phase.

When the reaction reached completion (about 2 h as confirmed by TLC), mPheo was partitioned into chloroform by adding equal parts chloroform and water. The chloroform fraction was washed several times with distilled water, and then washed with a 10% sodium bicarbonate solution to remove any remaining acid. The mPheo was obtained by drying with anhydrous sodium sulphate followed by evaporation of the solvent in a rotary evaporator.

Methyl pheophorbide *a* was purified to remove the alkyl debris, resulting from the excised phytyl chain, by silica column chromatography, using a 2.5 cm by 200 cm column with a mobile phase of 5% methanol in dichloromethane. The mPheo was dissolved in a minimum amount of the mobile phase (typically < 3 mL) and placed at the top of the column. After 10 min, to allow the mPheo to adhere to the silica, the mobile phase was added continuously until the dark green mPheo band was eluted from the bottom of the column. The silica containing the remaining pigments was then removed for bulk cleaning. The mPheo purity was tested by silica TLC, as per the method for Chl *a*. This method did not detect the presence of any alkyl fragments. In order to view the alkyl fragment band, the TLC was sprayed with concentrated H_2SO_4 and heated to 100 °C. This procedure chars hydrocarbons, thus allowing such bands to become visible. The mPheo fraction was dried as above and stored at -3 °C in vials purged with N_2.

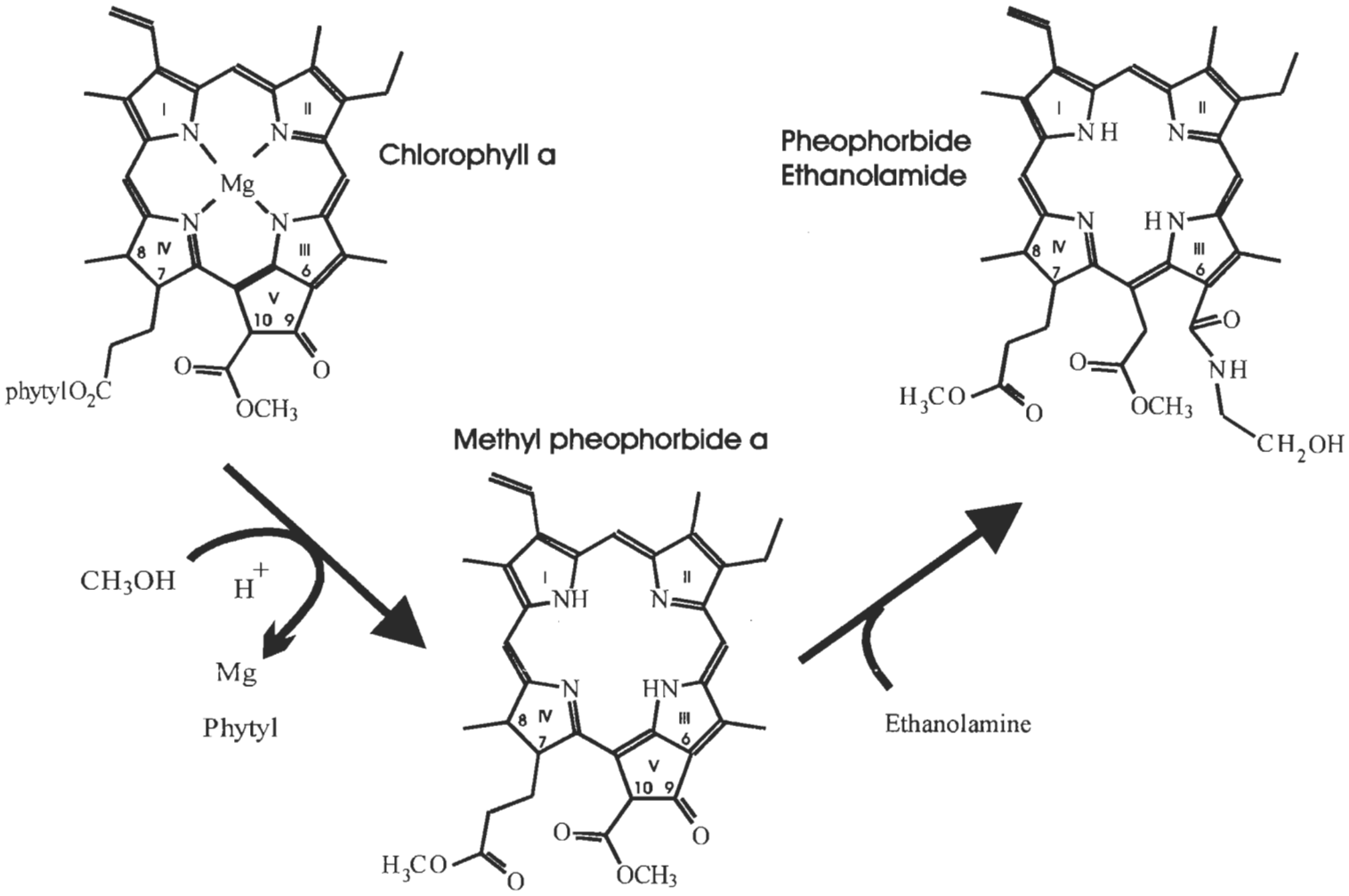

Figure 3.2 Synthesis of PEA from chlorphyll *a*. Chlorophyll *a* is converted to methyl pheophorbide *a* by the loss of Mg and the phytyl chain. Methyl pheophorbide *a* and ethanolamime react to produce PEA.

3.3 Ethanolamide synthesis

3.3.1 Pheophorbide *a* ethanolamide

PEA was synthesized from mPheo and ethanolamine (see Fig. 3.2). Methyl pheophorbide *a* (1 g) was added to dioxane (20 mL) and ethanolamine (10 mL). The reaction mixture was stirred under nitrogen. The progress of the reaction was monitored by regular samples tested on silica TLC plates using 5% methanol in dichloromethane as the mobile phase. The conversion reaction of mPheo to PEA usually took about 2 h.

When the reaction was completed (as determined by TLC), PEA was partitioned into chloroform by adding equal parts chloroform and water. The chloroform layer was washed several times with water, then neutralized by adding dropwise concentrated HCl and testing with pH paper until pH=7. The chloroform layer was dried with anhydrous sodium sulphate and evaporated. PEA was purified by silica column chromatography using the same procedure as outlined for mPheo. PEA eluted from the column was dried as above and then placed in a Fischer pistol for 7 h at 80 °C. PEA was stored in vials purged with nitrogen at -3 °C. The chemical structure of PEA was confirmed by IR and NMR spectroscopy data.

3.3.2 HPPEEA synthesis

It was necessary to synthesize large quantities of HPPEEA for comparison studies between HPPEEA and PEA. The synthesis was preformed exactly as outlined by Girard (1992) producing similar yields.

3.4 HPLC analysis of Pheophorbide *a* ethanolamide

The purity of PEA was tested by HPLC. HPLC techniques for analysis of chlorins have been reviewed by Roy (1987). The procedure of Mantoura and Llewellyn (1983) was used for the HPLC of PEA. An important point in this HPLC procedure was the use

of an ion pair reagent. The ion paired reagent improves the separation of compound that are very polar or can have multiple ionized forms (Roy, 1987). It was necessary to precondition the PEA sample prior to use in the HPLC in order to assure that the ion paired reagent functioned properly. This preconditioning involved dissolution of PEA (0.5 mg) in 1 mL of 90% acetone. Then 300 μL of the ion pair reagent was added and at least 5 min was allowed for ion pair association with the sample prior to analysis. If the ion pair association had not occurred then the separation on the column was found to be poor.

The HPLC column used was a 3x3 Econosphere, fully end capped, C18 (Mandel Scientific) in a gradient solvent system HPLC (ISCO model 2360). The gradient consisted of 100% solvent A to 100% solvent B in 10 min. Solvent A contained ion pair reagent/H_2O/methanol in a ratio of 10/10/80 (v/v/v) and solvent B contained acetone/ methanol in a ratio of 20/80 (v/v). The ion pair reagent contained 1.5 g tetrabutyl-ammonium acetate and 7.7 g ammonium acetate in 100 mL of distilled H_2O. Detection of the products was acheived by light absorption at 405 nm.

3.5 Spectroscopy of chlorins

Absorbance, fluorescence excitation, and fluorescence emission spectra were recorded for both mPheo and PEA. The compounds were dissolved in dichloromethane for absorption and fluorescence measurement since they were only slightly water soluble. All absorption measurements were recorded on a Shimadzu UV-160 spectrometer with a 3 nm spectral resolution, using 1 cm pathlength quartz cuvettes. All fluorescence and fluorescence excitation spectra were recorded on an LS-100 spectrofluorometer (PTI). This instrument has variable slit widths in both the excitation and emission monochromaters. Typical slit widths were 1 mm in both monochromaters, providing spectral resolutions of 0.5 nm. Emission spectra were obtained by excitation at the peak of the Soret band (413 nm and 401 nm for mPheo and PEA respectively). Excitation spectra were obtained by monitoring the intensity at the peak of fluorescence emission (680 nm for both mPheo and PEA) while scanning the excitation wavelengths. In order to prevent the phenomenon of self absorption in the sample cuvette, the absorbance of all

solutions studied was less than 0.1.

Infrared measurements were made on a Nicolet (model 510P) FTIR using a diffuse reflectance accessory (Harrick, model HVC-DR2). The spectral resolution of the instrument was set at 2 cm^{-1} and the spectral range was from 4000 to 600 cm^{-1}. The samples were prepared as a loose powder in ground KBr.

^{13}C NMR was preformed on a Varian (model Gemini 200) NMR. The samples were analyzed as solutions in deuterated chloroform.

3.6 Animal and tumour models

For the different types of experiments performed when evaluating the tetrapyrroles, several different breeds of mice were used (Table 3.1). The C57-BL6 mice are a black skinned and haired mouse commonly used in chemotherapy testing. The SKH-HR1 is a mouse breed that is genetically similar to the C57-BL6, therefore it can also carry the C57-BL6 tumour lines. The Balb C mice are pink skinned, white haired mice that are commonly used as mouse models for various cancer studies. The $B6D2F_1$ mice are black skinned and haired mice which are a cross between DBA and C57-BL6 mice, which can carry tumours from both breeds. These animals can carry a wide variety of available tumour lines.

Table 3.1. The different breeds of mice used and some of their physical characteristics.

Breed	Skin type	Hair type
SKH-HR1	Pink (similar to human)	Hairless
C57-BL6	Black pigmented	Black
$B6D2F_1$	Black pigmented	Black
Balb C	Pink (similar to human)	White

Tumours were purchased from the NCI-Frederic Cancer Research and Development Center (Building 432, Frederick, MD 21701). The tumour lines used in the investigations are summarized in Table 3.2. Tumours were maintained by live transfer into suitable hosts. For tumour suspension type implants of solid tumours, tumours were removed when they were approximately 10 mm in diameter and placed in physiological saline (150 nm NaCl). The tumour tissue was cut into 1 to 2 mm cubes. The tissue was further homogenized by repeatly passing through a syringe, which was performed by placing a 1 mL syringe at a slight angle against the bottom of a beaker and drawing the tumour tissue rapidly up and down in the syringe. The shear force, as the tissue passed through the syringe causes the tissue to break into smaller pieces. Thus, the generated tissue suspension was injected subcutaneously into the mouse using a 16 gauge needle. Animals were anesthetized with ketamine (Rogarsetic® (rogar/STB Inc, London Ont.), dose = 100 to 120 mg kg^{-1} body weight) by intraperitoneal injection. Tumours reached 10 mm diameters in about 10 days. The P388 leukemia was transferred differently because it was an ascites cancer. This cancer migrates throughout the whole body forming a cell-filled ascites fluid. This fluid is removed by a syringe and diluted to a suitable cell number, usually about 1000 cells. Then the cell suspension is injected intraperitoneal into another suitable host.

Table 3.2. Mouse tumour lines and their general characteristics.

Tumour line	Host	Characteristics
Lewis lung	C57-BL6 $B6D2F_1$ SKH-HR1	Solid tumour, lung carcinoma, metastatic
P388	$B6D2F_1$	Leukemia, ascites cancer
EMT-6	Balb C	Mammary adenocarcinoma, solid tumour
M4898	Balb C	Lung adenocarcinoma, solid tumour

3.7 Injectable solvent

Any new drug has to be tested for solubility in an injectable solvent formula. A suitable injection formulation for both HPPEEA and PEA was found to consist of a mixture of DMSO and serum. The drug studied was dissolved in DMSO and then diluted with human serum. The maximum concentration of DMSO used in the injection formulation was 10%, with human serum accounting for the balance of the solution. The maximum drug concentration obtained using this solvent formulation was typically 4 mg mL^{-1}. Other emulsifier formulations such as CRM were not able to provide sufficient drug concentrations with these ethanolamides.

3.8 Acute toxicity evaluation

The drug to be tested for toxicity was dissolved in the injectable solvent to produce a stock solution. The stock solution was either 1 or 4 to 5 mg mL^{-1}. The drug was injected intraperitoneally and the animals were observed for acute or chronic toxicity. Due to the limited drug solubility, it was necessary in some tests using the higher drug doses to administer the drug over several days, in several injections. No single injection into an animal exceeded 1 mL. The drugs tested for acute toxicity were HPPEEA, PEA, and polyhematoporphyrin. Polyhematoporphyrin, (University of Leeds, Leeds, UK) is believed to be equivalent to PFII (Vernon *et al.*, 1995). Due to the limited solubility the highest HPPEEA dose was injected as 7 daily injections of 100 mg kg^{-1} and the highest PEA dose was injected as 3 daily injections of 166 mg kg^{-1}.

3.9 Chemotherapy

3.9.1 MTT cytotoxicity assay

The MTT cytotoxicity assay involves the measurement of cell viability after treatment with cytotoxic agents by the colorimetric change of the MTT dye (Cole, 1986).

The cells are placed in 96-well flat bottomed tissue culture trays. The drug is added after 24 h at the stated concentrations (0.001 to 100 μM). The cells are grown in the presence of the cytotoxic drug for 4 days, then the MTT dye is added. The dye is enzymatically converted to a coloured formazan in metabolically active living cells (Slater *et al.*, 1963; Cole, 1986). Those cells that have been damaged or killed by the cytotoxic agent will not produce the blue coloured formazan dye, which is measured by light absorption at 570 nm using a Dynatech model MR600 plate reader. Each drug concentration was tested in quadruplicate in each experiment. The drugs tested were: adriamycin (Sigma Chemical Com, St. Louis, Mo, USA), a chemotherapeutic agent; polyhematoporphyrin (pHP); hematoporphyrin IX (HPIX) (Porphyrin products, Logan, Utah, USA); HPPEEA; mPheo; and PEA. The cell lines used for the assay are summarized in Table 3.3.

Table 3.3. Tissue culture cell lines used in MTT assay.

Line	Origin
K562	Human erythroleukemia
Raji	Human burkitt lymphoma
Daudi [a]	Human burkitt lymphoma
HeLa	Human cervical carcinoma
H69	Human small cell lung carcinoma
2780.9s	Human ovarian carcinoma
MDA.MB	Human breast adenocarcinoma
S1HA	Human cervical squamous carcinoma

(a) Used only for IC_{50} study (Table 4.7, Fig. 4.19 and 4.20)

3.9.2 Solid tumour in animals

Lewis lung carcinoma was implanted into C57-BL6 mice. The treatment began when the tumours reached 5-6 mm in diameter. The HPPEEA or PEA were administered by IP injections daily to the animals at a dose of 10 mg kg^{-1} body weight. The control

animals were administered the injection solvent only in a similar manner. The treatment was evaluated by measurement of the progression of tumour diameter. Animals were kept in the dark for the duration of the experiment in order to prevent any phototherapy.

3.9.3 Leukemia cancer in animals

P388 leukaemia cancer was established in $B6D2F_1$ mice. The following day after the cancer was injected, the chemotherapeutic treatment began. The drugs, HPPEEA and PEA, were injected intraperitoneally at the stated dose. The progression of the cancer was followed by monitoring the weight of the animal. The results are reported as the percent weight increase of the animals from the beginning of the treatment. Animals were kept in the dark for the duration of the experiment so that no phototherapy could occur.

3.10 Pharmacokinetics

3.10.1 *In vivo* pharmacokinetics

In vivo pharmacokinetics is a rapid qualitative method to follow drug clearance from various anatomical locations, which involves monitoring the drug non-invasively by measuring the drug fluorescence from the tissues. Three animals were injected intravenously via the femoral vein with each of the fluorescent drug tested (HPPEEA, mPheo, or PEA) at a dose of 10 mg kg^{-1} body weight. At 15 min intervals the animal was positioned at the analysis site of a bifurcated fiber bundle (Fig. 3.3). One branch of the fiber bundle provided the excitation irradiation and the other carried the fluorescence emission from the drug to the spectrograph and photodiode array (Princeton Instrument model SMCP 700G). The analysis end of the fiber bundle was in a coaxial configuration with the center leading to the excitation branch of the fiber and the outside ring leading to the photodiode array emission spectrophotometer (Fig. 3.4); the branch fiber ends were formed into a rectangle slit configuration with a two to one aspect ratio. The excitation source was a 75 W xenon arc lamp coupled to a 0.22 meter monochromater (PTI) set at

400 nm. The pharmacokinetic data were monitored via the fluorescence intensity of the drug at the peak of its emission spectrum (615 nm for HPPEEA; 680 nm for mPheo and PEA). The fluorescence intensity was corrected for instrumental variation within an experiment with a standard solution of uroporphyrin (Porphyrin Products, Logan, Utah, USA).

Several anatomical sites were monitored, namely the abdomen, thigh, tumour, and skinfold. Each site represents a composite fluorescence intensity arising from a group of organs. The abdomen site represents a combined signal from the skin, liver and internal organs; the skinfold represents the skin and some fat tissue; the thigh represents muscle and skin; and the tumour site represents skin and tumour tissue.

3.10.2 *Ex vivo* pharmacokinetics

Animals were injected intravenously into the femoral vein with the drug (HPPEEA or PEA) at a dose of 10 mg kg^{-1} body weight and sacrificed at timed intervals up to 48 h post injection.

3.10.2.1 Serum measurements

For the serum measurements the animals were asphyxiated to near death with propane. Immediately, the whole blood was removed by cardiac puncture and the serum was separated by centrifugation in a desk top centrifuge. The fluorescent drug (HPPEEA and PEA) was extracted into chloroform/methanol (2:1 v/v) from the serum (100 μL serum added to 4.9 mL of chloroform/methanol). The fluorescence of the drug in the chloroform/methanol was measured in a spectrofluorometer in a manner similar to that for fluorescence solution studies of HPPEEA and PEA (section 3.5). Drug concentrations were determined with the use of a standard curve of known drug concentration in the same solvent composition.

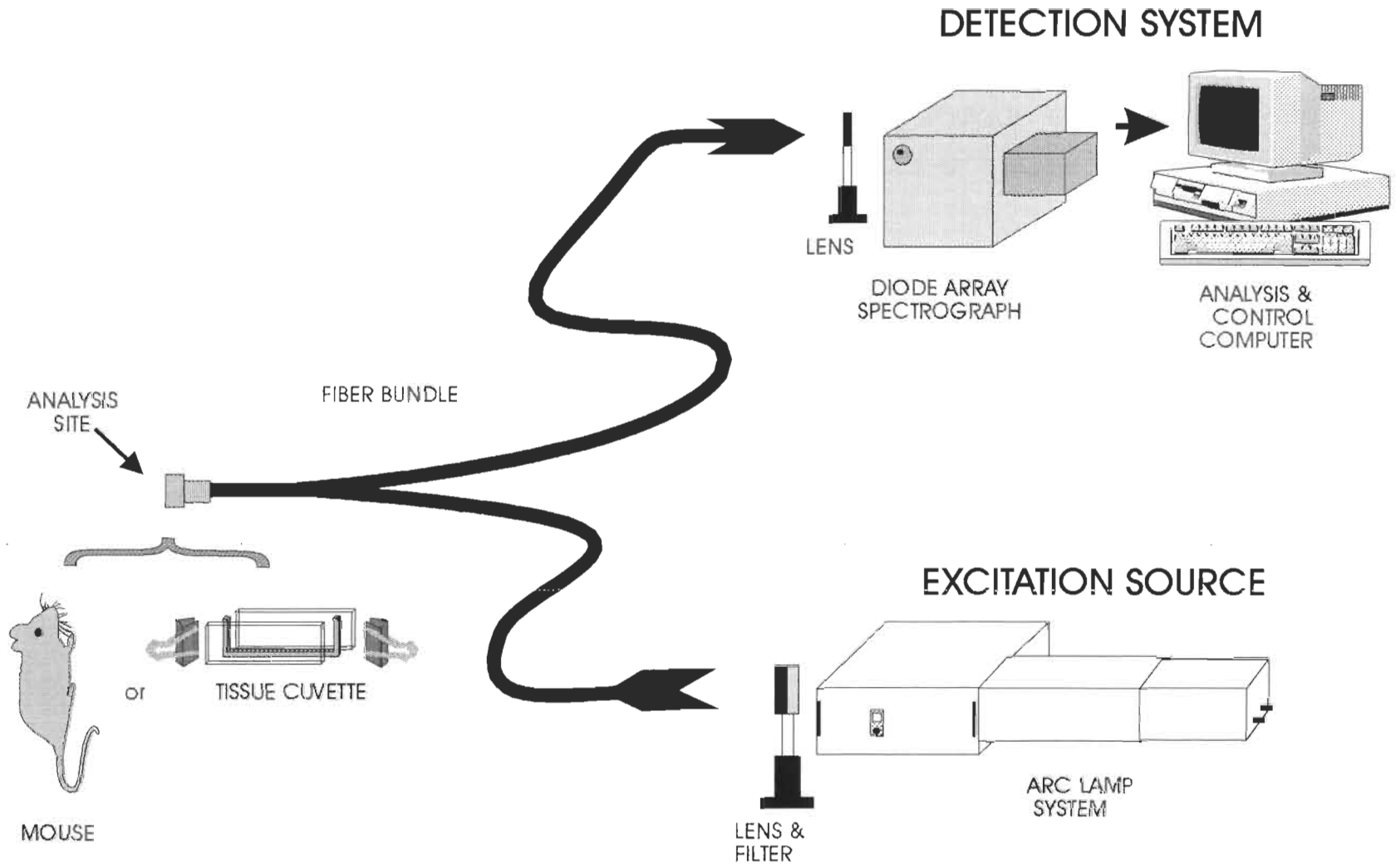

Figure 3.3. Instrumentation used for pharmacokinetics measurements.

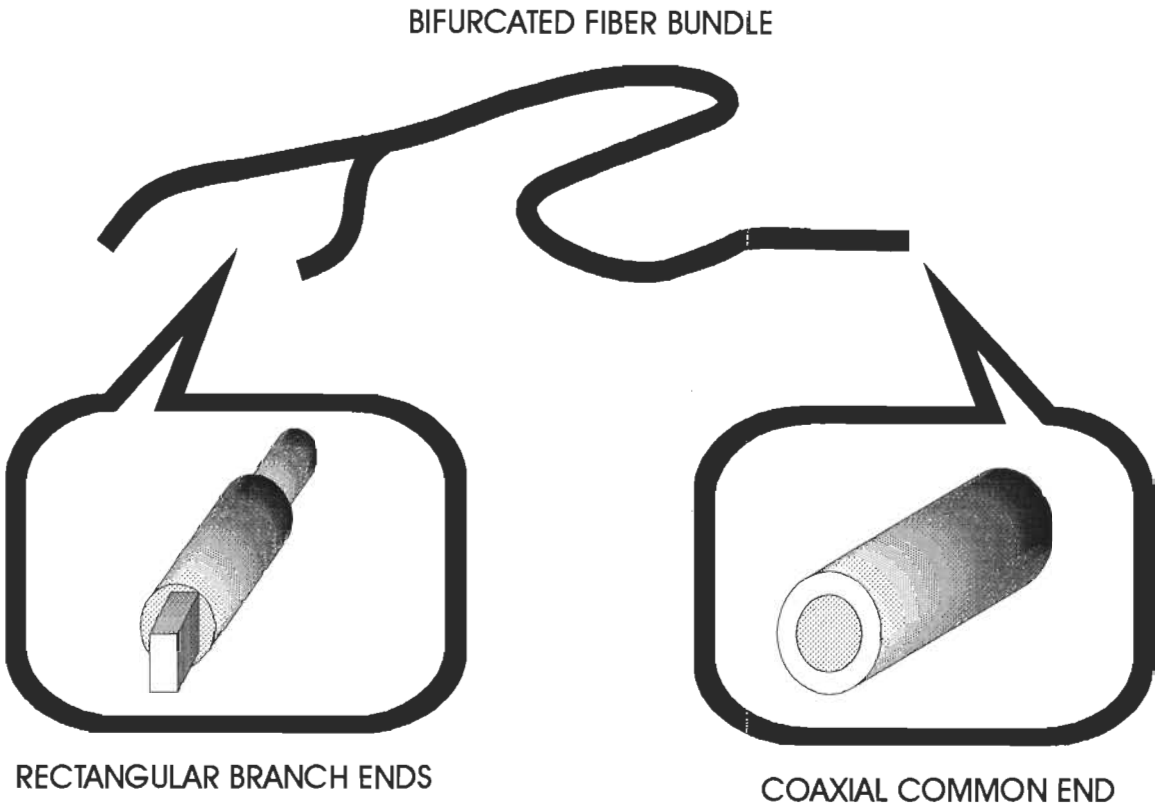

Figure 3.4. Fiber bundle conformation used for pharmacokinetic measurements.

The fluorescence intensity was also measured from a known concentration of PEA in the presence or absence of serum in order to determine whether or not the serum was affecting the fluorescence signal from the drug. The determination was achieved by comparing the fluorescence intensity from PEA, obtained from the following solvents: i) 5 mL of chloroform/methanol (2:1 v/v); and ii) 4.9 mL of chloroform/methanol plus 100 μL of mouse serum.

3.10.2.2 Tissue measurements

For the tissue measurements the animals were asphyxiated to death with propane. Each tissue of interest was removed, washed in physiological saline (150 mM NaCl) to

remove debris and body fluids, and placed in a tissue cuvette for fluorescence measurements. The tissue cuvette consisted of a 1 mm spacer between two 1 mm thick glass plates so that the tissue thickness was consistently 1 mm thick (Fig. 3.5). The tissue pharmacokinetics and clearance curves were then obtained from the tissue fluorescence, in the same manner as the *in vivo* measurements. The fluorescence measurements were corrected for instrumental variation in the same manner as the *in vivo* mesurements.

3.11 Photohemolysis

Photohemolysis involves the measurement of hemoglobin released from damaged red blood cells by absorption spectroscopy. The red blood cell damage is a result of photosensitization by the drug. The red blood cells and photosensitization drug are combined in the presence of light for a specified light dose. After 24 h in the dark the amount of hemoglobin released from the damaged cells was measured. A flow diagram of the procedure is presented Fig. 3.6.

Human whole blood (0.75 mL) was washed three times in TBS (5 mM tris and 150 mM NaCl, pH=7.4 unless otherwise stated) and added to 500 mL of TBS. This stock blood solution had an absorbance of about 1.5 at 414 nm when all hemoglobin was released from the cells. The blood stock solution was dispensed in 10 mL aliquots into 100 mm standard plastic petri dishes (Fig. 3.6). The drugs were dispensed in μL quantities into the petri dishes containing the blood in the dark in order to give the required nM drug concentrations. The solvent (95% ethanol) used did not cause any hemolysis. After addition of the drugs, the petri dishes were gently agitated. The drugs tested were: pHP; HPIX; HPPEEA; mPheo; and PEA.

The light source used for the light treatment is composed of a light table with a plexiglass top and with two 96" VHO cool white fluorescent lamps, giving 9 mW cm^{-2} of white light to the samples (Fig. 3.6). The petri dishes were exposed to: 1) no light; 2) 5 min; or 3) 10 min of light and then removed and placed in the dark for 24 h. The samples were then collected and centrifuged at 2000 rpm at 5 °C after the 24 h dark period. The released hemoglobin from lysed cells found in the supernatant was measured

by absorption at 414 nm (the peak of the hemoglobin Soret band). The percent hemolysis was calculated by comparison with a standard curve. The 100% hemolysis reference was generated by lysis of a 10 mL aliquot of the same washed red blood cells as used for the samples with distilled water. The hemoglobin absorption at 414 nm was not affected by the drug due to the low drug concentrations in the samples.

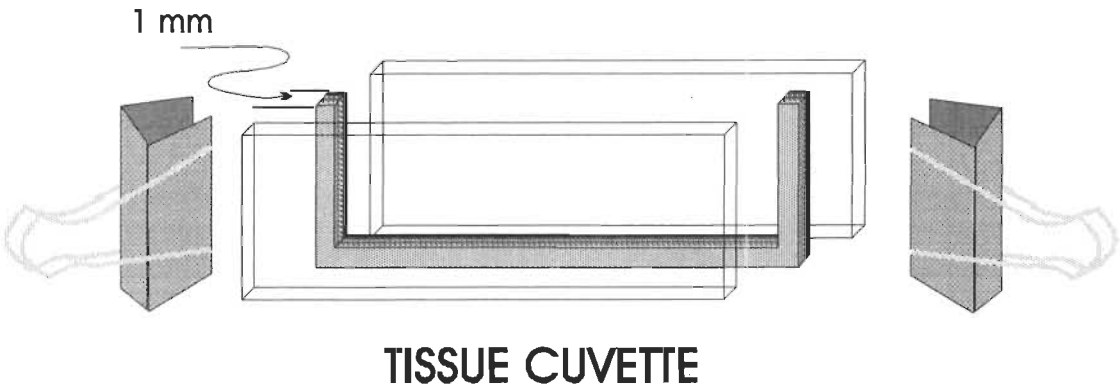

Figure 3.5. Tissue cuvette design. A 1 mm brass spacer separated the two glass plates.

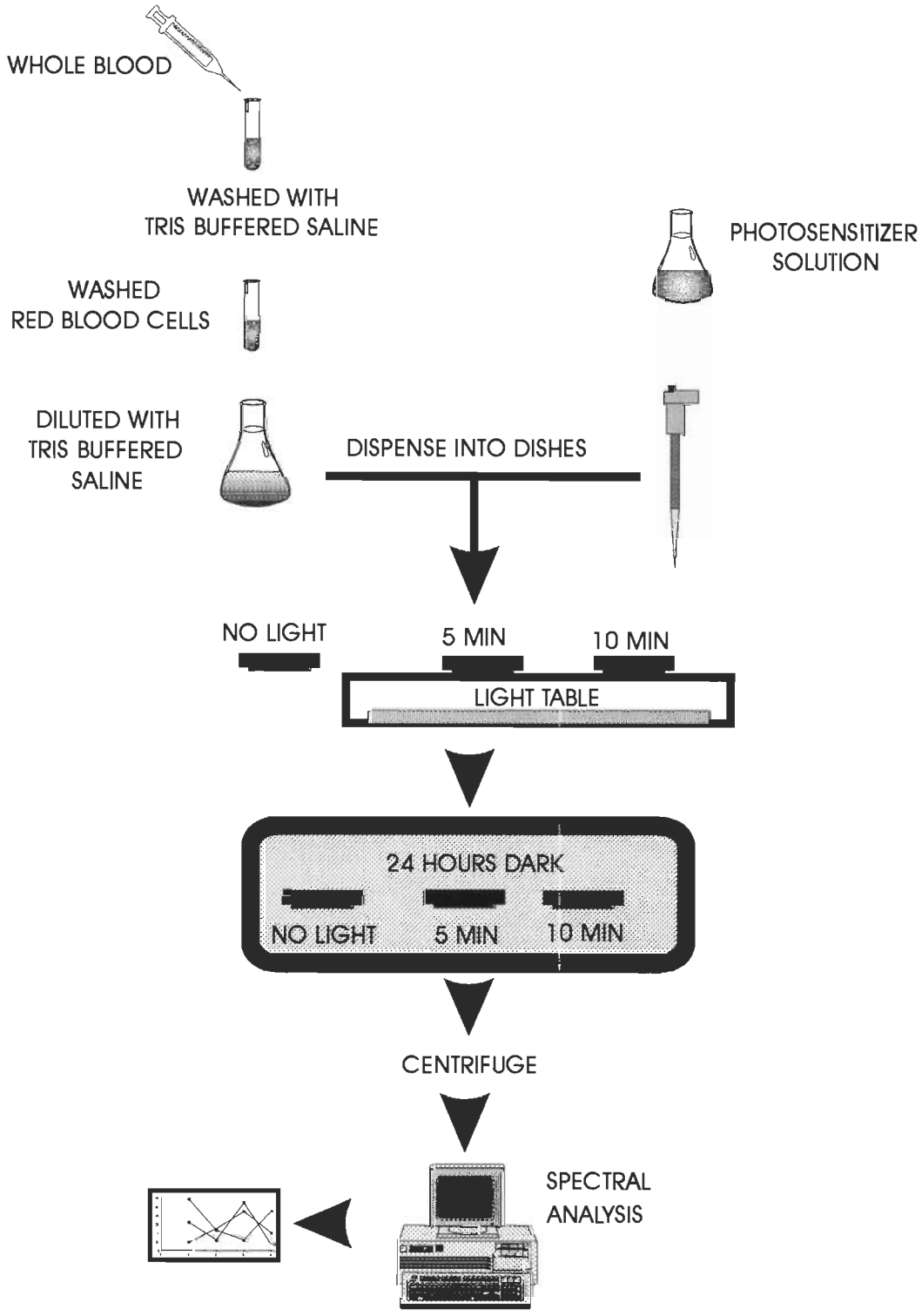

Figure 3.6. Flow diagram of photohemolysis procedure.

Chapter 4 Results

4.1 Isolation of chlorophyll *a*

The starting material selected for PEA synthesis was Chl *a*, isolated from spinach, because of the availability and reasonable cost. The pigments extracted from the spinach pulp, after partitioning into petroleum ether, were washed several times with 50 mM NaCl-H_2O (Folch *et al.*, 1957) to remove polar lipids. Poor separation of the ether and water phases resulted in a lower pigment yield if these salt washes were not performed, due to the pigment-ether being discarded with the H_2O washes.

Immediately after pigment extraction the Chl *a* was separated on the silica columns. The pigment sample was allowed to adhere to the silica on the column for at least ten minutes before the column elution began. The separation was poor if the pigment was not allowed to adhere to the silica for that time. The second visible band in the column was the blue-green Chl *a*. A typical elution time was about 1 h, but varied somewhat due to the packing of the silica in the column and the elution solvent flow rate. The purity of the Chl *a* eluted from the column was confirmed by thin layer chromatography (TLC).

4.2 Synthesis and purification of methyl pheophorbide *a*

The synthesis of mPheo proceeded immediately after Chl *a* was eluted from the column so that degradation of Chl *a* would be minimized. The alkyl fragments, a byproduct from the phytol chain cleavage, were detected by TLC in the mPheo product and removed by further silica column separation.

The typical yield of purified mPheo from spinach was 0.07 % by weight (0.752 g of mPheo was obtained from 1200 g fresh weight of spinach). If one assumes 98% water content in the fresh weight then a 1200 g sample is equal to 24 g dry weight; which results in a yield of 3.13 % for mPheo based on dry weight. A 1200 g fresh weight

spinach batch was the largest that could be utilized with the experimental equipment available in a single extraction procedure. Thus 0.75 g of mPheo could be produced in about two days laboratory work.

4.3 Synthesis and purification of PEA

PEA (Fig. 4.1) was synthesized from mPheo by replacing the methyl esters on mPheo with ethanolamine. The conversion from mPheo to PEA took approximately 2 h. The product (PEA) was partitioned into chloroform after completion of the reaction. The PEA containing chloroform layer required neutralization with HCl to a neutral pH for complete separation of the chloroform and aqueous phases.

PEA was purified by column chromatography similarly to mPheo. PEA was stored in sealed vials at -3 °C that had been purged with nitrogen gas. A typical yield of PEA from mPheo was about 45% by weight (2.11 g mPheo yielded 0.96 g PEA).

4.4 Verification of the purity of PEA by HPLC

It was necessary to confirm the purity of PEA after completion of its synthesis. HPLC analysis was performed although TLC had indicated a single homogeneous compound. Methyl pheophorbide *a* had a retention time of 7.2 min (Fig. 4.2). PEA, a more polar compound, had a retention time of 1.5 min (Fig. 4.3). PEA was estimated to have a purity of 95% based on the HPLC (Fig. 4.3). This purity is similar to other commercially available porphyrin products tested (Porphyrin Products, Logan Utah, USA).

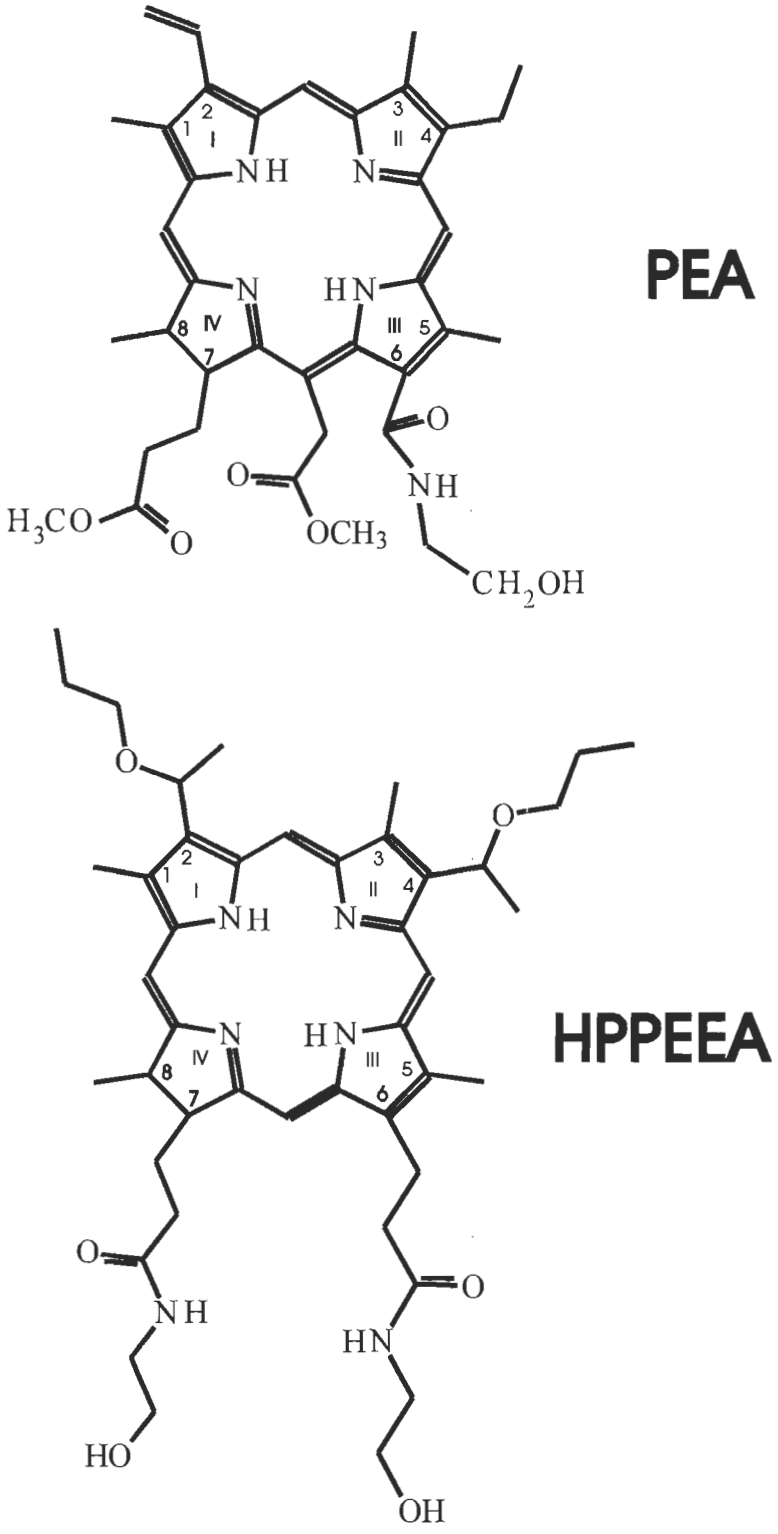

Figure 4.1. Molecular structure of pheophorbide *a* ethanolamide (PEA) and hematoporphyrin propyl ether ethanolamide (HPPEEA).

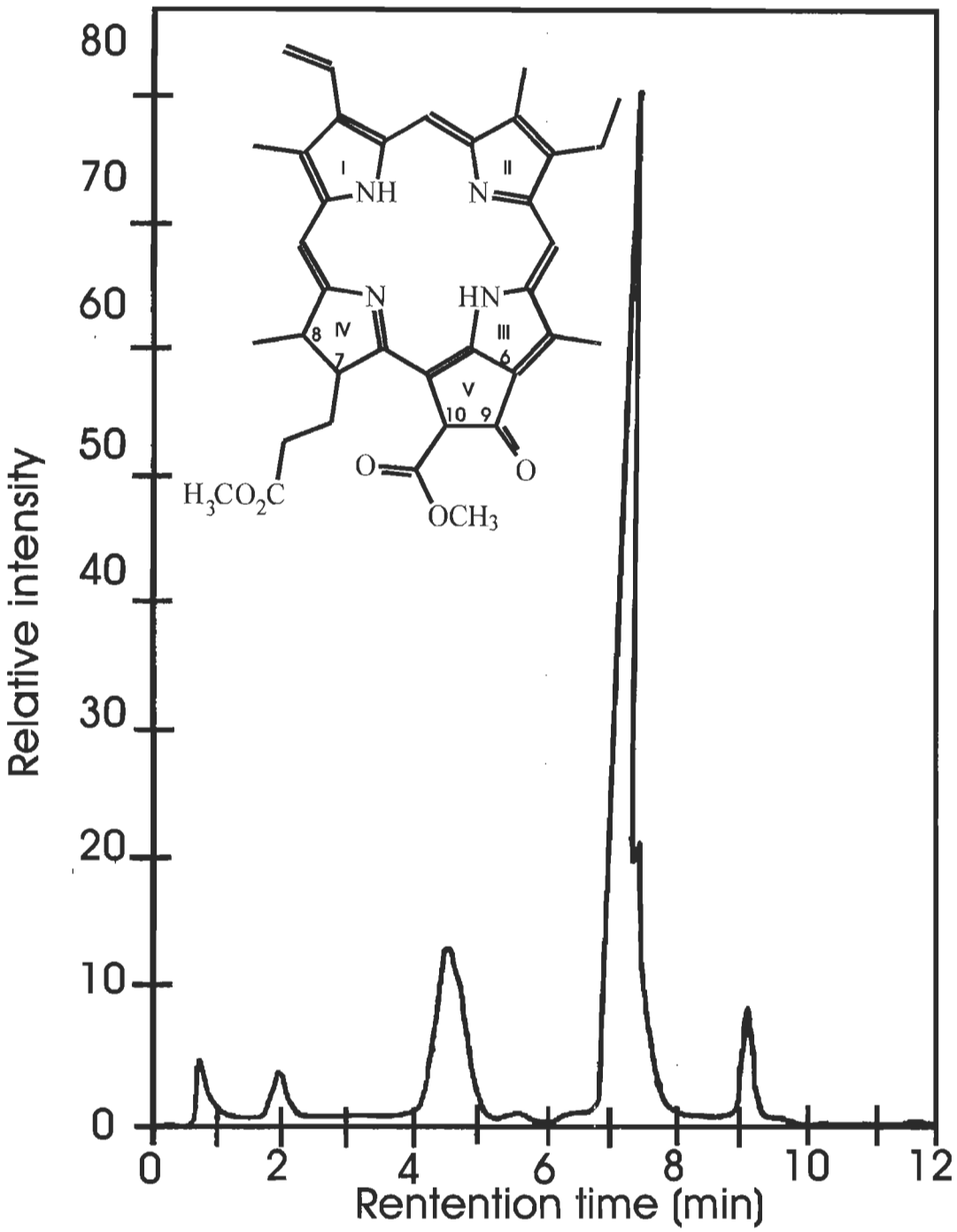

Figure 4.2. HPLC chromatogram of methyl pheophorbide *a* (mPheo). Peaks were detected by absorption at 405 nm, reported in relative units (left scale). The peak at 7.2 min is due to mPheo.

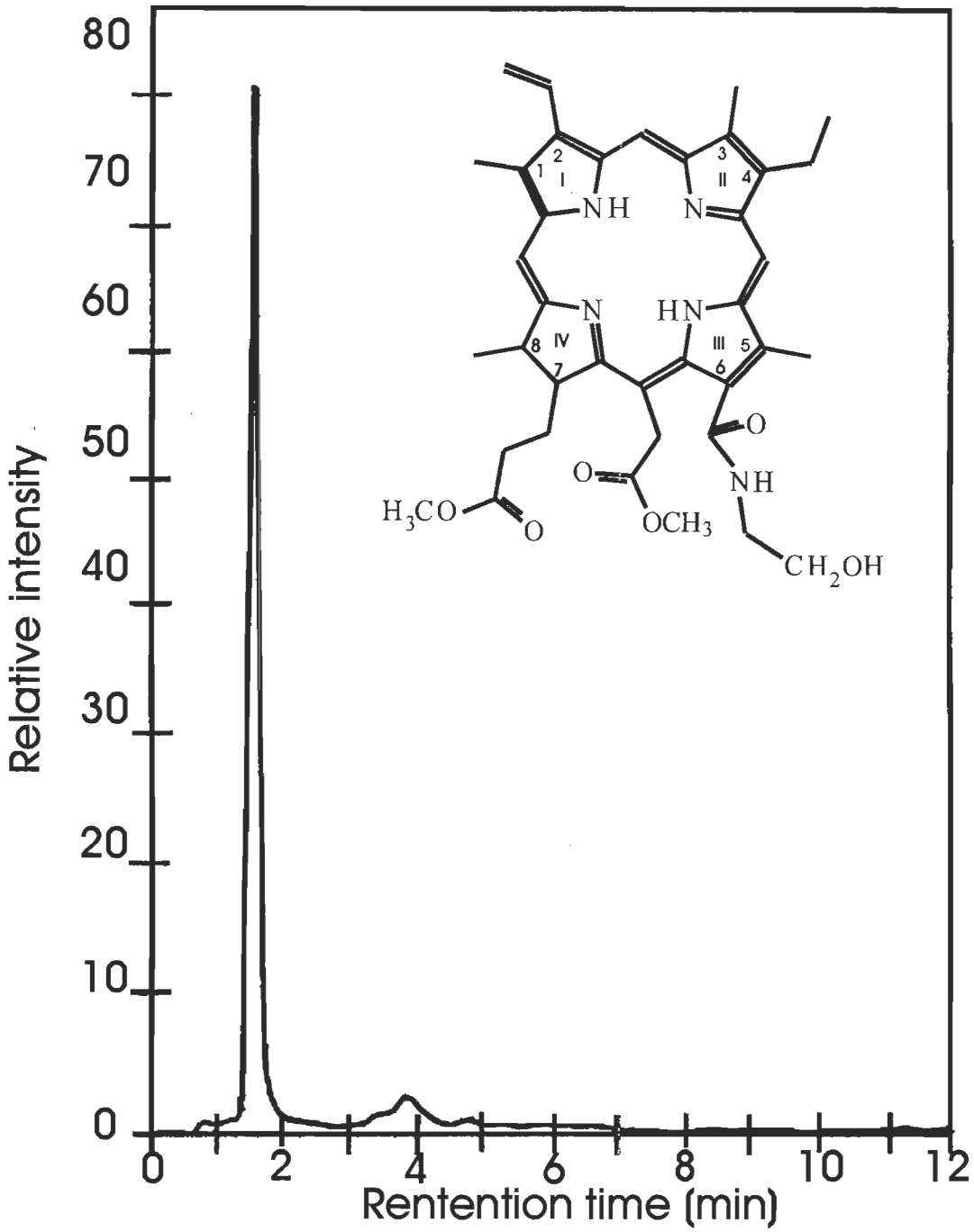

Figure 4.3. HPLC chromatogram of PEA. Peaks were detected by absorption at 405 nm, reported in relative units (left scale). The peak at 1.7 min is due to PEA. The trace contamination indicated by the peak at 3.8 min accounts for 5% of the peak total area, indicating that PEA is has 95% purity.

4.5 Molecular structure of PEA

4.5.1 Electronic absorption spectroscopy

The porphin ring must remain intact during the modification of the basic Chl *a* structure for the characteristic far red absorbance of these chlorins to be maintained. Fig. 4.4 shows the absorption, excitation, and emission spectra of mPheo. The high absorption of the first Q band at 665 nm indicates that the porphin ring is still intact. The similarity of the absorption and excitation spectra further indicates that a single molecular species is responsible for the fluorescence. The molar extinction coefficients for the Soret (413 nm) and the first Q band (667 nm) are 6.25 x 10^4 M^{-1} cm^{-1} and 2.80 x 10^4 M^{-1} cm^{-1}, respectively. The ratio of the Soret to the first Q band is 2.23 which is similar to that reported by Pennington *et al.* (1964).

The absorption spectrum of PEA has the shape of a typical chlorin type spectrum (Spikes, 1990), with a high absorption of the first Q band at 665 nm (Fig. 4.5). Again, the similarity of the fluorescence excitation spectrum and the absorption spectrum indicates only one fluorescent species. The molar extinction coefficients for the Soret (405 nm) and first Q band (665 nm) are 7.94 x 10^4 M^{-1} cm^{-1} and 2.64 x 10^4 M^{-1} cm^{-1} respectively. The molar extinction coefficient ratios of the respective bands (mPheo/PEA) are: Soret; 0.79 and first Q band; 1.06. The near unity of these ratios again infers that the major chlorin chromophore is retained in PEA. The ratio of the Soret to the first Q band in PEA is 3.03, being slightly higher than that for mPheo, due to the higher molar extinction coefficient of the Soret band of PEA.

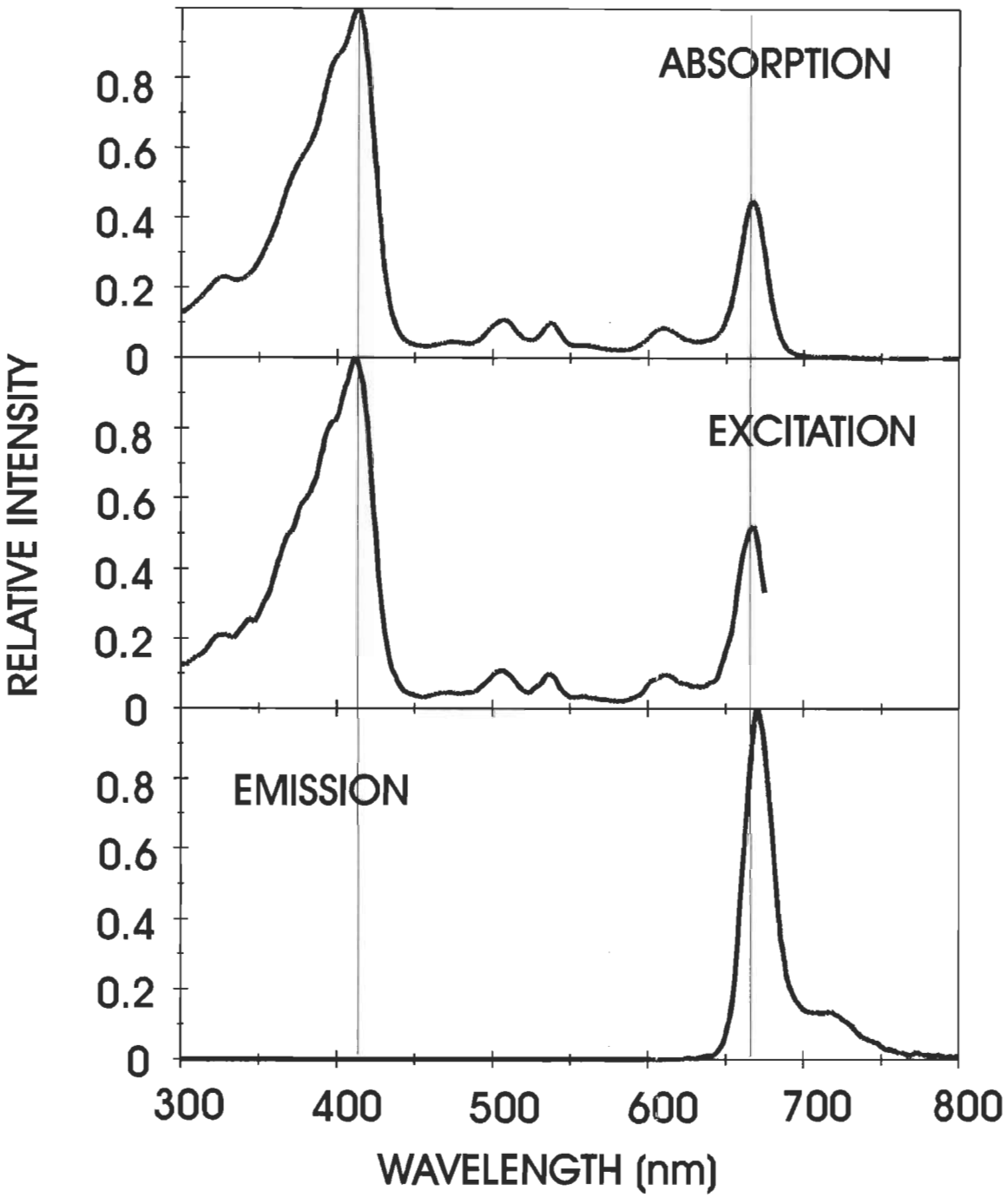

Figure 4.4. Absorption, fluorescence excitation, and fluorescence emission spectra of methyl pheophorbide *a* in dichloromethane: pathlength = 1 cm; concentration for absorption spectrum = 24.8 μM; concentration for fluorescence excitation and emission spectra = 1.24 μM; excitation λ at 400 nm for emission spectrum; emission λ monitored for excitation spectrum at 680 nm. Vertical lines are at 413 nm and 667 nm.

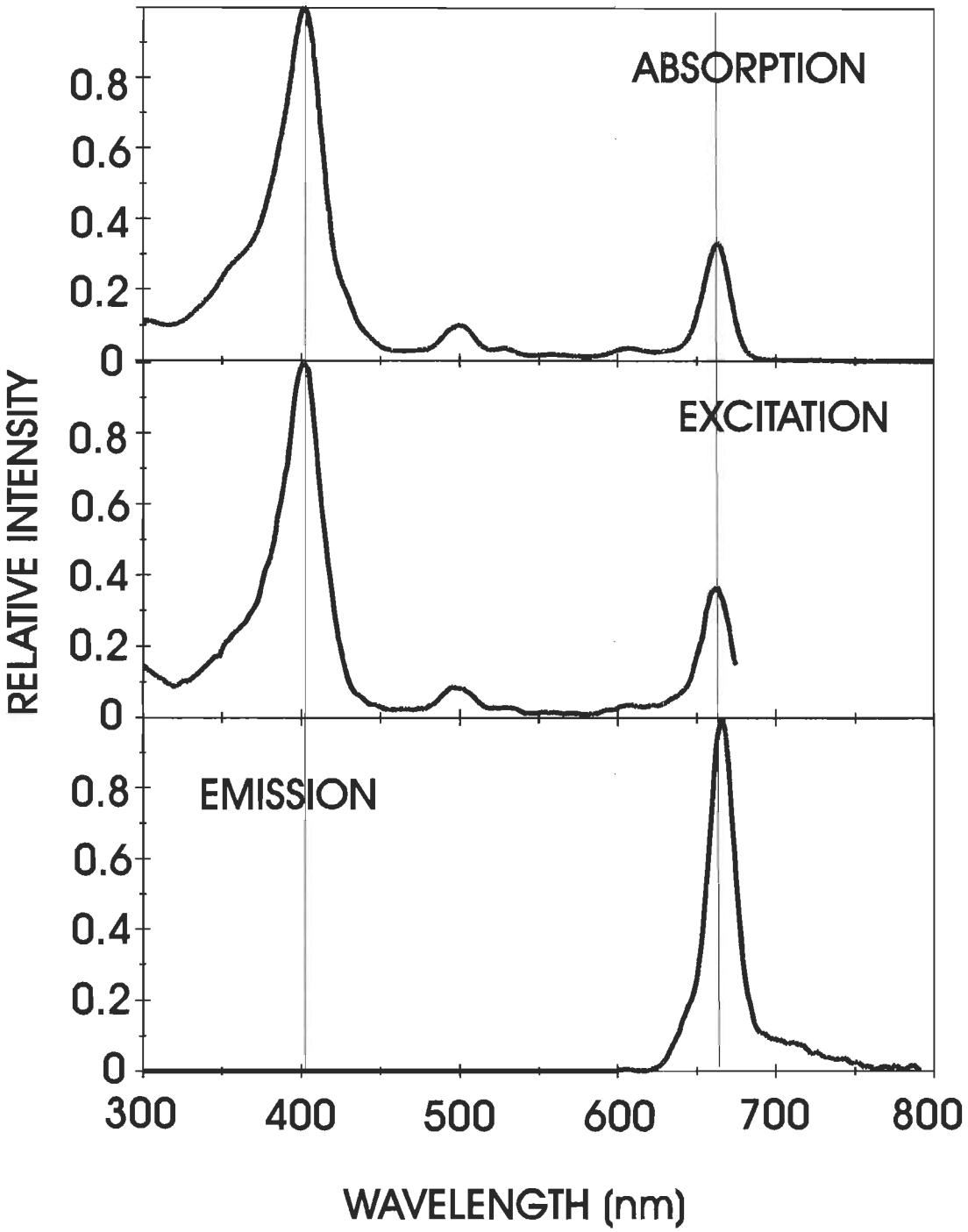

Figure 4.5. Absorption, fluorescence excitation, and fluorescence emission spectra of PEA in dichloromethane: pathlength = 1 cm; concentration for absorption spectrum = 30.2 μM; concentration for fluorescence excitation and emission spectra = 0.604 μM; excitation λ at 400 nm for emission spectrum; emission λ monitored for excitation spectrum at 680 nm. Vertical lines are at 405 nm and 665 nm.

4.5.2 IR spectroscopy

The presence of the carbonyl ketone, methyl ester, and amide groups of the various chlorin derivatives can be monitored by their IR spectra. Fig. 4.6 and 4.7 represent the FT-IR spectra of mPheo and PEA. Salient features of the mPheo spectrum include the strong methyl ester band at 1743 cm^{-1} and the strong free ketone carbonyl band at 1701 cm^{-1} which are similar to those reported for Chl *a* by Chapados (1988).

In the IR spectrum of PEA, the band at 3307 cm^{-1} (Fig. 4.7) indicates the presence of an NH amide and OH of the amide side group (Bellamy, 1975). Also 1655 cm^{-1} band is the ketone of the amide. The disappearance of the ketone band at 1700 cm^{-1} in the PEA IR spectrum indicates that the free ketone carbonyl at C-9 of ring V has changed. This suggests that perhaps ring V has opened and that the ketone is transformed into an amide.

4.5.3 NMR spectroscopy

The NMR spectra can provide further support for the molecular structures indicated by IR spectroscopy. The ethanolamide moiety could be located on the chlorin ring in one of two possible locations, either at position 6 or at position 7 (Fig. 4.1). Amino type compounds usually attach to chlorins at ring V (Pennington *et al.*, 1967; Gurinovich *et al.*, 1992). Ring V of the chlorin would likely be opened if the ethanolamide group attaches to position 6, and the ketone carbonyl carbon C-9 would be reassigned to C-6a and the peak in the ^{13}C NMR spectrum of PEA would disappear (Smith and Unsworth, 1975). Detailed ^{13}C NMR spectra analysis of mPheo has been discussed by Smith and Unsworth (1975), who indicate that the free ketone carbonyl carbon C-9 on ring V produces a peak at 190 ppm. That ketone carbonyl peak is shown in the ^{13}C NMR spectra of mPheo (Fig. 4.8). The C-9 ketone carbonyl peak is not present in the ^{13}C NMR spectrum of PEA, but the C-6a peak is found at 167 ppm indicating that during the reaction forming the ethanolamide, ring V is opened and the free ketone carbonyl is changed (Fig. 4.9). To be certain that the 190 ppm peak is not present in

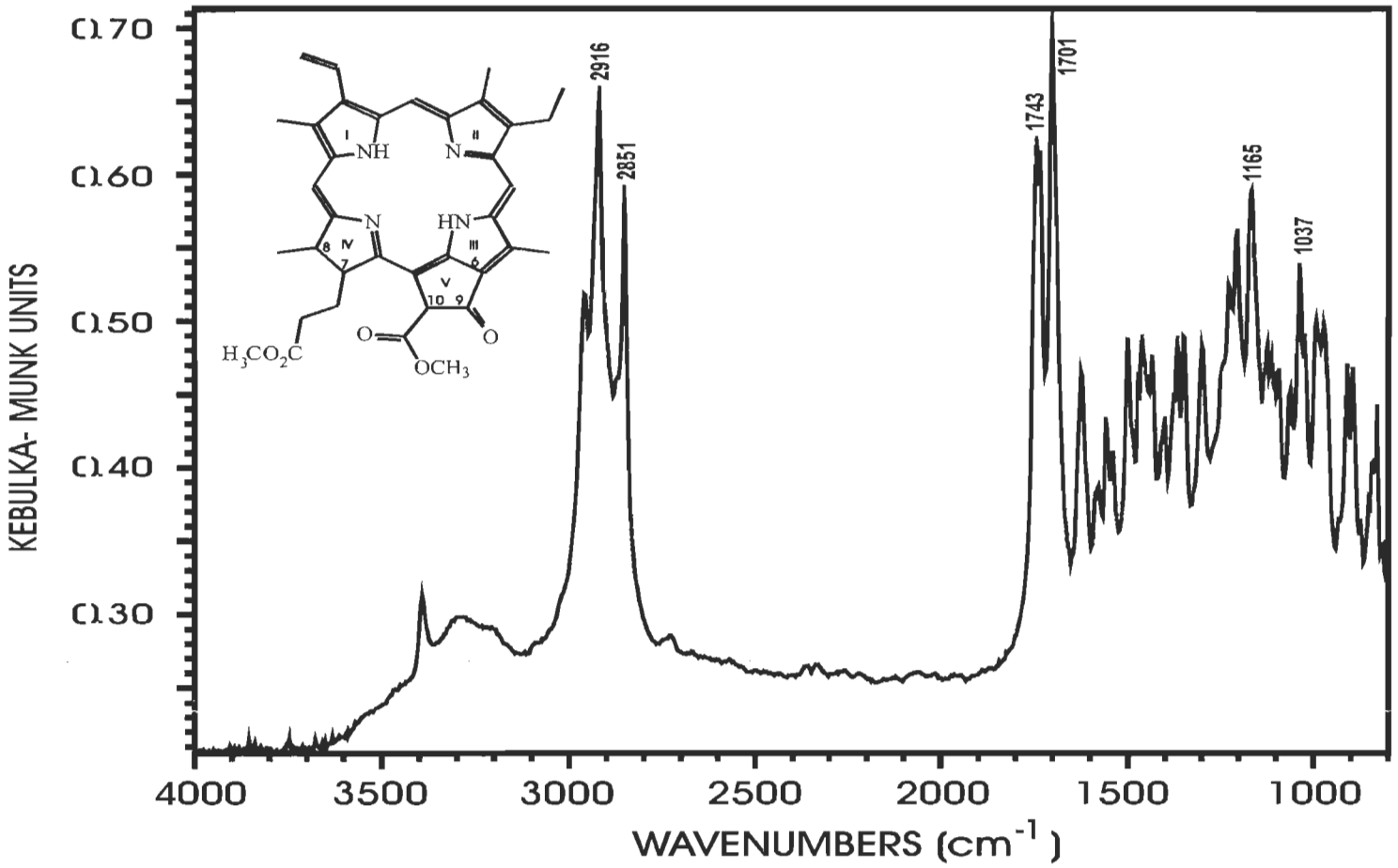

Figure 4.6 IR absorption spectrum of methyl pheophorbide *a*. Spectrum was taken by diffuse reflectance of the sample in powder form mixed with KBr. Intensity reported in Kebulka-Munk units. The peak at 3400 cm^{-1} is free N-H and at 3300 cm^{-1} is associated NH. The 1743 cm^{-1} peak is the C=O ester and the 1701 cm^{-1} peak is the C=O ketone carbonyl. The 1601 cm^{-1} peak is the ring C=N.

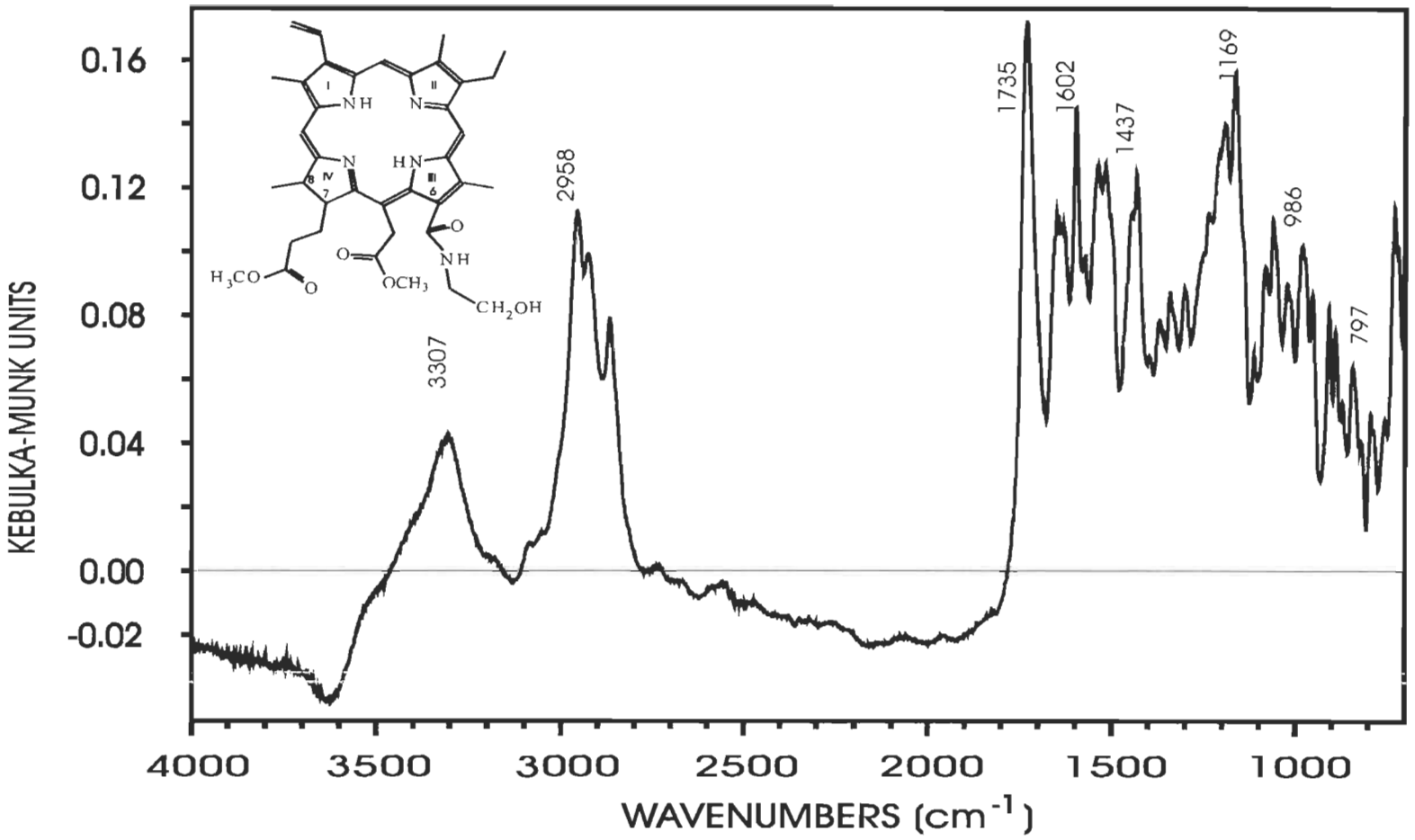

Figure 4.7 IR absorption spectrum of pheophorbide *a* ethanolamide. Spectrum was taken by diffuse reflectance of the sample in powder form mixed with KBr. Intensity reported in Kebulka-Munk units. The peak at 3307 cm^{-1} is N-H and the O-H of the amide side group. The 1735 cm^{-1} peak is the C=O ester and the small peak at 1655 cm^{-1} is the carbonyl of the amide. The 1602 cm^{-1} peak is the ring C=N.

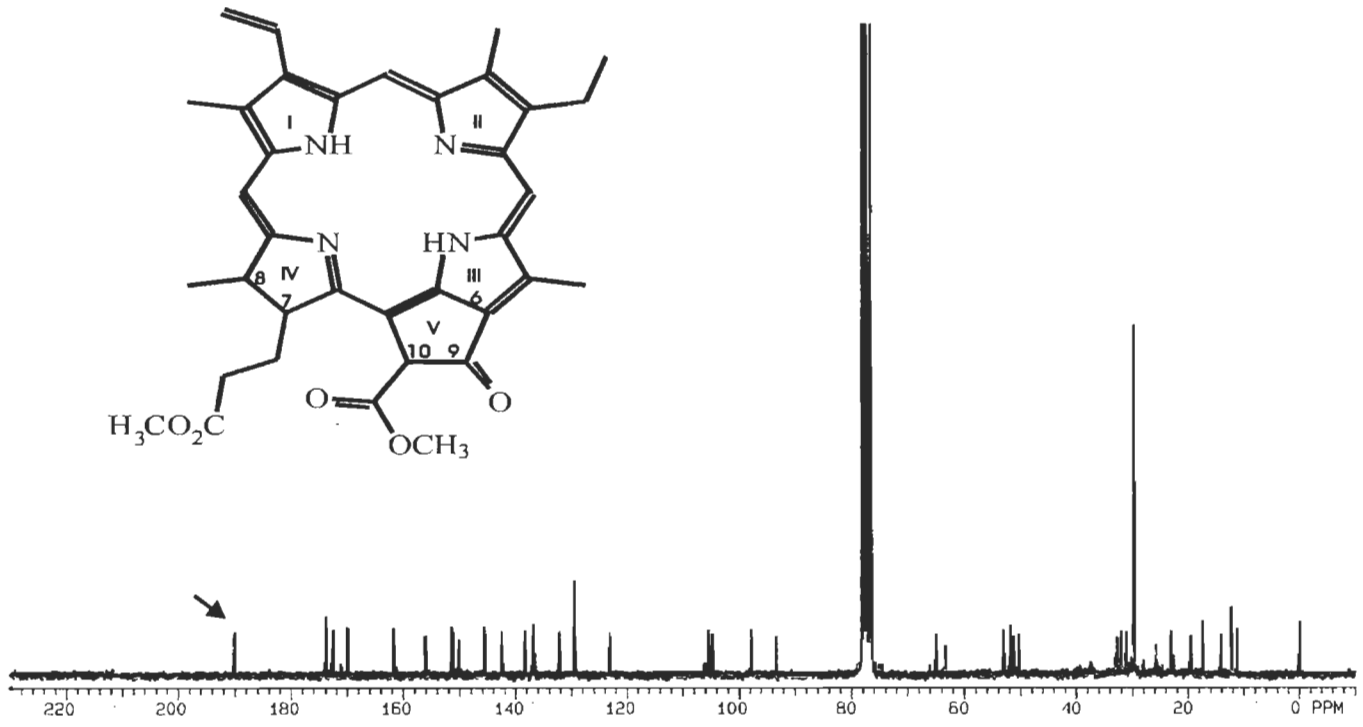

Figure 4.8 ^{13}C NMR spectrum of methyl pheophorbide *a* in deuterated chloroform. Peaks which have assignments are as follows: 190, C-9; 173, C-7c; 170, C-10a; 130, C-2a; 124, C-2b; 105.5, C-γ; 105, C-ß; 99, C-α; 93, C-δ; 65, C-10; 53, C-10b; 52.5, C-7d; 51, C-8; 32, C-7a; 31, C-7b; 23, C-8a; 20, C-4a; 19, C-4b; 14, C-5a; 12, C-1a; 11, C-3a.

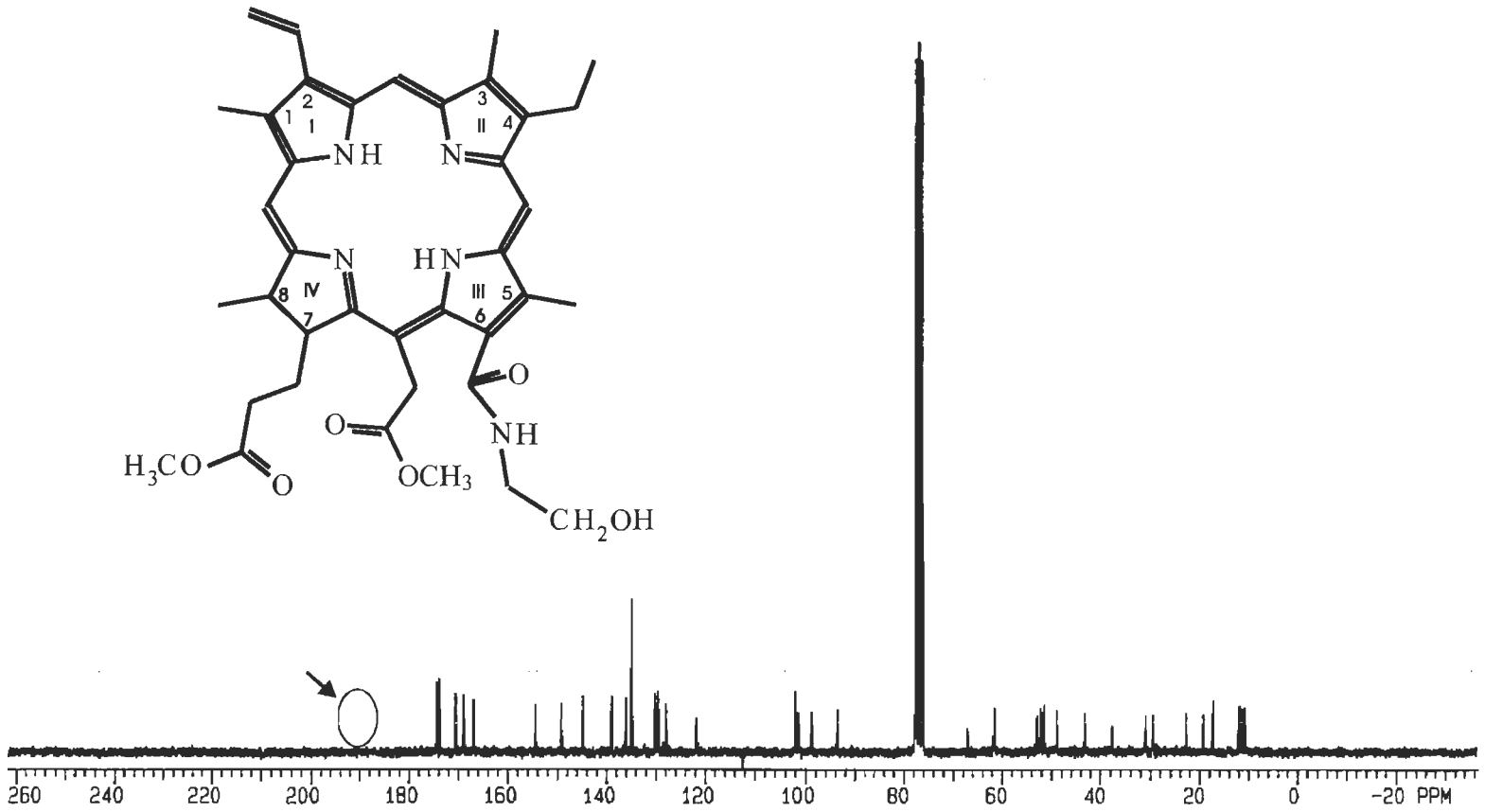

Figure 4.9. ^{13}C NMR spectrum of pheophorbide *a* ethanolamide in deuterated chloroform. Peaks which have assignments are as follows: 171, C-7c; 170, C-6a; 167, C-γb; 128, C-2a; 122, C-2b; 102.2, C-γ; 102, C-ß; 99, C-α; 94, C-δ; 62, C-6c (CH_2OH); 52, C-γc; 51.5, C-7d; 51, C-7; 49.9, C-8; 43, C-6b ($NH-CH_2$); 38, C-γa; 23, C-8a; 20, C-4a; 19, C-4b; 13, C-1a; 11, C-3a. Note that the ketone carbonyl peak of C-9 on ring V of the porphin is not observed at 190 ppm.

PEA its ^{13}C spectrum, shown in Fig. 4.9, was collected for several days. Pandey *et al.* (1991), who synthesized several chlorins which had opened ring V, found that when ring V was opened with the 5 % H_2SO_4 in methanol a methyl ester was attached at position C-6, and a strong methyl ester proton peak was observed at 4.25 ppm in the proton NMR. That 4.25 ppm peak is not observed in the proton NMR of PEA, further supporting that the ethanolamide was located at position C-6 on PEA. The singlet (6.2 ppm) from 10-H in proton NMR of mPheo (Fig. 4.10) is not observed in PEA, however a double doublet (5.5 ppm and 4.75 ppm) from γa-H_2 is observed in PEA (Fig. 4.11). In the proton NMR spectrum of PEA, the hydrogen on the NH of the amide at 6.8 ppm is identified (Fig. 4.11). This amide peak is not present in the proton NMR spectrum of mPheo (Fig. 4.10). A single hydrogen is indicated by the NH 6.8 ppm peak confirming that only one ethanolamide has attached to PEA. Thus the structure of PEA is believed to be as shown in Fig. 4.1 (pg 59) and 4.12 (pg 73).

4.6 Biological evaluation of new dual action drugs

4.6.1 Acute toxicity of the ethanolamides

Both HPPEEA and PEA were found to have low acute toxicity in a mouse model. No toxicity was observed after three daily injections of 166 mg kg^{-1} body weight of PEA, for a total of 500 mg kg^{-1} administered. No toxicity was observed after seven daily injections of 100 mg kg^{-1} body weight of HPPEEA for a total of 700 mg kg^{-1} administered. In both drugs the high dose had to be administered over several days due to the limited drug solubility in an injectable solution. No LD_{50} values can be quoted for either drug since at the doses administered no toxicity was apparent. Polyhematoporphyrin gave an LD_{50} of about 150 mg kg^{-1}.

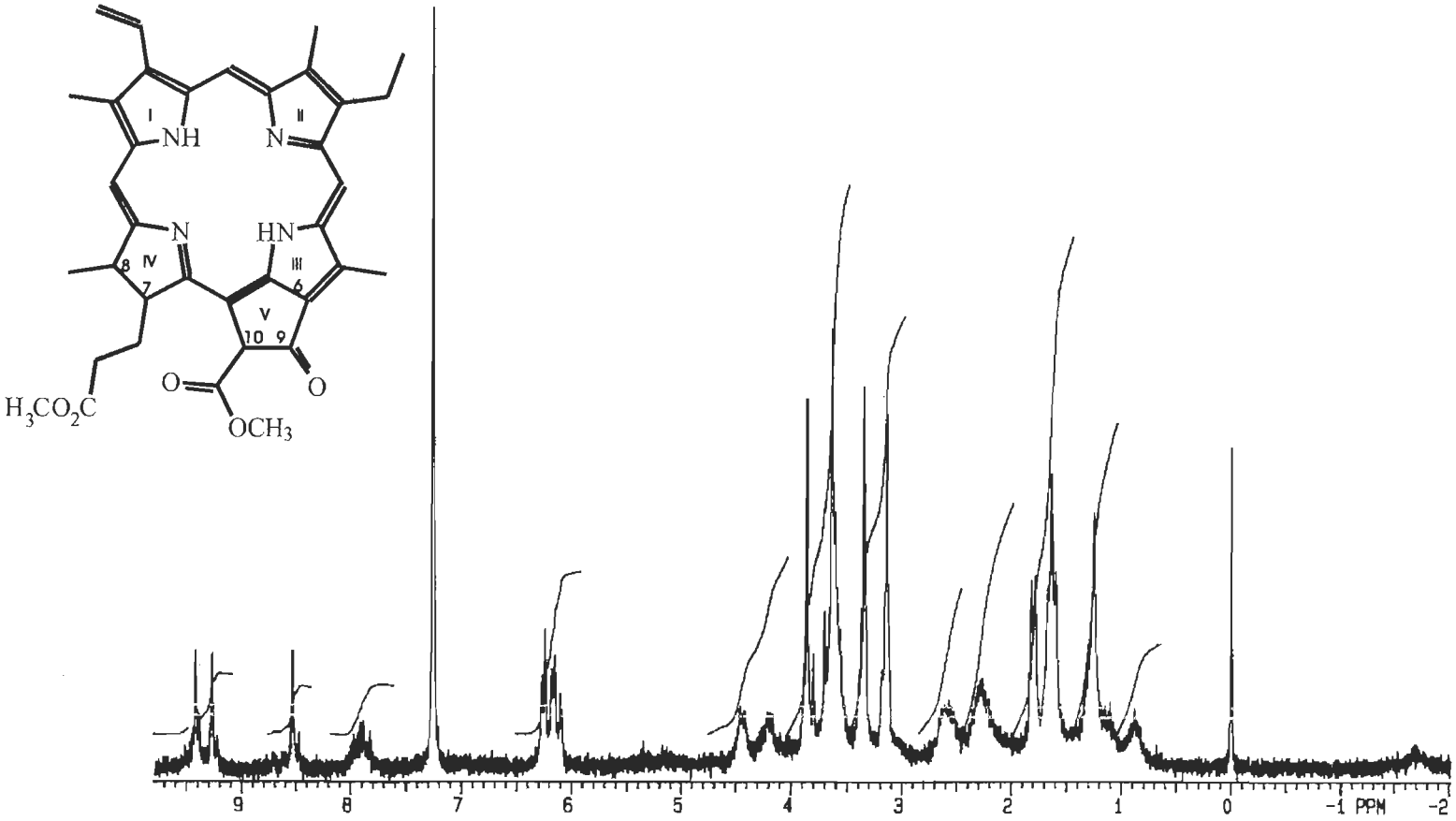

Figure 4.10 Proton NMR spectrum of methyl pheophorbide *a* in deuterated chloroform. Peaks which have assignments are as follows: 9.45, 1H, α-H, s; 9.32, 1H, ß-H, s; 8.5, 1H, δ-H, s; 7.9, 1H, 2a-H, dd, j=13Hz, j=22 Hz; 6.2, 2H, 2b-H, dd, j=12 Hz, j=17 Hz; 6.2, 1H, 10-H, s; 4.46, 1H, 8-H, d, j=8; 4.20, 1H, 7-H, d, j=8; 3.8, 3H, 10-$COOCH_3$, s; 3.65, 2H, 4a-H_2, q; 3.65, 3H, 7-$COOCH_3$, s; 3.65, 3.35, 3.19, 3H x 3, ring 1,3,5- CH_3, s; 2.6, 2H, 7a-H 7b-H; 2.25, 2H, 7a'-H 7b'-H; 1.8, 3H, 8-CH_3, d, j=9 Hz; 1.2, 3H, 4b-CH_3, t, j=7 Hz; -1.7, 2H, ring N-H, s.

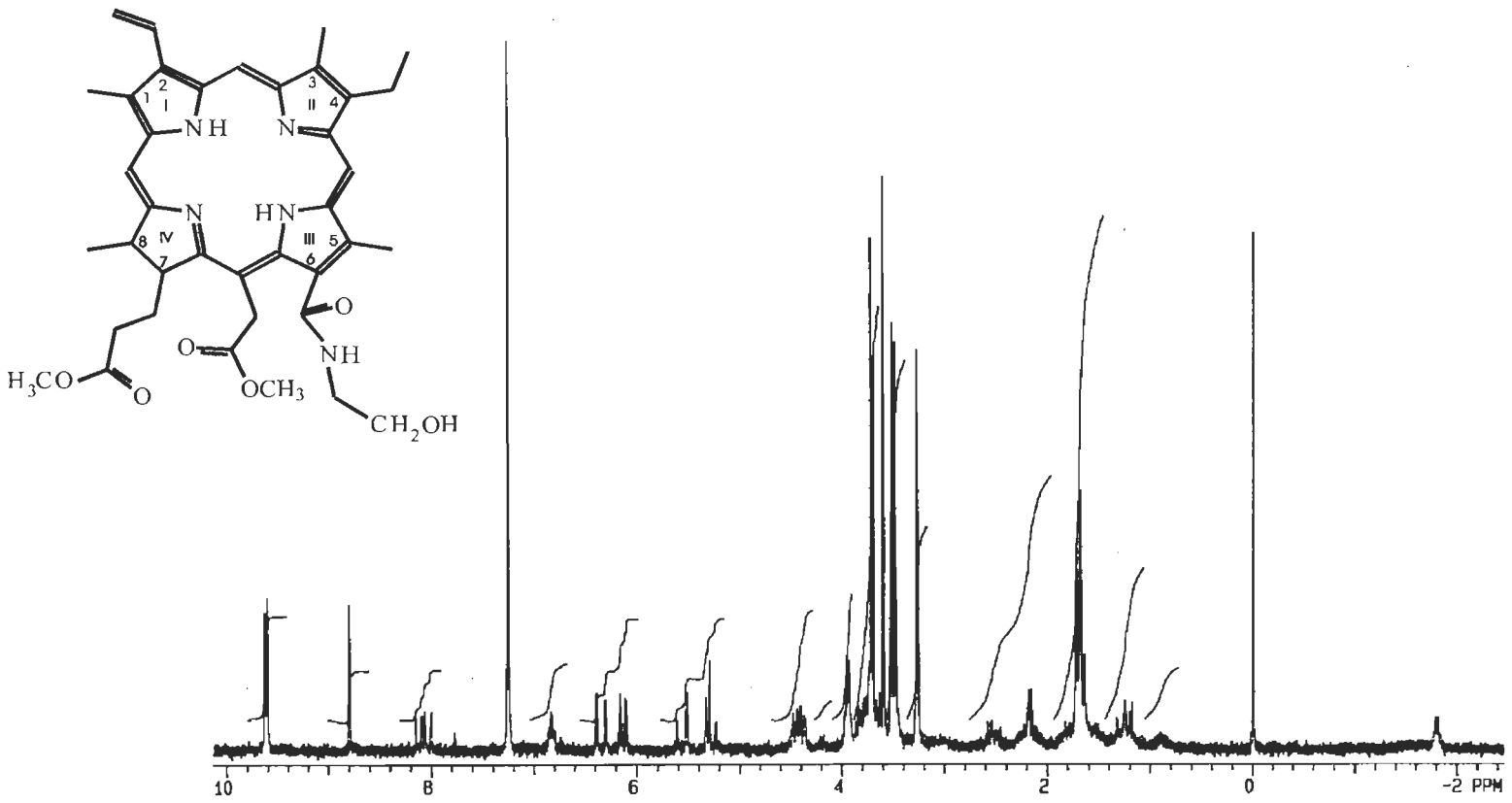

Figure 4.11 Proton NMR spectrum of pheophorbide *a* ethanolamide in deuterated chloroform. Peaks which have assignments are as follows: 9.62, 1H, α-H, s; 9.60, 1H, ß-H, s; 8.8, 1H, δ-H, s; 8.1, 2a-H, dd, j=12 Hz, j=19 Hz; 6.8, 1H, 6-NH, t, j=5 Hz; 6.35 & 6.15, 2H, 2b-H_2, d & d, j=18 & 13 Hz; 5.5 & 4.75, 2H, γa-H_2, d & d, j=19 & 19 Hz; 4.45, 1H, 8-H, d, j=8 Hz; 4.38, 1H, 7-H, d, j=8 Hz; 3.7, 3H, γ-$COOCH_3$, s; 3.7, 2H, 4a-H_2, q; 3.6, 3H, 7-$COOCH_3$, s; 3.5, 3.5, 3.3, 3H x 3, ring 1,3,5-CH_3, s; 2.45, 2H, 7a-H & 7b-H; 2.2, 2H, 7a'-H & 7b'-H; 1.6, 3H, 8a-CH_3, d, j=9 Hz; 1.2, 3H, 4b-CH_3, t, j=7 Hz; -1.8, 2H, ring NH, s.

A

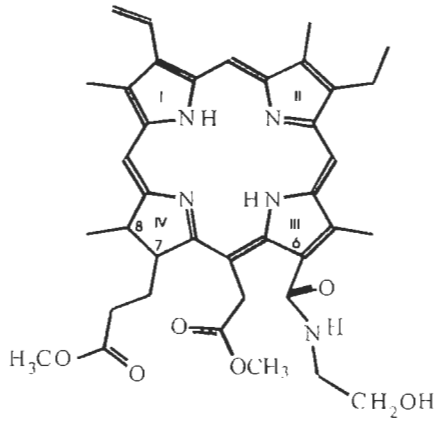

B

C

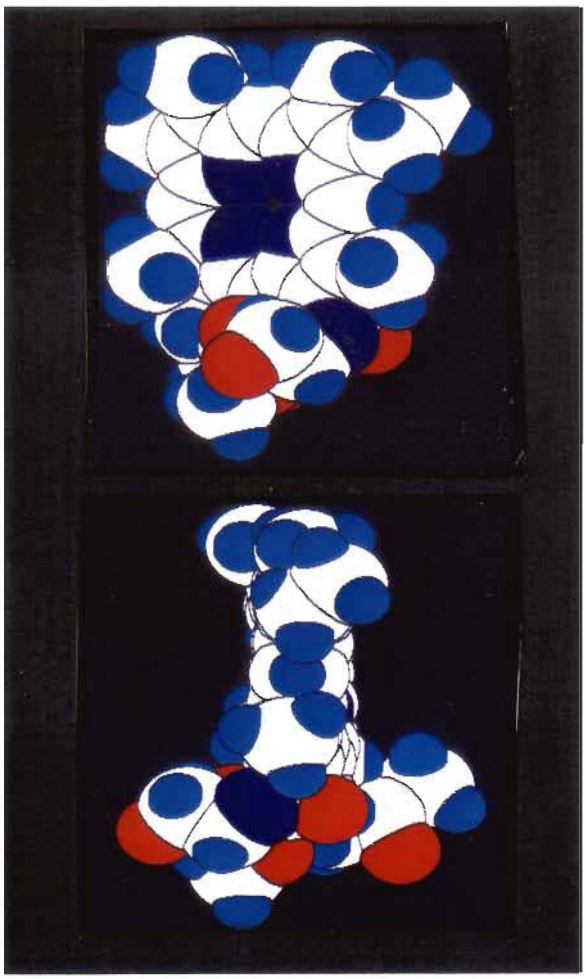

Figure 4.12. Proposed molecular structure of PEA. (A) Structural drawing, (B) space filling molecule viewed from above the plane of the porphin ring, (C) space filling molecule viewed from the edge (perpendicular to the plane). Space filling molecular configurations were generated by Desktop molecular modeller (ver. 2.0, Oxford university press, 1991).

4.6.2 Chemotherapy

4.6.2.1 MTT assay

The MTT assay tests the cytotoxic activity of cytotoxic compounds toward neoplastic cell lines by measuring spectroscopically the amount of blue formazan dye produced by surviving cells. Various human neoplastic cell lines were tested to evaluate the chemotherapeutic activity of the ethanolamide derivatives HPPEEA, PEA and their parent compounds, HPIX and mPheo from which they were synthesized. A well known chemotherapeutic drug, adriamycin, was used as a positive control, while the PDT drug pHP was used as a negative control.

The survival curves are shown in Fig. 4.13 to 4.18. In these curves the cell survival is expressed as a percent, compared with the blank untreated control cells which received no drug treatment, such that 100% survival refers to no cytotoxicity. The data for each survival curve is provided in an attached table (Table 4.1 to 4.6). Generally in any single experiment all the cell lines responded similarly to a particular drug.

For adriamycin, cytotoxicity began to be manifested in the cell lines at 0.01 μM and by 100 μM there was near 0% survival (Fig. 4.13 and Table 4.1).

For pHP, the negative control, some cytotoxicity was observed in the cell lines at about 50 μM and at the highest concentration (100 μM) the response was about 20-60% cell survival (Fig. 4.14 and Table 4.2).

HPIX (the parent compound of HPPEEA) exhibited very little cytotoxic activity. At the highest HPIX concentration tested (100 μM) some cytotoxicity was observed in the cell lines (Fig. 4.15 and Table 4.3), for example, 30% survival for the cell line K562.

HPPEEA exhibited significant cytotoxic activity. When 20 μM of HPPEEA was added the cell survival dropped to near 10% (Fig. 4.16 and Table 4.4). Below 20 μM, little cytotoxicity is observed.

Methyl pheophorbide showed very little if any cytotoxicity. At the highest concentration of mPheo tested (100 μM) cell survival was still approximately at 80% (Fig. 4.17 and Table 4.5).

PEA showed less than 10% cell survival at 40 μM indicating a similar response to HPPEEA, but at a higher concentration (Fig. 4.18).

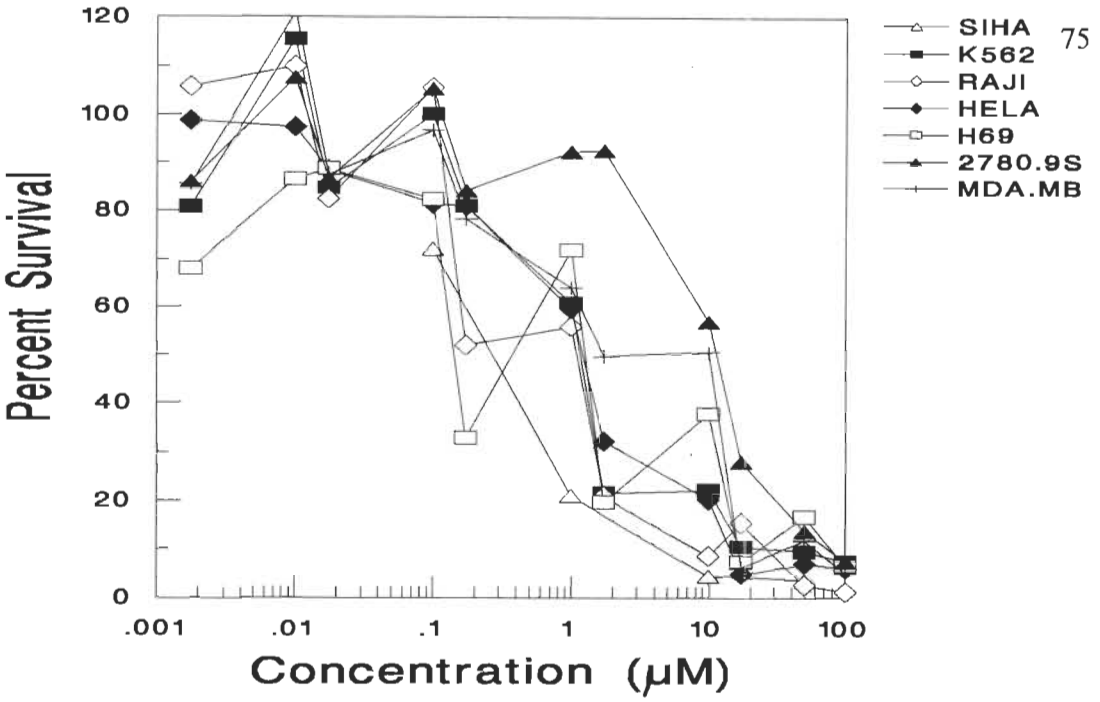

Figure 4.13. Cell survival curves for adriamycin treated cells in the MTT assay. Survival expressed as a percent of the control untreated cells.

Table 4.1. Percent cell survival of various neoplastic cell lines at various μM concentraions of adriamycin.

Concentration	SIHA	K562	RAJI	Hela	H69	H209	2780.9S	MDA.MD
0.00174		80.7±35.4	105.7±11.7	98.7±5.1	68.1±3.5	90.8±5.5	86.0±6.2	85.5
0.01		115.5±23.9	110.0±23.9	97.5±9.7	86.5±13.5	85.6±14.0	107.6±14.2	121.3±16.9
0.0174		84.7±19.9	82.3±27.7	88.4±0.4	88.7±48.4	68.0±3.0	86.7±1.5	87.5
0.1	72.2±16.3	100.1±25.8	105.6±14.3	81.4±13.3	82.2±16.7	85.6±17.1	105.4±12.0	96.8±12.9
0.174		80.9±25.0	52.0±28.7	80.9±3.5	32.9±12.1	21.5±6.8	84.1±1.5	78.1
1	21.0±12.5	60.8±37.9	55.9±31.5	59.6±34.4	71.9±20.9	56.9±30.9	92.3±9.9	64.0±28.2
1.74		21.6±22.1	20.8±12.4	32.1±19.2	19.7±6.0	17.9±8.6	92.6±5.1	49.7
10	4.4±2.8	22.1±8.5	8.6±6.0	20.2±24.2	37.71±23.2	23.1±18.7	56.9±24.5	50.48±29.2
17.4		10.6±9.6	15.5±17.0	4.8±0.5	7.4±2.5	7.9±2.8	28.0±7.4	6.2
50	3.5±1.9	9.5±6.3	2.5±2.9	7.0±4.7	16.8±16.4	5.8±2.9	13.8±16.8	11.8±10.2
100		7.5	1.1	6.1	6.6	1.5	7.4	5.0

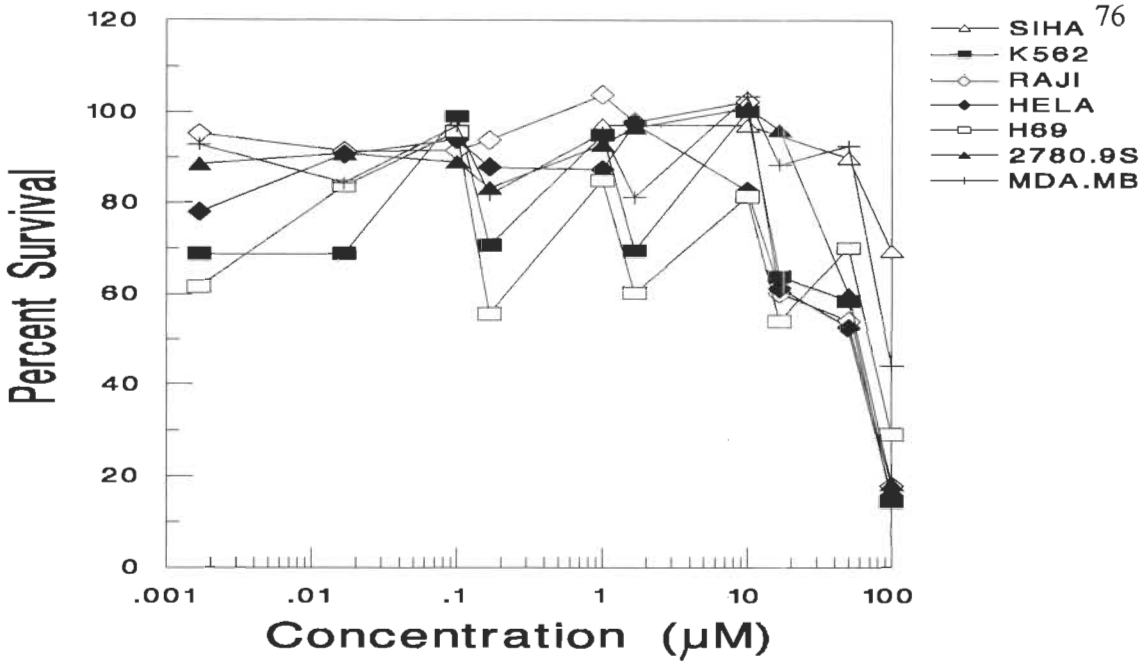

Figure 4.14. Cell survival curves for polyhematoporphyrin treated cells in the MTT assay. Survival expressed as a percent of the control untreated cells.

Table 4.2. Percent cell survival of various neoplastic cell lines at various μM concentraions of polyhematoporphyrin.

Concentration	SIHA	K562	RAJI	Hela	H69	H209	2780.9S	MDA.MD
0.00167		68.8	95.2	78.0	61.6	94.6	88.5	92.8
0.0167		68.8	91.3	90.6	83.6	91.1	90.7	84.4
0.1		99.1	91.5	93.9	95.7	91.2	88.9	97.0
0.167		70.6	93.8	87.8	55.7	94.6	83.2	81.8
1	97.1±13.0	94.9±9.0	103.9±11.8	87.3±5.8	84.9±7.8	95.7±8.9	92.8±8.8	95.4±0.2
1.67		69.4	97.4	97.4	60.2	93.8	96.6	81.1
10	97.0±11.7	100.2±3.0	102.4±0.7	82.6±24.7	81.4±7.7	101.0±11.8	101.0±11.7	103.5±5.8
16.7		63.8	60.1	61.3	54.2	77.8	96.0	88.4
50	89.9±16.7	58.4±17.1	54.2±3.4	52.6±25.8	70.0±1.1	65.7	60.0±0.5	92.5±22.5
100	69.4±34.4	14.3	17.7±8.4	15.6±7.6	29.0±13.7	53.7±26.6	18.1±1.0	44.2±10.6

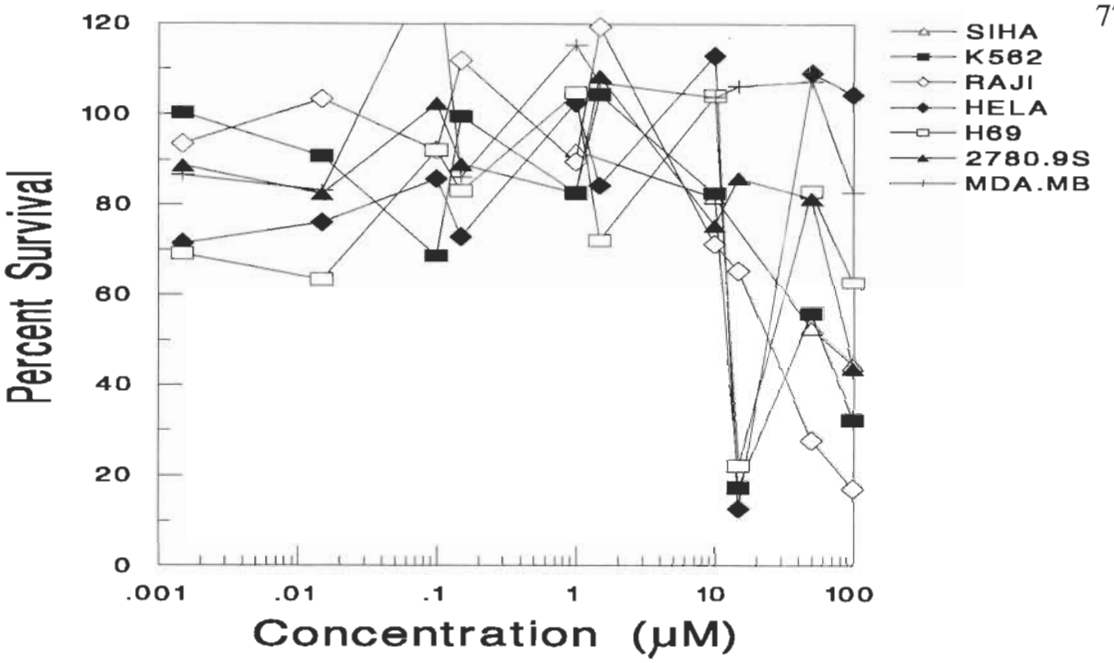

Figure 4.15. Cell survival curves for hematoporphyrin treated cells in the MTT assay. Survival expressed as a percent of the control untreated cells.

Table 4.3. Percent cell survival of various neoplastic cell lines at various μM concentraions of hematoporphyrin.

Concentration	SIHA	K562	RAJI	Hela	H69	H209	2780.9S	MDA.MD
0.00149		100.3	93.5	71.5	69.2	88.9	88.8	86.6
0.0149		90.8	103.4	76.1	63.4	97.5	82.4	83.1
0.1		68.7	92.1	85.8	92.2	91.4	102.4	135.7
0.149		99.6	111.8	72.9	83.1	98.3	89.1	86.2
1	92.2±5.2	82.7±13.3	89.6±15.9	102.6±24.3	104.8±16.4	94.0±14.7	82.5±15.3	115.4±50.5
1.49		104.4	119.3	84.3	72.2	116.3	108.5	106.9
10	81.6±9.3	82.5±9.1	71.4±24.1	113.0±25.6	104.1±12.3	99.5±13.9	75.5±28.8	103.8±27.2
14.9		17.3	65.4	12.6	21.9	18.5	85.9	106.2
50	52.6±7.7	55.9±13.4	27.6±14.7	109.1±5.9	82.9±6.2	93.3±3.3	81.4±22.7	107.3±34.0
100	44.5±18.9	32.1±23.4	17.0±4.6	104.4±35.0	62.6±1.3	84.6±1.2	43.8±37.4	82.8

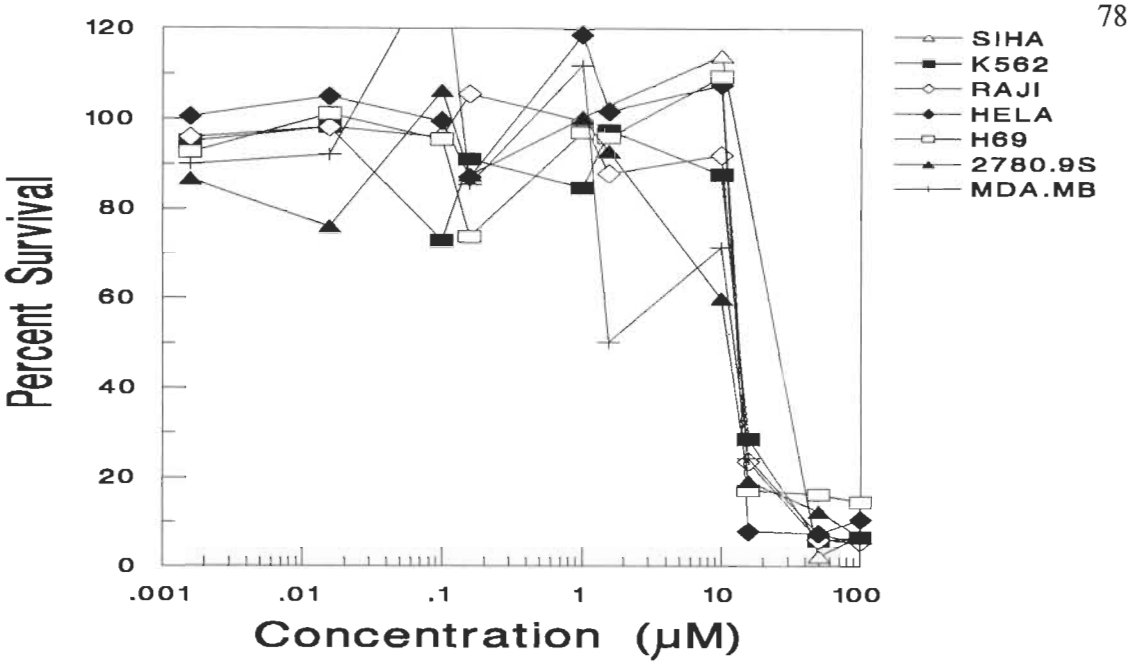

Figure 4.16. Cell survival curves for HPPEEA treated cells in the MTT assay. Survival expressed as a percent of the control untreated cells.

Table 4.4. Percent cell survival of various neoplastic cell lines at various µM concentraions of HPPEEA.

Concentration	SIHA	K562	RAJI	Hela	H69	H209	2780.9S	MDA.MD
0.00157		95.7	95.9	100.5	92.5	85.4	86.6	90.0
0.0157		98.2	98.2	105.1	101.1	82.2	76.0	92.0
0.1		72.9	96.1	99.6	95.5	97.8	106.4	137.4
1.157		91.1	105.6	87.0	73.8	67.9	87.5	85.5
1	100.4±13.4	84.7±9.2	99.5±7.0	118.7±22.9	97.0±19.8	104.9±5.2	100.2±0.2	112.0±33.1
1.57		97.5	87.8	101.8	95.9	68.1	92.7	50.2
10	114.2±21.2	87.6±4.5	92.0±6.7	107.7±14.6	109.5±14.0	99.2±13.3	59.9±20.1	71.3±37.8
15.7		28.5	23.6	7.8	17.1	16.1	19.3	24.3
50	2.2±1.4	5.7±0.5	5.9±3.0	7.4±2.5	16.1±1.5	8.6±5.1	12.3±4.0	7.4±4.7
100	6.7±3.5	6.6±0.7	5.4±0.9	10.5±7.1	14.4±1.3	9.8±5.9	6.5±1.6	5.2±0.1

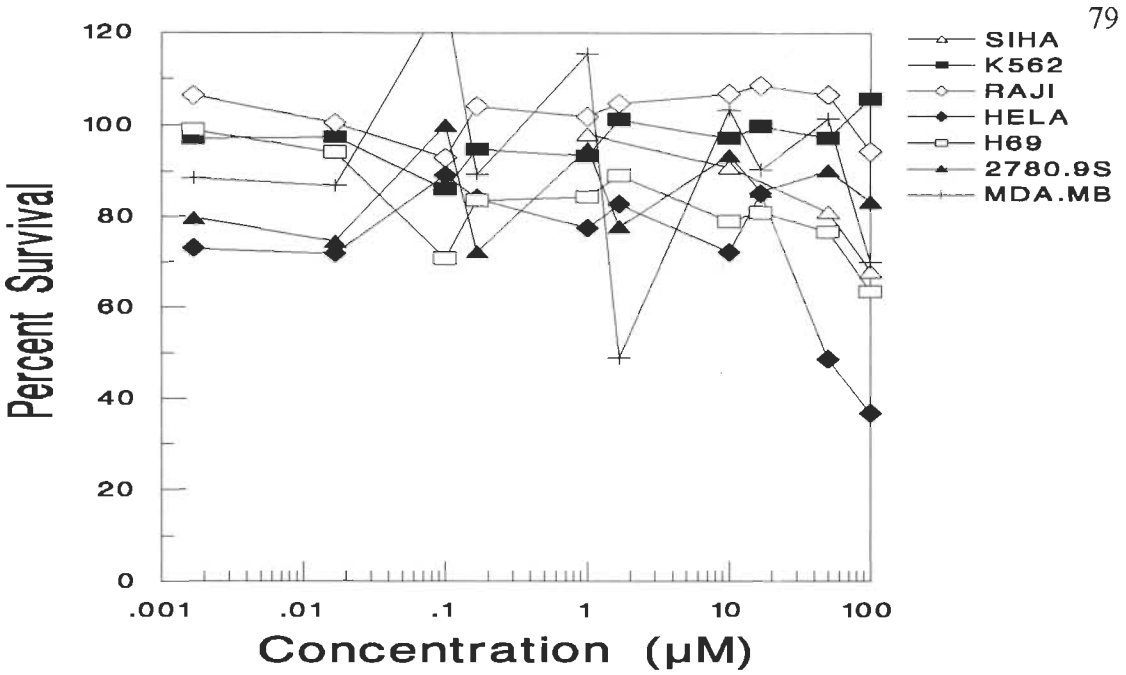

Figure 4.17. Cell survival curves for methyl pheophorbide *a* treated cells in the MTT assay. Survival expressed as a percent of the control untreated cells.

Table 4.5. Percent cell survival of various neoplastic cell lines at various µM concentraions of methyl pheophorbide *a*.

Concentration	SIHA	K562	RAJI	Hela	H69	H209	2780.9S	MDA.MD
0.00167		97.2	106.4	73.0	99.1	89.7	79.7	88.5
0.0167		97.4	100.4	71.8	94.1	85.9	74.5	86.8
0.1		86.0	92.9	89.1	70.7	83.6	100.0	128.2
0.167		94.7	104.0	84.0	83.5	83.0	72.2	89.2
1	98.0±5.4	93.3±1.4	101.8±17.9	77.4±8.5	84.3±2.6	90.2±8.4	94.9±4.3	115.4±31.1
1.67		101.2	104.7	82.7	89.1	94.0	77.8	48.9
10	90.8±11.1	97.3±3.1	106.7±7.6	72.1±3.6	79.0±8.6	91.7±2.1	93.4±6.2	103.3±16.1
16.7		99.7	108.5	85.1	80.9	92.3	85.6	90.4
50	81.0±10.0	97.3	106.4±7.8	48.7±26.7	76.7±12.2	85.2±1.8	90.1±19.9	101.3±15.8
100	68.0±8.1	105.7±15.0	94.3±1.1	36.7±34.1	63.6±12.9	82.3±3.7	83.2±10.4	68.9

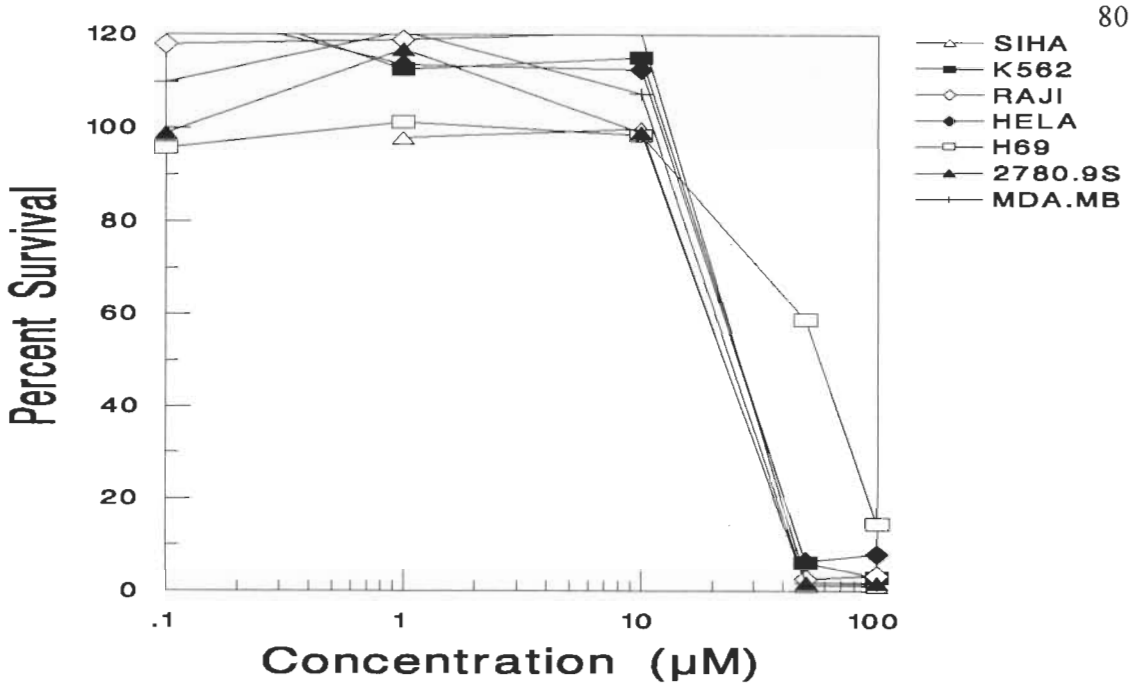

Figure 4.18. Cell survival curves for PEA treated cells in the MTT assay. Survival expressed as a percent of the control untreated cells.

Table 4.6. Percent cell survival of various neoplastic cell lines at various µM concentraions of PEA.

Concentration	SIHA	K562	RAJI	Hela	H69	H209	2780.9S	MDA.MD
0.1		129.4	117.9	126.0	95.7	101.9	98.8	109.8
1	97.8±5.6	112.6±24.8	119.0±8.0	113.6±57.0	101.3±10.5	102.0±10.2	117.0±7.1	120.7±16.8
10	99.9±8.6	115.2±28.9	120.6±0.1	112.6±51.7	98.4±14.8	106.0±1.0	99.0±9.7	107.4±13.0
50	1.2±1.0	6.1±3.4	2.5±3.1	6.3±4.1	58.7±7.9	59.4±25.5	1.7±1.1	1.6±0.9
100	1.1±0.7	2.9±3.0	3.3±4.5	7.8±8.9	14.4±12.3	5.2±4.2	1.7±0.4	1.6±0.4

The cytotoxic activity of both ethanolamide compounds occurred over a very small concentration range compared to adriamycin. The ethanolamide compounds had no effect at 10 μM and caused almost 100% cell death by 20-40 μM (Fig. 4.16 and 4.18).

For a comparison of the response of the different cell lines to the various drugs tested, the IC_{50}, or drug concentration required to cause a 50% survival, was examined (Fig. 4.19, 4.20 and Table 4.7). From these two figures, it is apparent that the ethanolamides can exhibit some cytotoxic activity at a higher concentration than that of adriamycin. It is also apparent from Fig. 4.19, 4.20 and Table 4.7 (cell lines 2780.9S; MDA.MB; H69) that PEA requires about twice the concentration of HPPEEA to accomplish the 50% cell kill in some of the cell lines, while the parent compounds of the ethanolamides, and pHP, had very little cytotoxic activity.

Table 4.7. Summary of the concentrations[a] derived from MTT cytotoxicity assay required to obtain an IC_{50}.

Cell lines	Adriamycin	pHP	HPIX	HPPEEA	mPheo	PEA
2780.9S	15±1	65±7	>100	16±8	>100	35±7
Daudi	0.3±0.2	28±4	15±5	22±6	25	35±7
H69	3±3	75±7	70±52	22±6	>100	55±7
Hela	2±1	73±39	71±50	21±6	25	35±7
K562	1±1	75±35	44±29	22±6	>100	35±7
MDA.MB	9±1	85±21	>100	12±12	>100	35±7
Raji	2±1	60±14	57±40	21±6	>100	35±7
SIHA	0.5±0.3	95±6	56±12	44±18	>100	35

(a) All concentrations values are in μM.

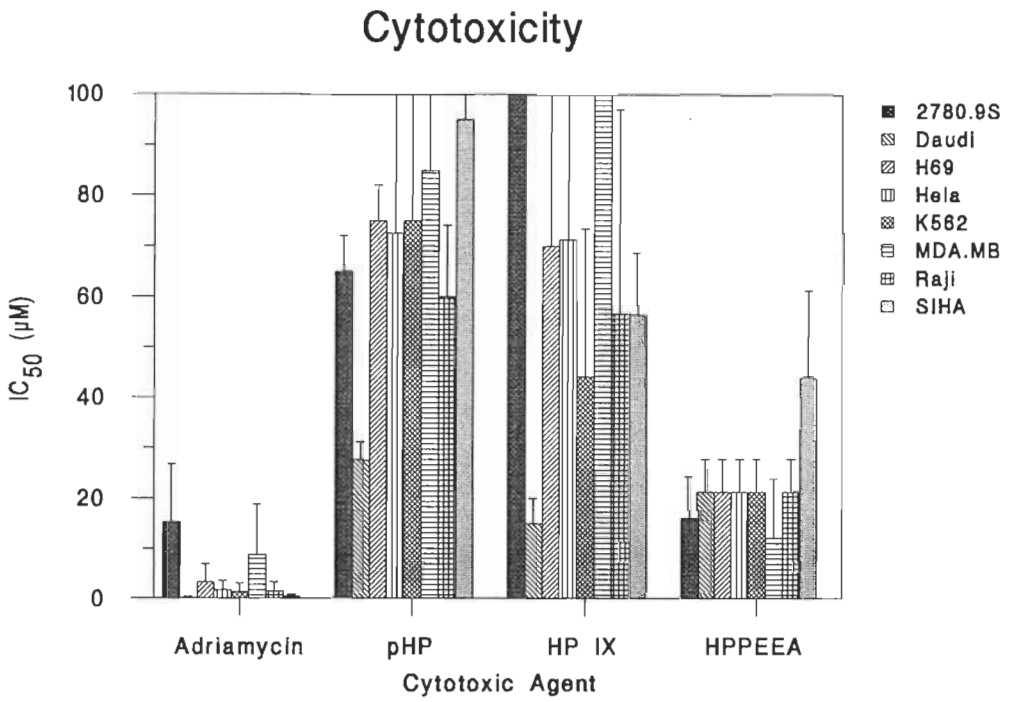

Figure 4.19. IC_{50} of various cytotoxic agents on several human neoplastic cell lines: Part 1.

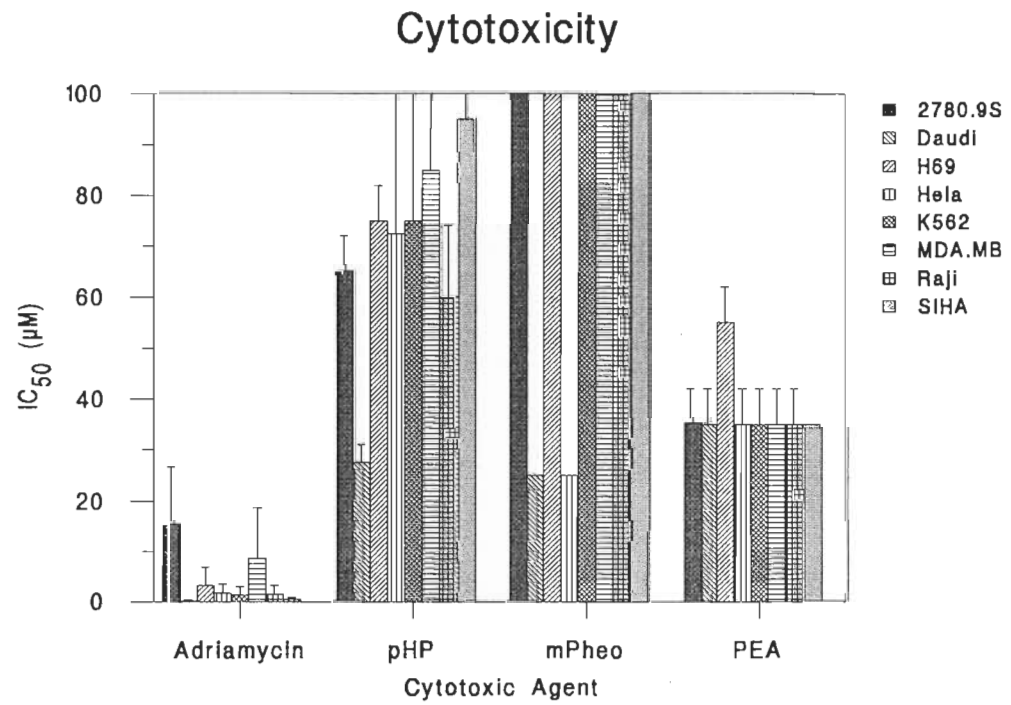

Figure 4.20. IC_{50} of various cytotoxic agents on several human neoplastic cell lines: Part 2.

4.6.2.2 Animal tumour studies

The MTT assay is useful for the preliminary evaluation of cytotoxicity, but it is necessary to investigate the entire living systems in order to assess anti-cancer drug response of tissues. This can be achieved using animal models which have implanted tumours. For these tests, two cancer types were used, the solid tumour Lewis lung carcinoma and the ascites leukemia cancer P388, representing both localized and non-localized forms of cancer respectively.

4.6.2.2.1 Lewis lung carcinoma in C57BL6 mice

The growth progression of the Lewis lung carcinoma in C57BL6 mice is illustrated in Fig. 4.21. The control animals, which received no drug, died at 8 to 10 days with small tumour diameters (about 15 mm) (Fig. 4.21). Numerous secondary tumours were observed in many anatomical locations when the control animals were examined, by dissection after death.

The animals treated with either HPPEEA or PEA (10 mg kg^{-1}) survived up to 25 days, which is an increase of over 100% in "Time to death" (TD). The primary tumour did not stop growing when subjected to either HPPEEA or PEA. Unlike a study using adriamycin at 7 mg kg^{-1} where 80% of the primary tumours were stopped (Corbett *et al.*, 1984). However, in this study no secondary tumours were observed when the animals were examined after death. The results thus indicate that under these study conditions treatment with the ethanolamide drugs appeared to prevent secondary tumours, but does not stop the primary tumour. The prevention of secondary tumours suggests that metastasis was stopped by intervention from the ethanolamide derivatives.

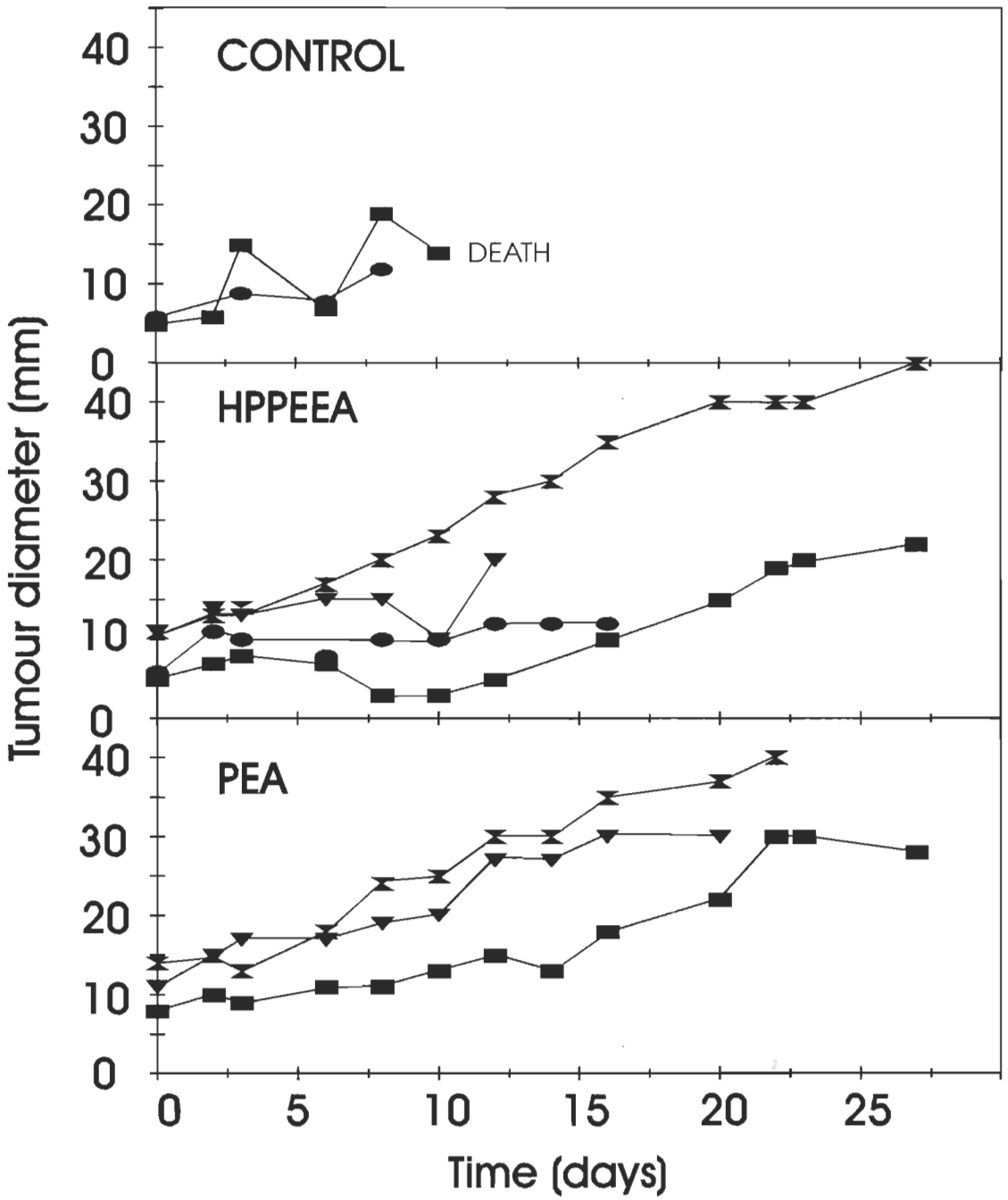

Figure 4.21. Chemotherapeutic treatment of the solid tumour Lewis lung carcinoma in C57BL6 mice, with HPPEEA and PEA at a dose of 10 mg kg^{-1} daily IP. Control animals received injection solvent only. Each point represents the tumour diameter of a single animal with the different symbols representing individual mice. The time of death (TD) for each mouse is at the last corresponding time point.

4.6.2.2.2 Ascites leukemia P388 in B6D2F$_1$ mice

To test the hypothesis that the ethanolamide derivatives can prevent metastasis, the chemotherapeutic activity of the ethanolamides was evaluated using the metastatic cancer, leukemia (P388), that does not form a distinct solid tumour. The progression of this cancer can be evaluated by the animal's weight gain expressed as a percent of the original weight. The control animals showed a 20-30% increase in weight at death, occurring in about 8 days (Fig. 4.22). No increase in TD in HPPEEA treated animals, and only a slight TD increase in PEA treated animals, was observed, indicating that the cancer response to the ethanolamides (dose = 10 mg kg^{-1}) was minimal (Fig. 4.22).

Another experiment was performed using a higher drug concentration, since the MTT cytotoxicity test had indicated that the IC_{50} of the ethanolamides were ~22 μM for HPPEEA and ~35 μM for PEA (Table 4.7 in section 4.6.2.1). The higher dose used was 100 mg kg^{-1}, which is 10 times the previous dose. The results (Fig. 4.23) were similar to the previous P388 experiment indicating a slight increase in TD compared to the controls. However, a notable lag before commencement of animal weight gain, of several days, was observed in both experimental trials where the animals were treated with ethanolamides.

4.6.3 Pharmacokinetics

A new PDT drug must demonstrate selective retention in neoplastic tissues, and have relatively low accumulation in the skin in order to be clinically useful. The tissue selectivity of PDT drugs is evaluated by their tissue pharmacokinetics by the means of fluorescence intensity measurements. The pharmacokinetic data for HPPEEA and PEA have been separated into three categories: i) serum measurements; ii) *in vivo* measurements; and iii) *ex vivo* measurements.

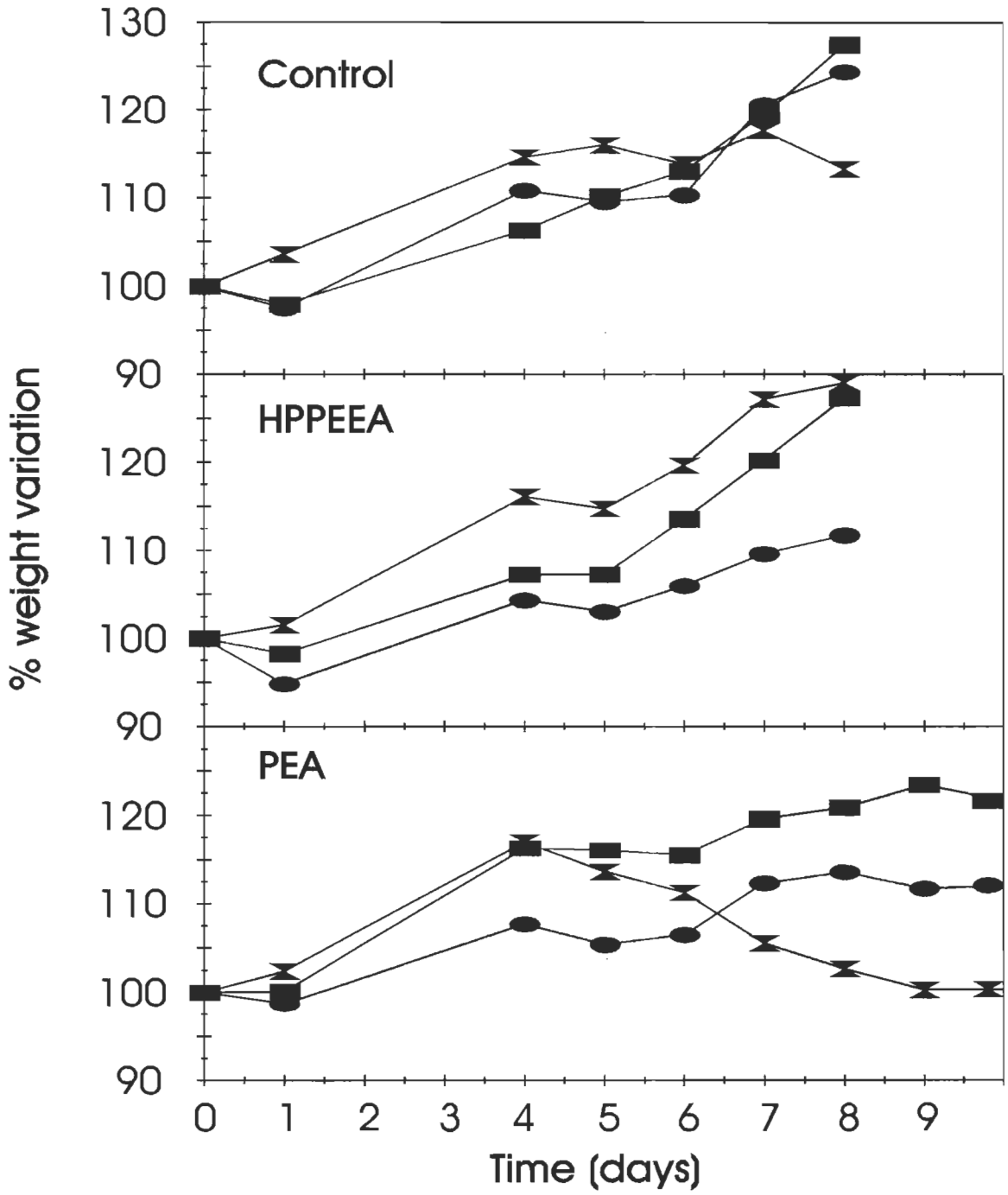

Figure 4.22. Chemotherapeutic treatment of leukemia P388 in $B6D2F_1$ mice with HPPEEA and PEA at a dose of 10 mg kg^{-1} daily IP. Control animals received injection solvent only. Each line represents the percent weight variation after cancer implantation of a single animal with the different symbols representing individual measurements. The time of death (TD) for each mouse is at the last time point.

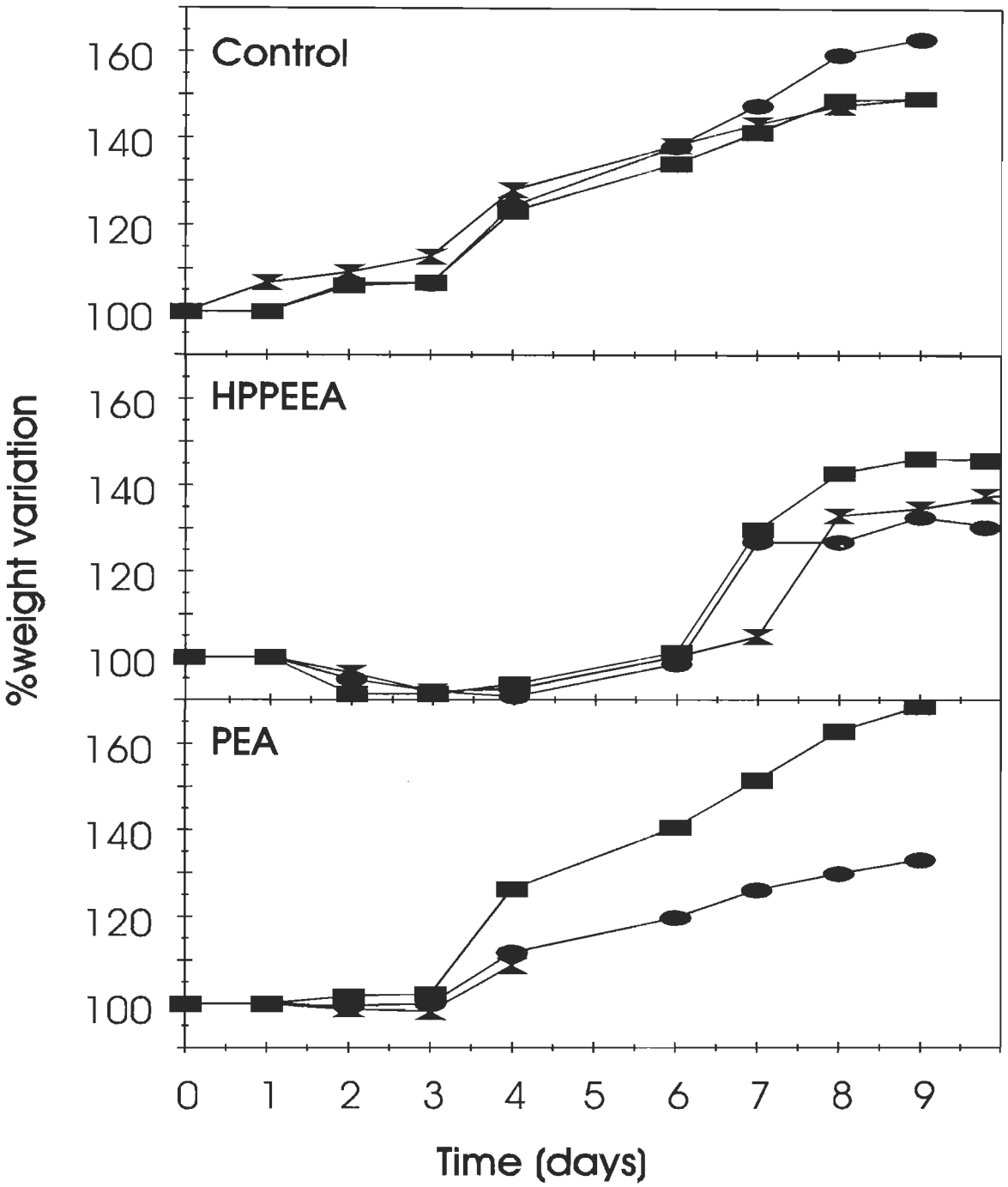

Figure 4.23. Chemotherapeutic treatment of leukemia P388 in $B6D2F_1$ mice with HPPEEA and PEA at a dose of 100 mg kg^{-1} daily IP. Control animals received injection solvent only. Each line represents the percent weight variation after cancer implantation of a single animal with the different symbols represent individual measurements. The time of death (TD) for each mouse is at the last time point.

4.6.3.1 Serum measurements

The serum clearance curve of HPPEEA and PEA are presented in Fig. 4.24. Both the HPPEEA and PEA concentration in the serum returned to background levels by about 30 h post IP injection (injection solvent formulation was DMSO/human serum in a 10/90 (v/v) ratio). The peak HPPEEA concentrations measured in serum (2800 ng mL^{-1}) were comparable to those reported for other PDT drugs (Biolo *et al.*, 1991). However, the PEA concentration measured in the serum was low. The curve profile was typical but the peak drug concentration measured (75 ng mL^{-1}) was lower than expected of a typical photosensitizer by a factor of almost 40. These have been confirmed by another series of measurements.

The fluorescence signal measured from several concentrations of PEA was the same with and without serum in the solvent, indicating that the serum was not quenching the fluorescence signal of PEA.

4.6.3.2 *In vivo* measurements

The *in vivo* pharmacokinetic data for HPPEEA in mice bearing Lewis lung carcinoma is shown in Fig. 4.25. HPPEEA fluorescence had decreased to background in all tissues by about 24 h. No significant selectivity is apparent in any tissue.

The *in vivo* pharmacokinetics of mPheo in mice bearing Lewis lung carcinoma is shown in Fig. 4.26. Methyl pheophorbide *a* cleared from the thigh and tumour sites rather quickly, reaching background levels at around 10 h. The skin and abdomen sites indicated a slower clearance, reaching background fluorescent levels at around 25 h.

The clearance (about 25 h) of PEA from tissues measured by *in vivo* pharmacokinetics was similar to mPheo (Fig. 4.27).

The *in vivo* clearance curves of tissue sites can not be compared to each other due to different fluorescence characteristics of each site. Also, tissue sites of different studies should not be compared since the instrumentation is standardized within each experiment but not between experiments. The main focus of the *in vivo* pharmacokinetics is to determine within a single animal the clearance of a drug from various tissues.

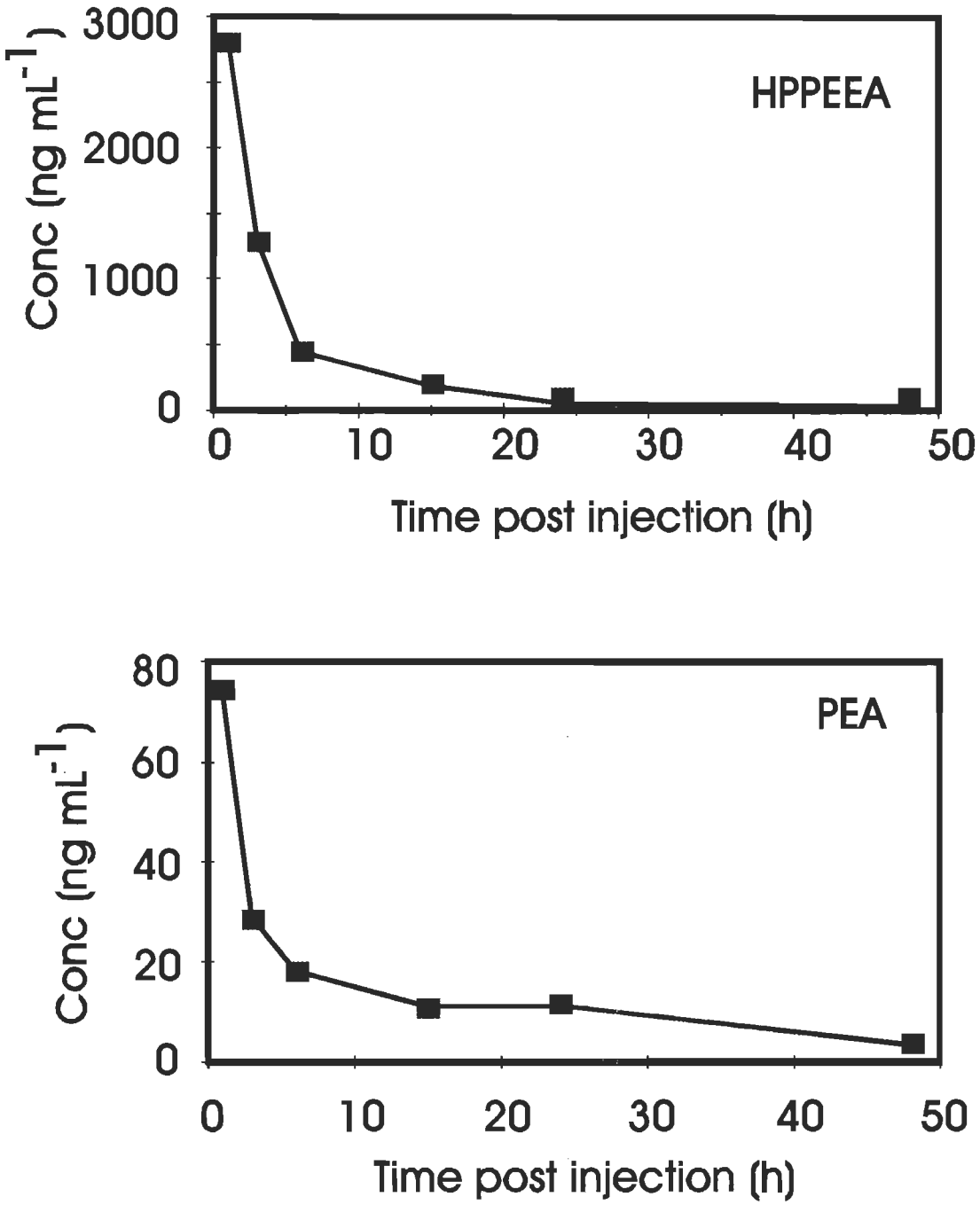

Figure 4.24. Serum pharmacokinetics of HPPEEA and PEA in B6D2F$_1$ mice, administered a single IP injection of 10 mg kg^{-1} of the drug. At various time points the animals were killed and the blood was removed by cardiac puncture. The serum was separated from the blood, and drug concentrations were measured by fluorescence. Each point represents at least three animals and has an error of less than 20%.

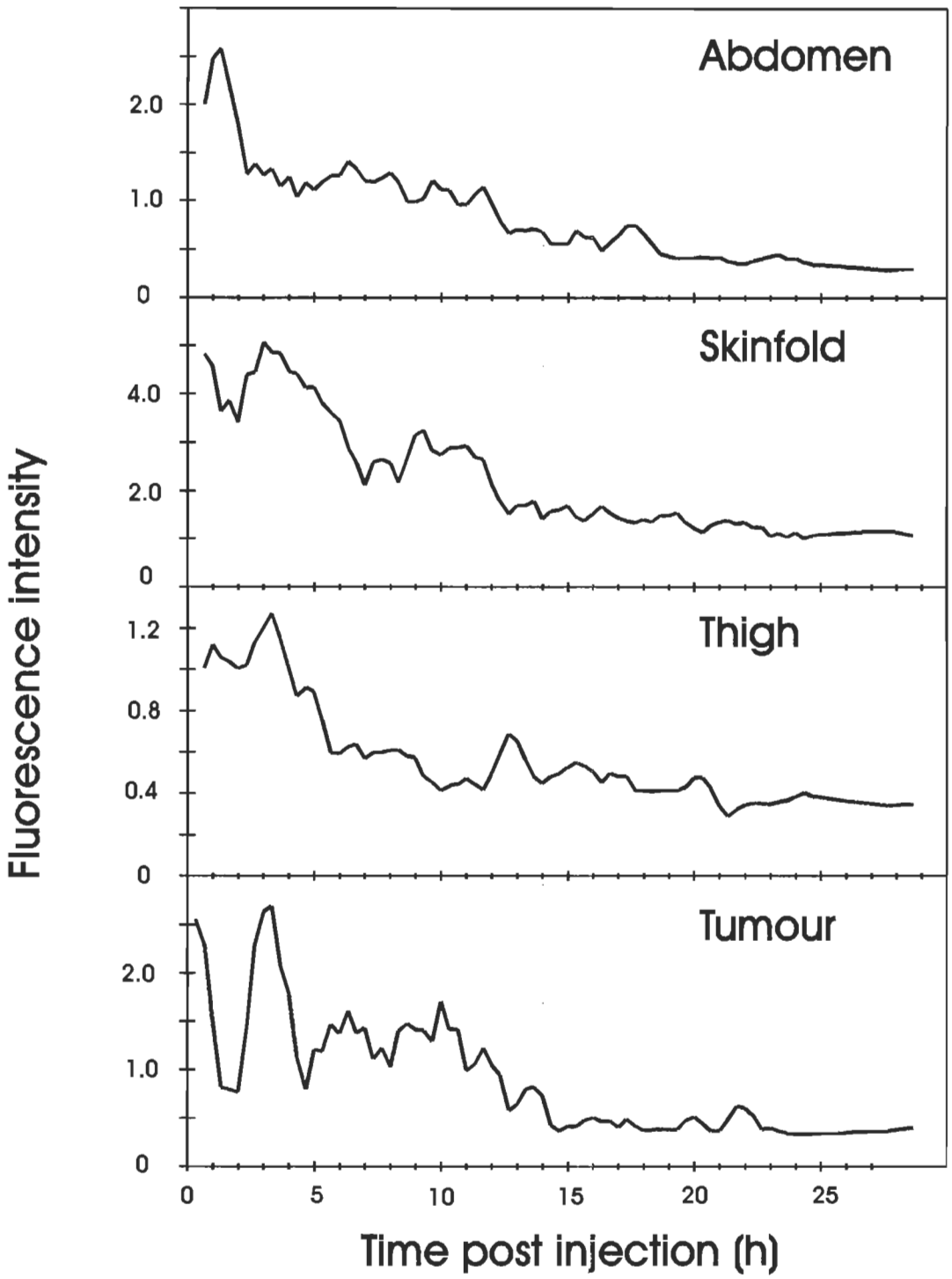

Figure 4.25. *In vivo* pharmacokinetics of HPPEEA (dose = 10 mg kg^{-1}) in SKH-HR1 mice bearing Lewis lung carcinoma. Curves are expressed as fluorescence intensity relative to a standard solution of uroporphyrin. The maximum error on any individual datum point is 20%.

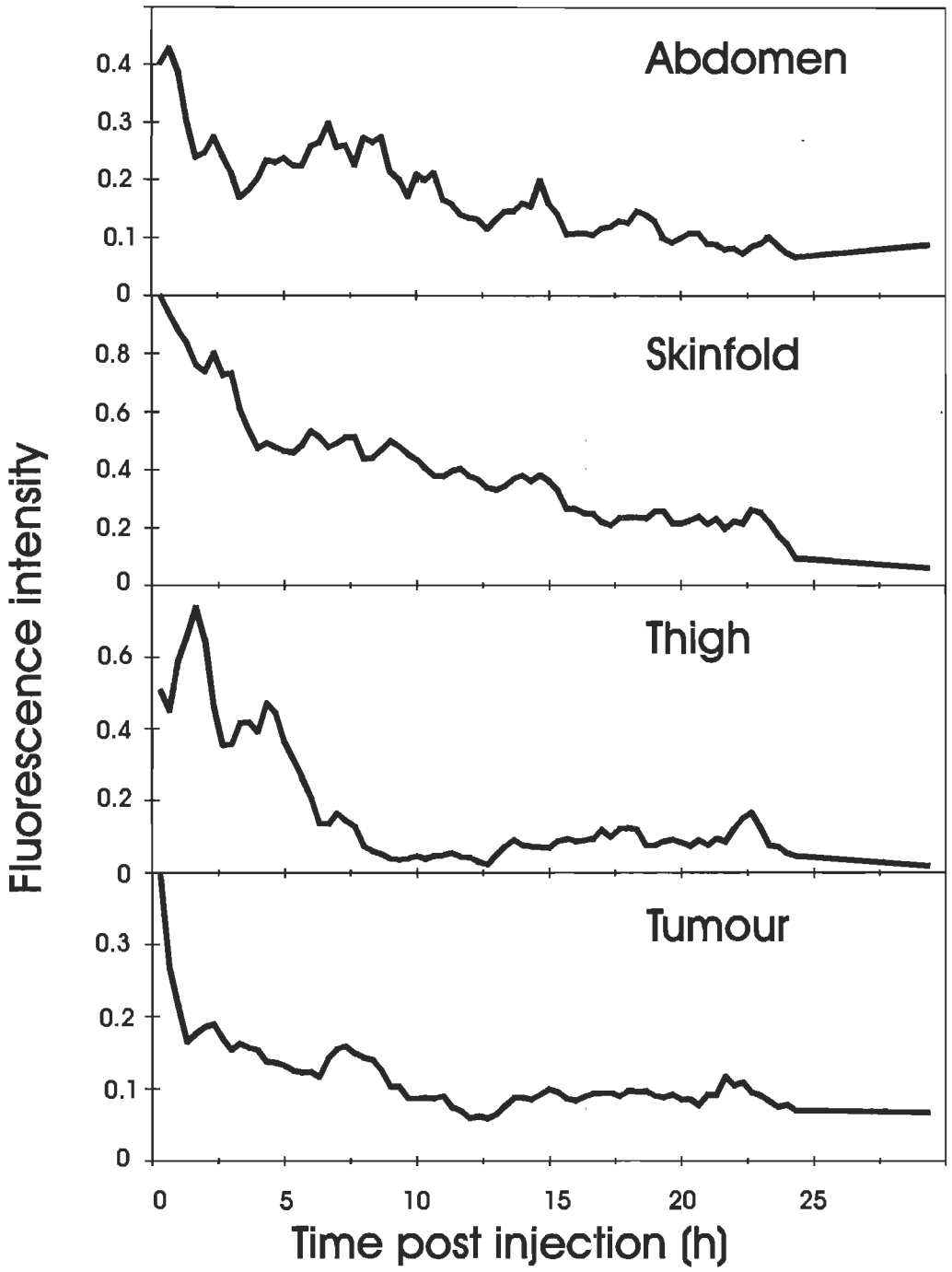

Figure 4.26. *In vivo* pharmacokinetics of methyl pheophorbide *a* (dose = 10 mg kg^{-1}) in SKH-HR1 mice bearing Lewis lung carcinoma. Curves are expressed as fluorescence intensity relative to a standard solution of uroporphyrin. The maximum error on any individual datum point is 20%.

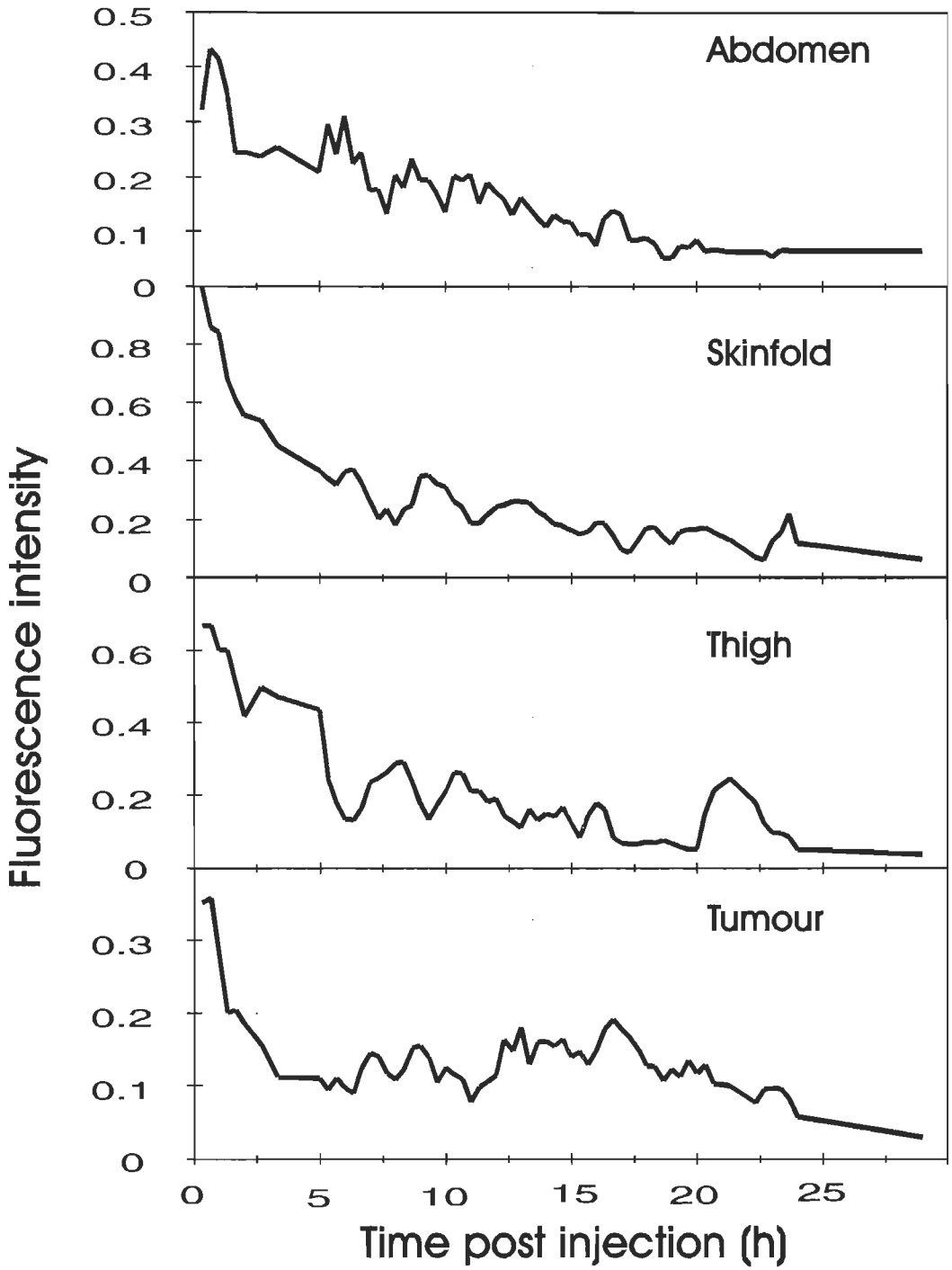

Figure 4.27. *In vivo* pharmacokinetics of PEA (dose = 10 mg kg^{-1}) in SKH-HR1 mice bearing Lewis lung carcinoma. Curves are expressed as fluorescence intensity relative to a standard solution of uroporphyrin. The maximum error on any individual datum point is 20%.

4.6.3.3 *Ex vivo* measurements

The *ex vivo* tissue pharmacokinetics of HPPEEA in mice bearing Lewis lung carcinoma measured by drug fluorescence intensity is shown in Fig. 4.28. The drug fluorescence was the highest in the skin followed by kidney, liver, tumour, and muscle, and the lowest in the brain. The drug fluorescence had returned to background intensity in all tissues after 25 to 30 h.

The tissue pharmacokinetics of PEA in mice bearing Lewis lung carcinoma is shown in Fig. 4.29. The drug fluorescence was the highest in the skin followed by the liver, kidney, muscle, and tumour, and the lowest in the brain. PEA fluorescence was at background intensity in all tissues by about 25 to 30 h.

The tissue pharmacokinetics of PEA was also studied using another animal tumour model (Balb c mice bearing a lung carcinoma M4898) (Fig. 4.30). In this experiment PEA was at background levels by 24 h. The drug fluorescence was the highest in the skin followed by the tumour, liver and muscle. There was a marked selective accumulation of PEA in the tumour at 3 h post injection relative to the skin or muscle (tumour/muscle = 6, tumour/skin = 2).

4.6.4 Photosensitization activity measured by photohemolysis

The ethanolamide photosensitization activity was evaluated by photohemolysis. In the photohemolysis assay the amount of hemoglobin released from damaged red blood cells as a result of photosensitization is measured. The concentrations of drugs used in the assay were comparable to those typically measured in tissues by pharmacokinetics.

The percentage of hemolysis as a function of drug concentration is presented in Fig. 4.31 to 4.36. The hemolysis from the solvent alone was always less than 14% (Fig. 4.31). The no light control in each test indicates that the drug alone had no effect on the hemolysis of the red blood cells, with the possible exception of PEA where a small increase is noticable (Fig. 4.35). At the maximum concentration, the % hemolysis is 17%, slightly higher than the control.

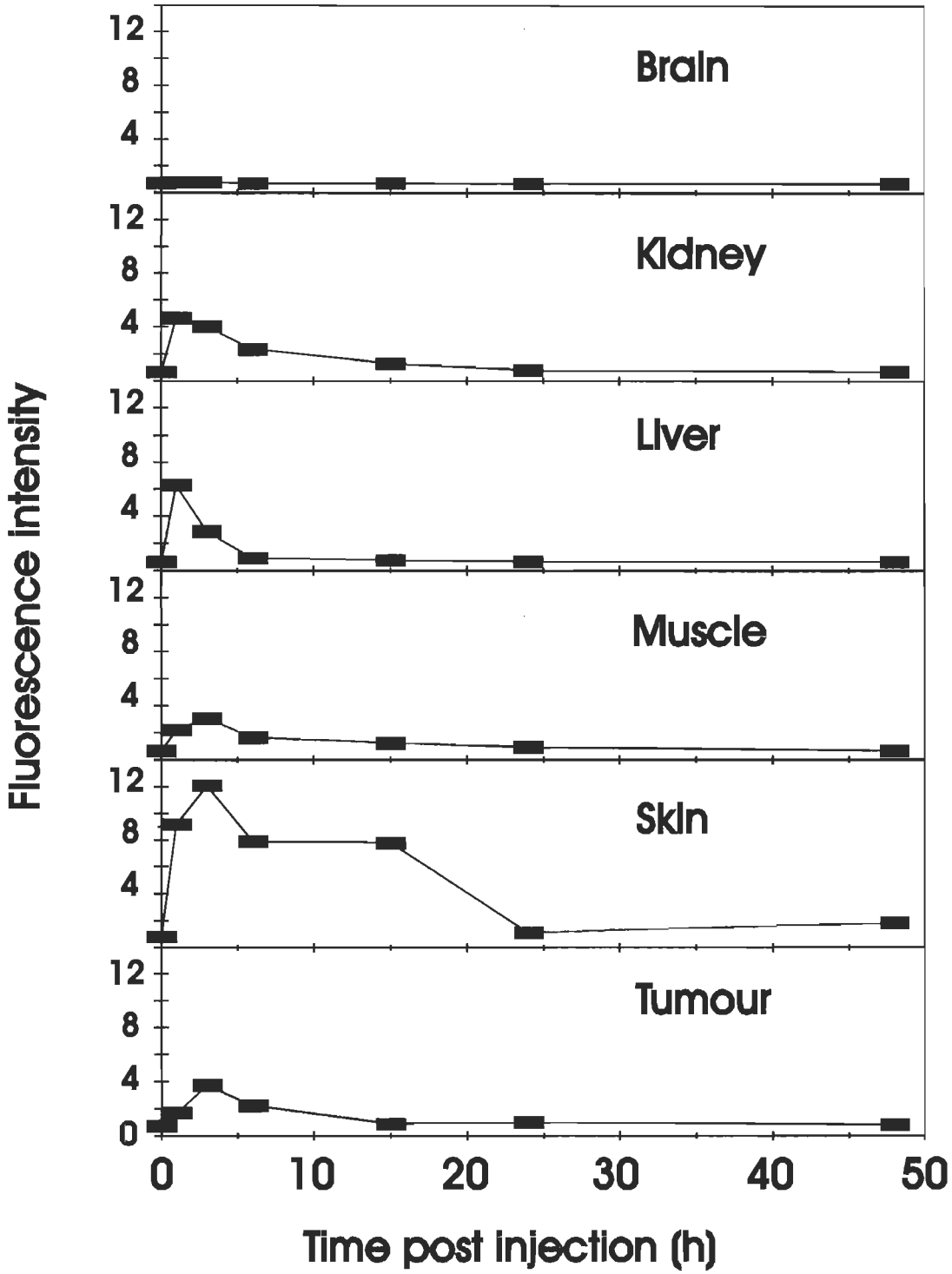

Figure 4.28. *Ex vivo* pharmacokinetics of HPPEEA (dose = 10 mg kg^{-1}) in SKH-HR1 mice bearing Lewis lung carcinoma. Curves are expressed as fluorescence intensity relative to a standard solution of uroporphyrin. The maximum error on any individual datum point is 15%.

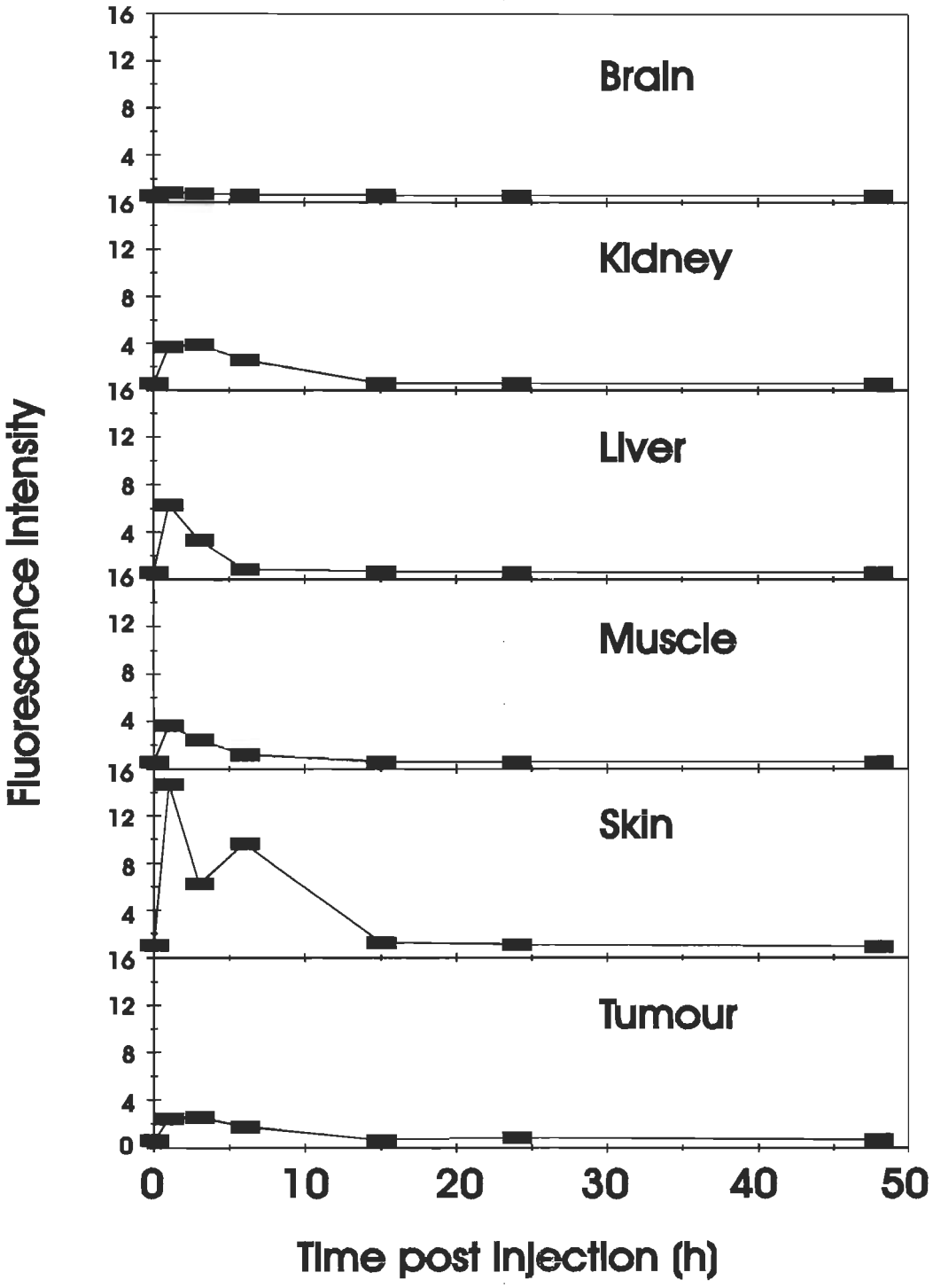

Figure 4.29. *Ex vivo* pharmacokinetics of PEA (dose = 10 mg kg^{-1}) in SKH-HR1 mice bearing Lewis lung carcinoma. Curves are expressed as fluorescence intensity relative to a standard solution of uroporphyrin. The maximum error on any individual datum point is 15%.

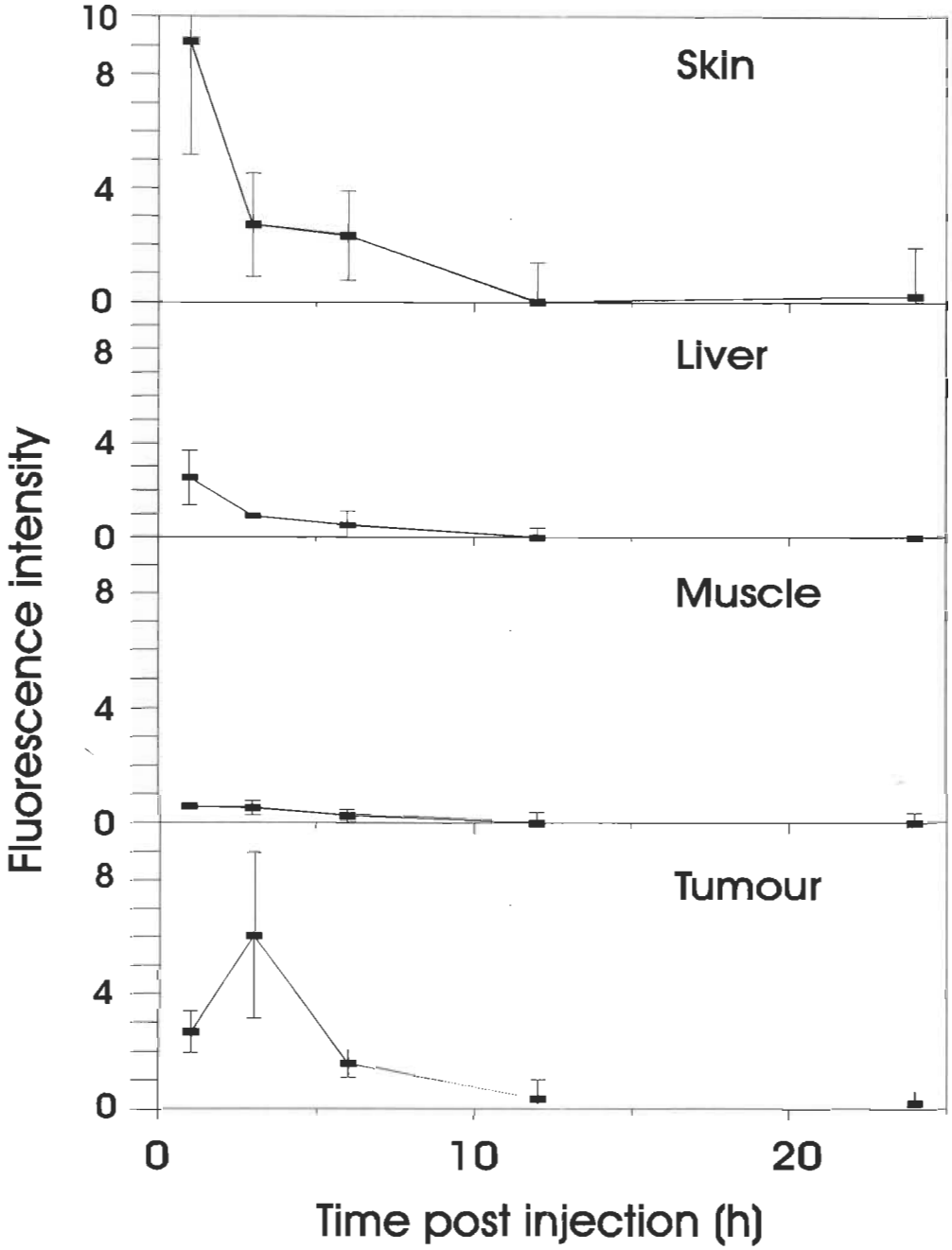

Figure 4.30. *Ex vivo* pharmacokinetics of PEA (dose = 10 mg kg^{-1}) in Balb c mice bearing a lung adenocarcinoma. Curves are expressed as fluorescence intensity relative to a standard solution of uroporphyrin. Error is given for each datum point in the figure.

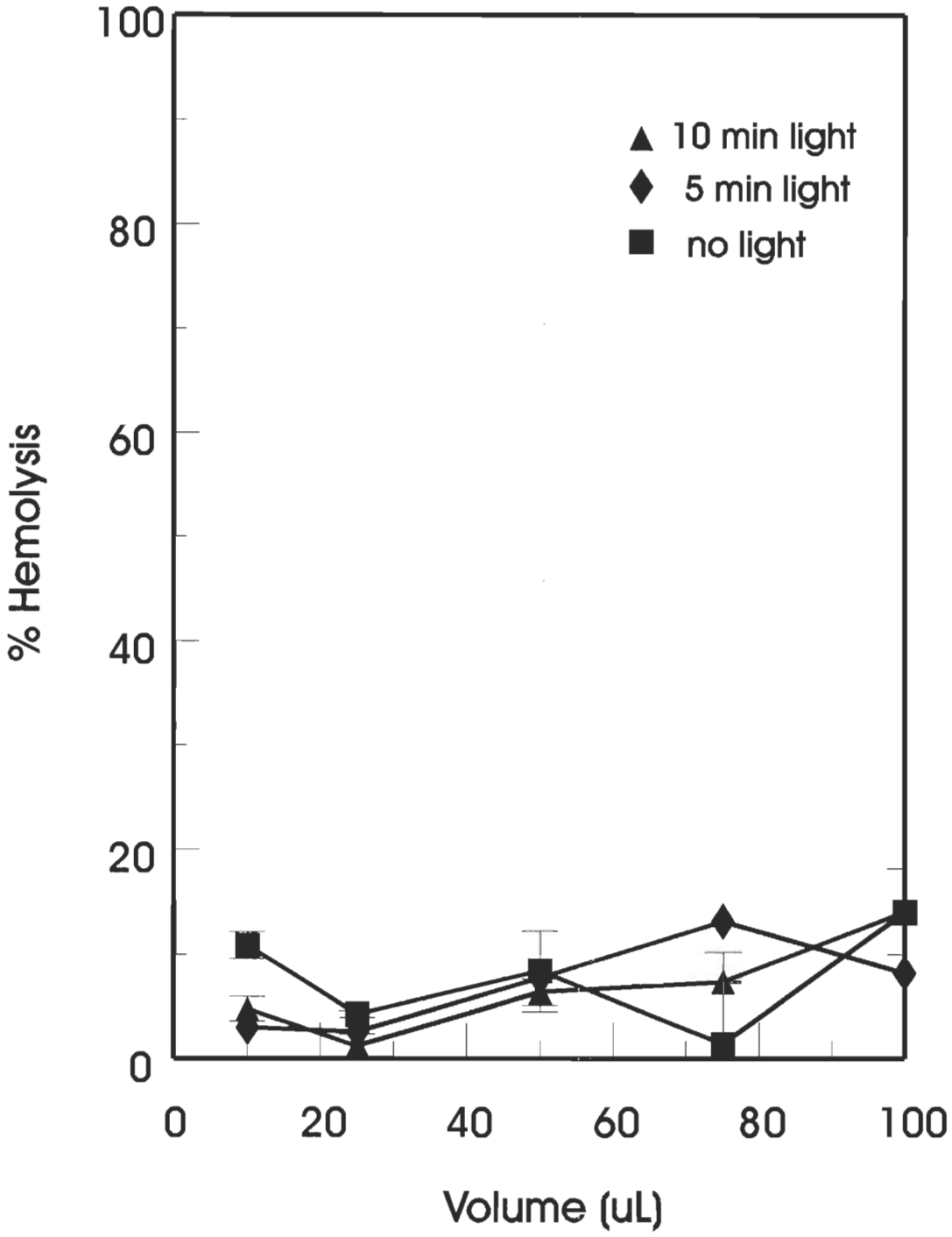

Figure 4.31. Percent photohemolysis of red blood cells measured at the solvent volumes used for testing the potential photosensitizers. Relative hemoglobin concentrations were measured by absorption at 414 nm.

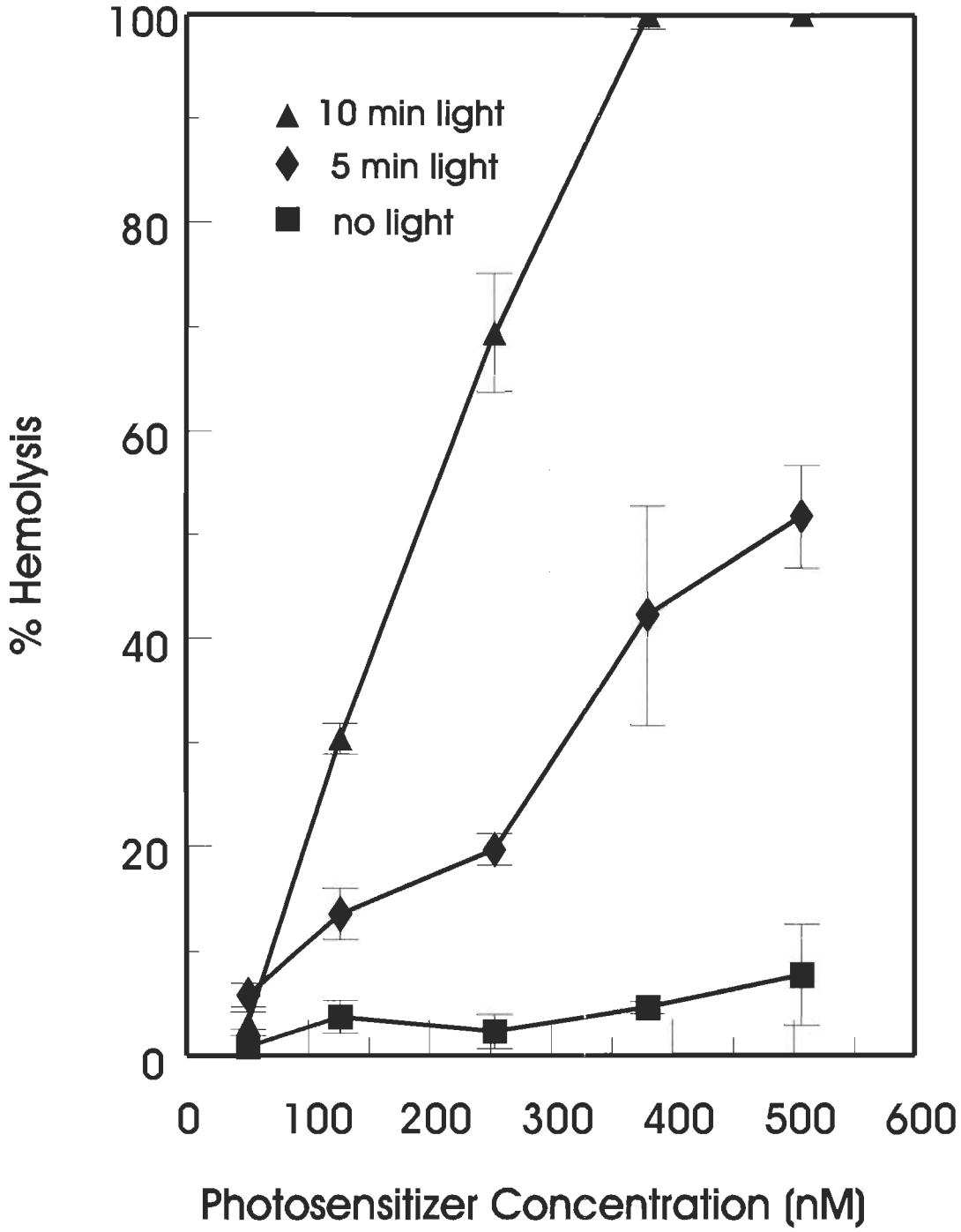

Figure 4.32. Percent photohemolysis measured for HPIX treated red blood cells with varying drug concentrations and light doses. Relative hemoglobin concentrations were measured by absorption at 414 nm.

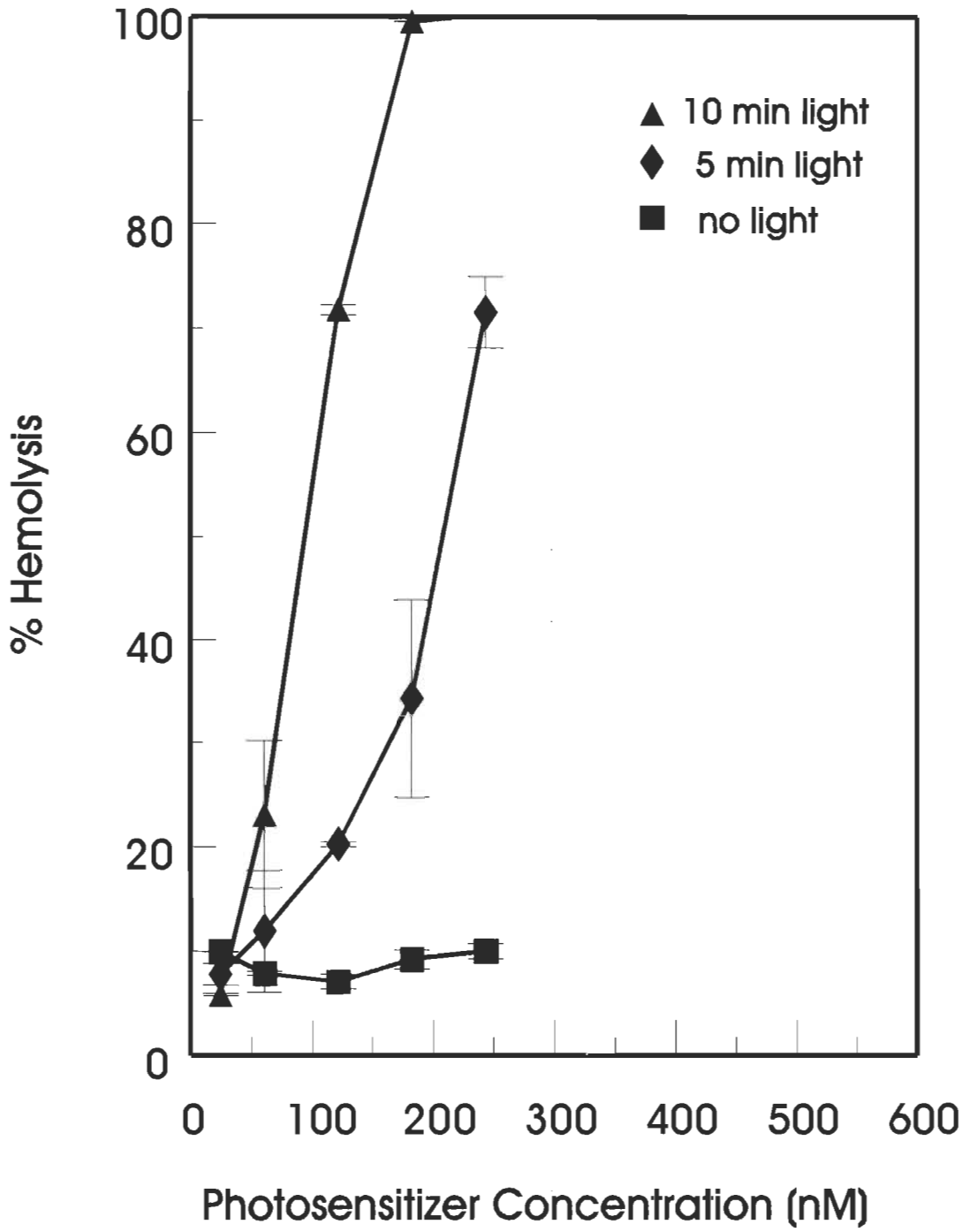

Figure 4.33. Percent photohemolysis measured for HPPEEA treated red blood cells with varying drug concentrations and light doses. Relative hemoglobin concentrations were measured by absorption at 414 nm.

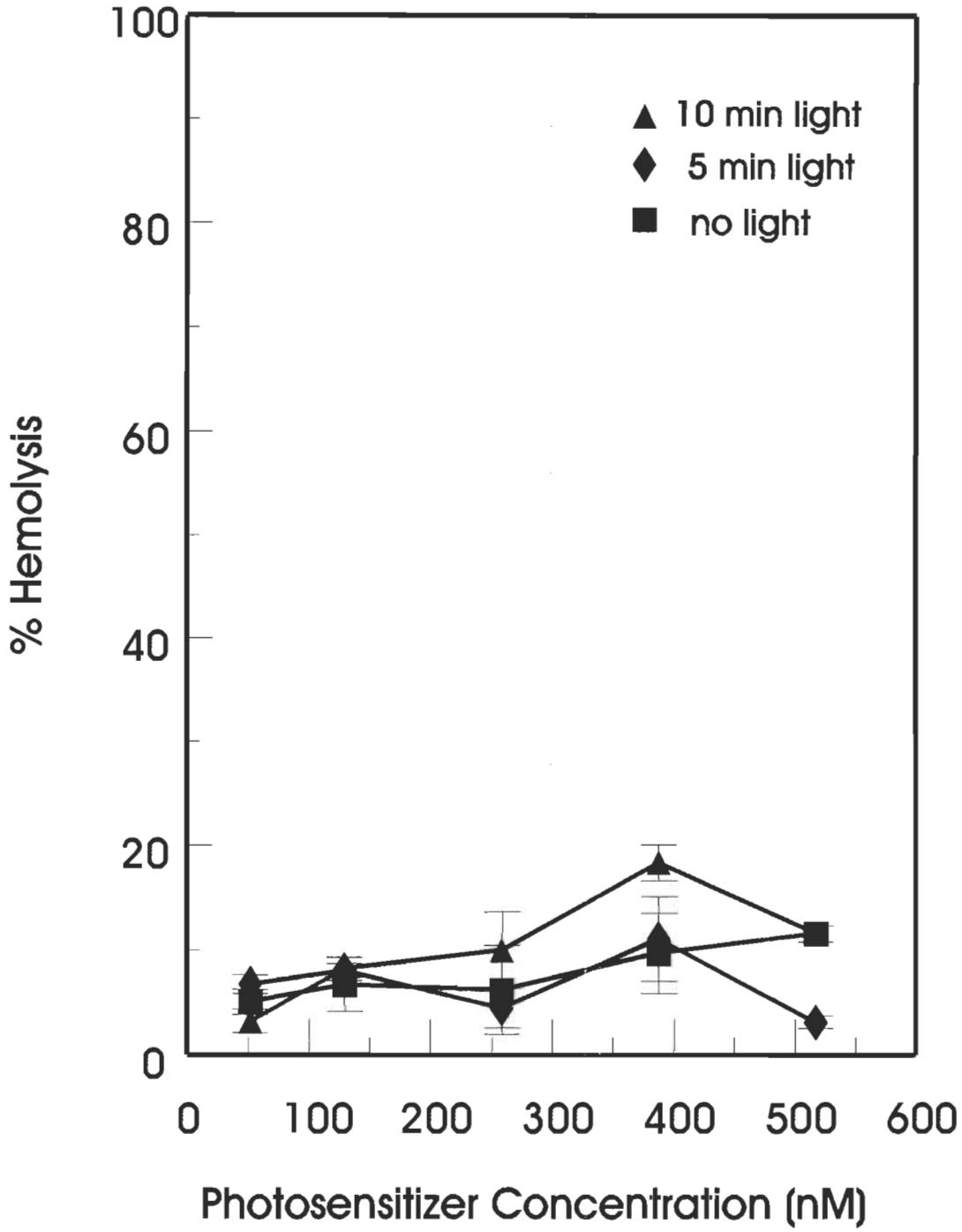

Figure 4.34. Percent photohemolysis measured for methyl pheophorbide *a* treated red blood cells with varying drug concentrations and light doses. Relative hemoglobin concentrations were measured by absorption at 414 nm.

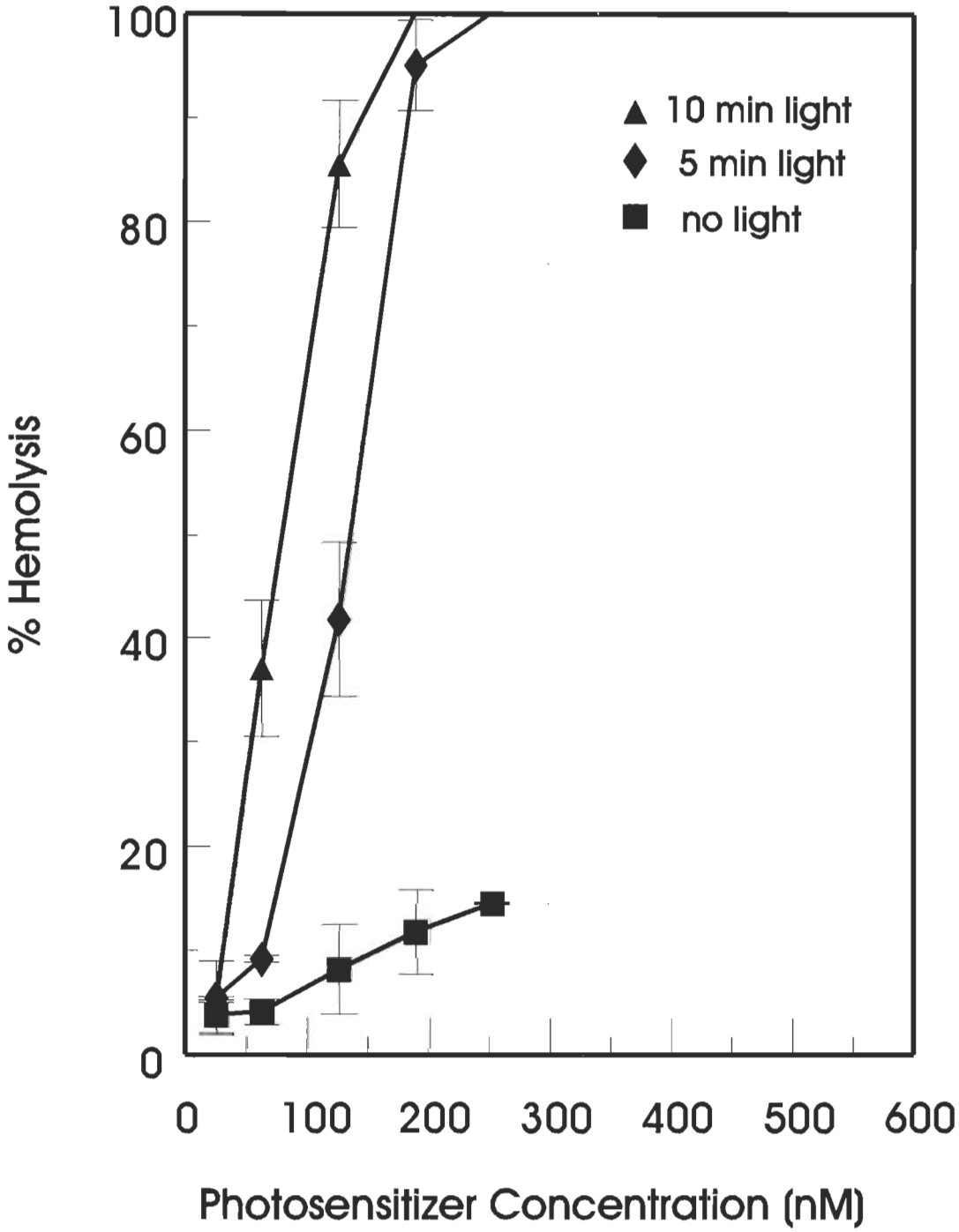

Figure 4.35. Percent photohemolysis measured for PEA treated red blood cells with varying drug concentrations and light doses. Relative hemoglobin concentrations were measured by absorption at 414 nm.

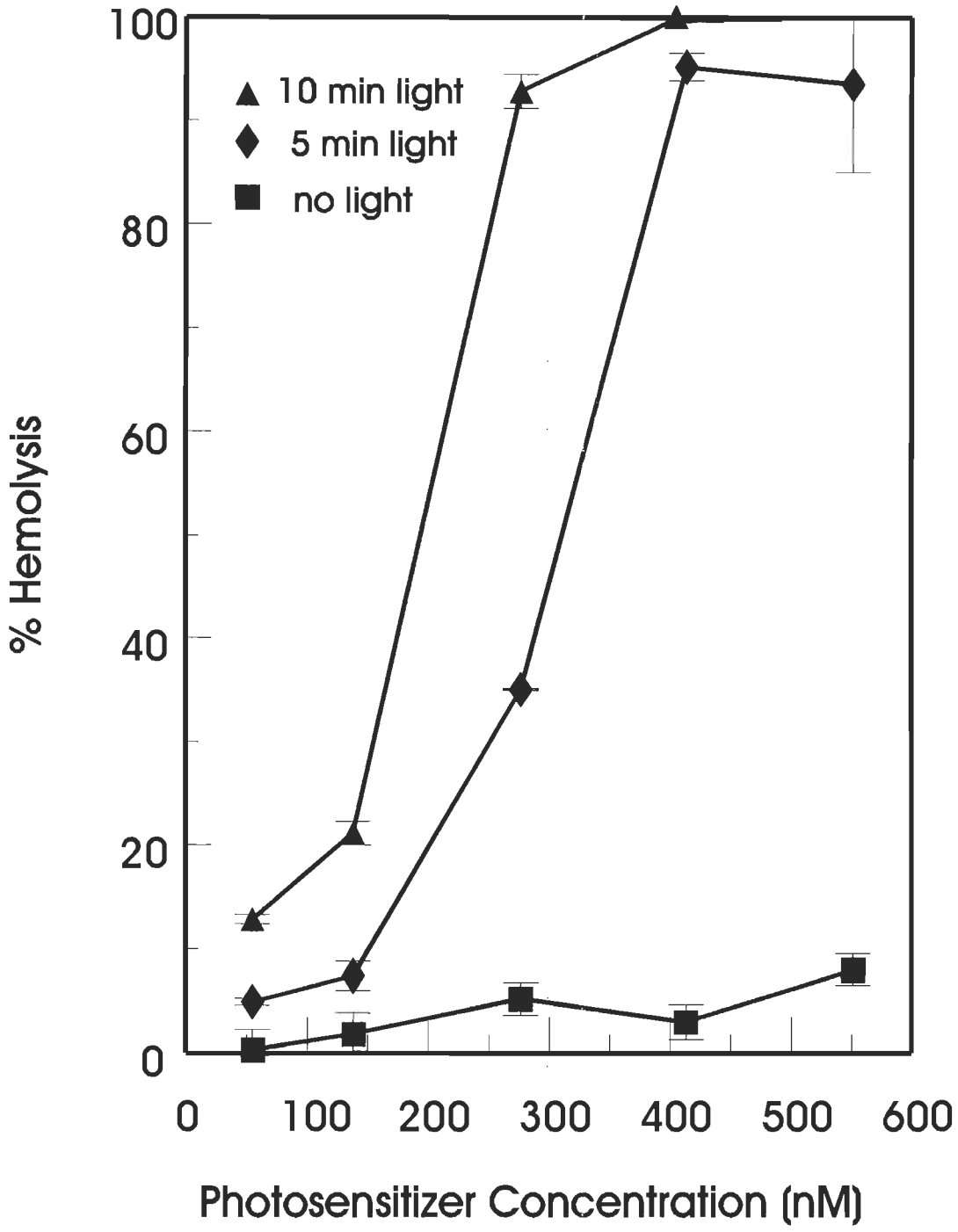

Figure 4.36. Percent photohemolysis measured for polyhematoporphyrin treated red blood cells with varying drug concentrations and light doses. Relative hemoglobin concentrations were measured by absorption at 414 nm.

HPIX produced 100% hemolysis at a concentration of about 375 nM with a 10 min light exposure (Fig. 4.32).

HPPEEA produced 100% photohemolysis at a concentration of 125 nM and a 10 min light exposure, indicated 3 times higher photohemolytic activity then HPIX (Fig. 4.33).

Methyl pheophorbide *a* had very little photohemolytic activity (Fig. 4.34). At the highest mPheo concentrations tested (520 nM), only 18% photohemolysis was observed. This value is almost at background level.

At about 190 nM, and a 10 min light exposure, PEA caused 100% hemolysis (Fig. 4.35). The concentration of PEA to produce 100% hemolysis with 5 min of light was only slightly higher. PEA showed high photohemolytic activity.

Polyhematoporphyrin at a concentration of about 420 nM (concentration of pHP is reported as HPIX equivalents (Delettre *et al.*, 1991)) was required to produce 100% hemolysis with a 10 min light exposure (Fig. 4.36). Polyhematoporphyrin showed lower photohemolytic activity than either of the ethanolamide derivatives.

Table 4.8 is a summary of the photohemolysis data. For this comparison, the drug concentration required to produce 50% hemolysis is tabulated. PEA exhibited the highest photohemolytic activity, followed by HPPEEA, HPIX, pHP, and lastly mPheo. While PEA showed slightly higher activity in the 5 min light exposure both ethanolamides have about twice the photohemolytic activity of pHP and higher activity than their parent compounds.

Table 4.8. Summary of photohemolysis results: concentration of photosensitizer required for 50% hemolysis.

Photosensitizer	10 min light conc in nM	5 min light conc in nM	Figures
PEA	80	140	4.35
HPPEEA	90	210	4.33
HPIX	170	460	4.32
pHP [a]	190	300	4.36
mPheo[b]	> 525	>525	4.34

(a) pHP concentration is reported in HPIX equivalents. The molecular weight of HPIX was used to calculate the Molar equivalents of HPIX using the mass weight of pHP (Delettre *et al.*, 1991).

(b) Only a small amount of photohemolysis is observed.

Chapter 5 Discussion

5.1 Objectives for the ethanolamide drugs

For the ethanolamides studied in this project to be useful as dual action anti-cancer drugs the proposed requirements were: possible synthesis of gram size quantities, high absorption in the far red, high neoplastic tissue selectivity, high photosensitization activity, and high chemotherapeutic activity. Large quantities are required for the various biological tests used to assess these new drugs. The far red absorption requirement stems from the higher light transmittance of far red light through tissues, such that more photons are available for absorption by the drug at deeper tissue location. High selectivity for neoplastic tissue is required in order to restrict the PDT response to only cancerous tissues. High photosensitization efficiency is required so that a significant response can occur with a minimum amount of light and drug. Chemotherapeutic activity is required if such molecules are to be representative of a new class of dual action anti-cancer drugs. The newly synthesized drug PEA will be discussed in the following sections based on its success at meeting the requirements outlined above. Also, PEA will be compared to HPPEEA for several of the tests as the latter is also a potential member of this new class of drugs (Girard, 1992).

5.2 Synthesis and purity of PEA

There were five concerns in the synthesis of PEA: i) producing sufficient quantities of the final product for biological testing; ii) testing the purity of the final product; iii) maintaining the far red absorption as provided by the chlorin ring; iv) identification of the number of ethanolamide moieties present and; v) the identification of the location on the molecule where the ethanolamide groups(s) attach. The first concern is answered by the product yield. The second concern can be answered by HPLC analysis. The third concern can be answered by an examination of the molecule's electronic absorption spectrum; the absorption spectrum of PEA would be significantly

different from mPheo, its parent compound, if the chlorin ring had been changed and the conjugated ring structure disturbed (Spikes, 1990). The fourth and fifth concerns can be answered by examination of the IR and NMR spectra of PEA. The discussion of the results in light of these concerns are covered in the following sections.

5.2.1 Quantity of PEA synthesized

The synthesis of PEA had to provide sufficient product (typically gram size quantities) for biological evaluation. The obtention of sufficient product was a noted difficulty with the preliminary chemotherapeutic evaluation of HPPEEA (Girard, 1992). Thus it was a goal of this synthesis to produce gram quantities of product. A single batch process of Chl *a* produced typically 0.75 g of mPheo. For 1 g of PEA about 2 g of mPheo was required, thus three batch processes of Chl *a* provided sufficient mPheo to synthesize 1 g of PEA. The procedure involved about 1 week of laboratory time. Recently, since pheophorbide *a* has become commercially available in larger quantities at competitive prices (Porphyrin Products, Logan, Utah, USA), the procedure to obtain PEA may be shortened in future preparations.

5.2.2 Purity of PEA

It is desirable for a new synthetic product to be a pure compound; the complex mixture Photofrin II® is a clear example (Bonnett and Berenbaum, 1989) of the difficulties in evaluating biological response from a mixture. Bonnett and Berenbaum suggest that many of the conflicting results in Photofrin II® studies are due to its complex nature. PEA was found to contain about 5% impurities (Fig. 4.3) which makes it comparable to porphyrin products commercially available.

5.2.3 Far red absorbance of PEA

The absorption spectra of mPheo and PEA (Fig. 4.4 and 4.5) are quite similar.

This indicates that the porphin ring of the PEA was not affected during the synthesis procedure. The first Q band of PEA has a high molar extinction coefficient of 2.64 x 10^4 M^{-1} cm^{-1} which is comparable to the value of 2.80 x 10^4 M^{-1} cm^{-1} for mPheo. These values are typical of chlorins (Spikes, 1990). The far red absorption of the chlorins as well as the higher far red light transmittance of tissues provides a better opportunity for photosensitization in deeper tissues (van Lier, 1988, Spikes, 1990). However, as suggested by Dougherty and Potter (1990), if the absorption is very high then optical screening can become a problem, such as observed in the phthalocyanines (Henderson, 1989). The chlorin type photosensitizers provide an intermediate position (Fig. 2.2), having higher absorption, further in the red then porphyrins (Spikes, 1990), but not to the extent of the phthalocyanines. Thus PEA should have a suitable absorption wavelength and efficiency for PDT without a screening effect.

5.2.4 Number of ethanolamide groups present

The number of ethanolamide moieties present on PEA could potentially affect its chemotherapeutic activity. PEA has one ethanolamide present, as indicated by the amide peak in the proton NMR spectrum for PEA (6.8 ppm) (Fig. 4.10). In comparison, the porphyrin ethanolamide HPPEEA contains two ethanolamides groups and has an amide peak at 6.7 ppm in the proton NMR spectrum (Girard, 1992).

5.2.5 Location of the ethanolamide group

The position of the ethanolamide(s) on the molecule can affect the biological activity of PEA. The position of polar groups on a molecule can effect the amphiphilic character of that molecules and its tissue localization (Moan *et al.*, 1987; Moan and Berg, 1992). For example in the sulfonated phthalocyanines (van Lier and Spikes, 1989), when the polar sulfonated groups are adjacent (on one side of a molecule) the molecule has amphiphilic character and higher tumour tissue selectivity, whereas if the sulfonates are opposite the molecule has poor tissue selectivity. The ethanolamide, also polar, could

have a similar affect. It is preferable to have all the polar groups located at one end of the porphin molecule to increase its amphiphilicity. This is the case for PEA, where the ethanolamide is located at position 6, and the two methyl esters are on the side chains at positions 7 and γ (Figs. 4.1 and 4.12). In Fig. 4.12 the proposed molecular shape of PEA illustrates how the methyl esters and the ethanolamide moieties are clustered together at one end.

5.3 Biological evaluation of the ethanolamides

The biological evaluation of the ethanolamides was divided into four sections: i) acute toxicity; ii) chemotherapeutic activity; iii) tissue selectivity and pharmacokinetics; and iv) photosensitization activity.

5.3.1 Acute toxicity of the ethanolamides

Table 5.1 is a summary of some PDT and chemotherapeutic drug LD_{50} toxicity values obtained in this study (section 4.6.1) compared with LD_{50} values reported in the literature for other selected potential and actual anti-tumour drugs.

Table 5.1. LD_{50} toxicity values for ethanolamide derivatives in comparison to selected chemotherapeutic agents and potential PDT photosensitizers.

Compound	Drug type	LD_{50} (mg kg^{-1})	Conditions	Reference
Chlorin e_6	PDT	189	mice	Kostenich *et al.*, 1994
Chlorin e_6	PDT	113	rats	Kostenich *et al.*, 1994
AlSPc	PDT	>100	IV in rats	Tralau *et al.*, 1990
HpD	PDT	275	IP in mice	Tralau *et al.*, 1990
PII	PDT	130	IP in mice	Tralau *et al.*, 1990
pHP	PDT	~150	IP in mice	this work (4.6.1)
HPPEEA	Both	unknown[b]	IP in mice	this work (4.6.1)
PEA	Both	unknown[c]	IP in mice	this work (4.6.1)
Mechlorethamine[a]	Chemo	1.1	IV in rats	Windholz *et al.*, 1983
Adriamycin	Chemo	21.1	IV in mice	Windholz *et al.*, 1983

(a) A commonly used chemotherapeutic nitrogen mustard drug (treatment dose = 0.4 mg kg^{-1} in humans (Calabresi and Chabner, 1990)). (b) >700 as a total of 7 daily injections of 100 mg kg^{-1}. (c) >500 as a total of 3 daily injections of 166 mg kg^{-1}.

The determination of the acute toxicity limit of any new drug is required before it can be administered to a patient, since it indicates the treatment dose upper limit. The therapeutic index provides an estimate of the toxic risk involved in a drug treatment (Gilman *et al.*, 1990). The therapeutic index is calculated by dividing the LD_{50} concentration of a drug by the treatment dose (Gilman *et al.*, 1990). For example the nitrogen mustard mechlorethamine has a poor therapeutic index of 2.75 (treatment dose = 0.4 mg kg^{-1} (Calabresi and Chabner, 1990) and LD_{50} = 1.1 mg kg^{-1}), which indicates

that the toxicity risk is quite high. The typical therapeutic index for PII would be greater than 13 since the treatment doses are typically less than 10 mg kg^{-1} (Marcus, 1992). One of the reasons PDT is viewed favourably as a form of chemotherapy is because the therapeutic index is higher than other chemotherapeutic treatments. The ethanolamides have very low toxicity (Table 5.1), which suggests an even higher therapeutic index than other PDT drugs. Specific values of LD_{50} are not reported for the ethanolamides since no treated animals died. The therapeutic index can only be estimated as greater than 70 for HPPEEA and greater than 50 for PEA based on the highest dose tested.

It should be cautioned that the estimated LD_{50} values expressed for the ethanolamides may be higher than reality, since the drugs were administered over several days. Also, the clearance time of these drugs, as indicated from the pharmacokinetics, is about 24 h. At this time it is not known what the actual tissue concentrations of the drugs were after the several daily drug injections.

It is not clear why the ethanolamides have such low toxicity. It can only be suggested that they may be in a non-toxic, perhaps bound, form in the tissues. Whatever the non-toxic conditions are, they must change in neoplastic cells, since the neoplastic cell cytotoxicity study did indicate that the ethanolamides were chemotherapeutically active in the absence of light.

5.3.2 Chemotherapeutic activity

The chemotherapeutic activity of the ethanolamides was tested after the acute toxicity of the drugs had been determined. The first chemotherapy test was the cytotoxicity of the ethanolamides toward human neoplastic cell lines. A nitrogen mustard would have been an ideal positive control for these experiments, but due to their short lifetime *in vivo* (Calabresi and Chabner, 1990), the nitrogen mustards were not a suitable positive control. The positive control selected was adriamycin because it also is very reactive and does not have the short lifetime of nitrogen mustards. Polyhematoporphyrin was used as a negative control, since it has not been reported to have any chemotherapeutic activity. Further, pHP is a well documented PDT agent (Vernon *et al.*,

1995). The drug concentration required for chemotherapeutic activity must be much lower than that which causes acute toxicity or the therapeutic index would be too low for practical use (Tibbetts *et al.*, 1977). For example, the average adriamycin concentration causing 50% cytotoxicity in the MTT assay was 4.06 μM. That concentration can be expressed as 2.2 mg L^{-1} (MW of adriamycin is 543.54) which can be compared to about 2.2 mg kg^{-1} and the LD_{50} *in vivo* in mice is 21.1 mg kg^{-1} thus the therapeutic index is equal to about 10. As expected, neither pHP nor both of the parent compounds of the ethanolamides, HPIX and mPheo, demonstrated any significant cytotoxicity. The ethanolamides were expected to have chemotherapeutic activity, but lower than nitrogen mustards, based on the background discussion in section 1.5.2. It was also predicted that a di-ethanolamide such as the porphyrin HPPEEA would have a higher chemotherapeutic activity than a mono-ethanolamide such as PEA, based on the reactivities observed for mono and di-functional nitrogen mustards (Calabresi and Chabner, 1990). This prediction was apparent from the MTT assay results (Figs. 4.18, 4.19, and Table 4.7) where HPPEEA had about twofold higher activity than PEA. The doubling of the activity for the di-ethanolamide thus lends support to the hypothesis that ethanolamide derivatives of both porphyrins and chlorins can act as chemotherapeutic agents with a mechanism of action possibly similar to that of the nitrogen mustards. Thus the MTT assay suggests that the ethanolamides exhibit chemotherapeutic activity at a concentration lower than that which causes acute toxicity *in vivo*. Also, as predicted the di-ethanolamide (HPPEEA) exhibited higher cytotoxic activity than the mono-ethanolamide (PEA), but the ethanolamides were not as cytotoxic as adriamycin.

The MTT cytotoxicity indicated that the ethanolamides were chemotherapeutically active *in vitro*; however animal testing was required to evaluate their tissue activity. The animals tumour model used was the $B6D2F_1$ mice bearing Lewis lung carcinoma. These animals had been used in other chemotherapeutic studies, however with different tumour lines (Tibbetts *et al.*, 1977). The dose selected for treatment was 10 mg kg^{-1}, (a typical PDT dose) since the ethanolamides were expected to be used in combined treatment therapy. It is noteworthy however, that since HPPEEA and PEA have low toxicity, higher

doses could have been used for chemotherapy. The observed increase in time to death (TD) in the treated animals is a typical positive result for chemotherapy studies in animals models. The animal survival is often increased but rarely is the cancer stopped (Tibbetts *et al.*, 1977). The primary tumour did not stop growing in this study. It is possible that the lack of tumour regression was due to the poor tumour selectivity of the ethanolamides for that tumour, as was indicated by the pharmacokinetics. It would have also been informative if a typical chemotherapeutic drug, such as adriamycin, had been tested in this animal model to permit comparison between the different agents. However, animals studies are frequently difficult with chemotherapeutic drugs since the therapeutic index of these drugs is very low (Tibbetts *et al.*, 1977). The effect of the ethanolamides on a primary tumour could be further studied with an animal-tumour model which exhibits tumour localization of the ethanolamides, such as the Balb c mice with the lung adenocarcinoma studied here.

The observation of a lack of secondary tumours in the ethanolamide-treated animals for this first chemotherapy test is worthy of further discussion. It has been observed upon dissection, that many animals carrying Lewis lung carcinoma have secondary tumours that develop within 5 to 8 days from the day when the primary tumour was implanted. Previous to this ethanolamide treatment study, no animals had survived for such an extended time periods. Perhaps, although the ethanolamide did not localize in the tumour tissue, the drug was able by some unknown mechanism to prevent any secondary tumours from forming in other anatomical locations. This finding suggests that metastasis had stopped.

To test the hypothesis that the ethanolamides were preventing metastasis, the chemotherapeutic activity was assessed with a metastatic leukemic cancer that does not form a distinct solid tumour. The leukemia P388 is a very aggressive cancer. It requires only a 10 cell inoculum to be established and causes death in 8-10 days. Treatment of this cancer with conventional chemotherapeutic drugs does not stopped the cancer, but only increases the TD (Sobrero *et al.*, 1991). Thus, it was not expected that the ethanolamides would stop or kill this leukemia, but that the survival time or TD would increase. The little if any increase in TD observed in both tests (Fig. 4.21 and 4.22) on

P388 suggests that, at least under these study conditions, the ethanolamides have weak chemotherapeutic activity, insufficient to slow an aggressive cancer such as the P388, even at the higher dose of 100 mg kg^{-1}. This was expected since the ethanolamides were not expected to have as high a chemotherapeutic activity as, for example, a nitrogen mustard.

A significant observation in the P388 tests was the increased lag in initial weight gain (Fig. 4.23). Such a lag phase could possibly indicate that the cancer was responding to the treatment, but that after several days the cancer had adapted to overcome the drug, or the body had adapted to more effectively eliminate it. Adaptation of carcinoma cell lines is not uncommon and has been reported for other chemotherapeutic agents such as adriamycin (Ozol and Goldstein, 1994).

The animal chemotherapeutic studies, as well as the MTT assay, indicate that the ethanolamides have less chemotherapeutic activity than conventional chemotherapy drugs. Response of the primary tumour could not be demonstrated during this study, but it is suspected that the poor tumour localization of the ethanolamides may be a limiting factor towards the attainment of such activity. The prevention of secondary tumours may indicate an affect by the ethanolamides on metastasis. However, it was not possible to clearly demonstrate an affect on metastasitic cancer with the study of the leukemia P388. Thus the results obtained in these chemotherapeutic studies suggest that the ethanolamides may be useful as a chemotherapeutic agent, but not necessarily as a principal treatment. It should be noted that chemotherapeutic results from animal models are difficult to apply to human studies (Tibbetts *et al.*, 1977). Further, the ethanolamides may work quite well as a dual action drug, where the chemotherapeutic action is required to destroy only residue neoplastic tissue and not the bulk of the tumour. The potential use of the ethanolamides toward the complete destruction of deep seated tumours, such as nodular basal cell carcinoma, is promising since tumour recurrence is a major problem of such tumours.

5.3.3 Pharmacokinetics of the ethanolamides

The tissue distribution and clearance of a drug can be evaluated by that drug's pharmacokinetics. The most common method of estimating a drug's pharmacokinetics is with animal-tumour models but the extrapolation from such models is often difficult (Tibbett *et al.*, 1977). However, animal models are still the easiest subjects to study and are the best approximations available. Thus, the pharmacokinetics results reported here are based on mouse-tumour models which were the best available.

In vivo studies are somewhat limited in usefulness for localization studies unless there is a significant accumulation in a tissue. The *ex vivo* investigations permitted the tissue selectivity of the ethanolamides to be evaluated. However this procedure requires the use of many animals and is rather time consuming. It was thus necessary to investigate both *in vivo* and *ex vivo* procedures in order to obtain a more complete picture of the pharmacokinetics behaviour of the ethanolamides.

The serum is generally the main carrier of PDT drug to and from tissues if the drug is administered IV or IP. The drug is often carried bound by a protein fraction in the serum (Rosenberger, 1993). The drug selectivity toward different tissues is often affected by the blood fraction to which the drug is bound (Jori, 1992; Hamblin and Newman, 1994). For this reason the solvent formula selected for the ethanolamides was a serum based formulation which would contain blood proteins.

The results of the serum pharmacokinetics for HPPEEA, were typical of other PDT drugs as given by Biolo *et al.* (1990) with a similar clearance curve (Fig. 4.24). The results observed for PEA serum pharmacokinetics are not as clearly understood. The serum clearance curve profile was typical (Fig. 4.24), but the total concentration of PEA was about a factor of almost 40 times lower than that of HPPEEA. Even with the low serum levels of PEA, the tissues that were measured had typical drug concentrations as seen in the *ex vivo* study (Fig. 4.29). There are no indications in the literature of a similar observed low serum concentration of a PDT drug and typical tissues levels. The concentrations of PEA in the serum were derived from fluorescence intensity

measurements and it was originally thought that the fluorescence of PEA may have been quenched in some manner by the serum. However, the fluorescence was unaffected at several PEA concentrations which were measured with and without serum, indicating that the serum was not affecting the fluorescence signal. There are at least two other possible explanation for the low serum levels of PEA: i) PEA may have localized into body tissues such as the liver before the first time point measured at 1 h so that the serum levels were already decreasing; or ii) PEA may be transported in the circulatory system by some means other than the serum.

The *in vivo* pharmacokinetics provide a rapid qualitative method to follow the drug clearance and determine total clearance times by monitoring the drug fluorescence. However, it is difficult to assess individual tissue selectivity from the *in vivo* pharmacokinetics results due to the composite fluorescence signal source (Biolo *et al.*, 1990). The composite fluorescence signal measured from any given site can originate from several tissues. Attempts to account for the *in vivo* fluorescence by a summation of the different possible sources has to date not been very successful (Biolo et al, 1990). The *in vivo* pharmacokinetics can provide information on localization within a tissue (if the selectivity is high) as well as the overall drug clearance. Thus the principal information that may be obtained from the *in vivo* pharmacokinetics is related to the overall drug clearance pattern. The 24 h total clearance time from skin indicated by the *in vivo* results for both of the ethanolamides HPPEEA (Fig. 4.25) and PEA (Fig. 4.27) is much faster than for compounds such as PII (about 2 months) (Henderson and Dougherty, 1992). It would have been informative if the *in vivo* pharmacokinetics of PII could have been studied by fluorescence in a manner similar to that described here in order to permit a more direct comparison, but such a study was unfortunately not possible due to limited availability of PII. A compound very similar to the ethanolamides, namely chlorin e_6 ethylenediamide (EDA), has been reported in which a similar fast clearance from Af mice was observed (46 h) (Gurinovich *et al.*, 1992).

Thus the *in vivo* pharmacokinetics results show that the ethanolamides exhibited a fast clearance from all tissues. This is a requirement for a good PDT agent.

Neither ethanolamide exhibited any tumour tissue selectivity in Lewis lung carcinoma, as observed by both the *in vivo* (Fig. 4.25 and 4.27) and *ex vivo* (Fig. 4.28 and 4.29) pharmacokinetics. Poor tumour selectivity by drugs in some animal-tumour models is not unusual (Henderson and Dougherty, 1992). Such negative results are often related to the model used. For example, a selection of metallo-naphthalocyanines have recently been shown to only partially localize in Lewis lung carcinoma (Shopova *et al.*, 1994). Further, it was recently observed that the same mouse breed as that used in this study is a poor model for demonstrating selectivity (Biolo, 1995). A large variation in tumour selectivity by photosensitizer drugs in different animals-tumour models is indicated in Table 1.2. Similarly Kostenich *et al.* (1993,1994) have found that different tumours in the same mouse model gave different results, for example chlorin e_6 gave a T/M ratio of 8.8 in the M1 tumours but the T/M ratio was only 6 in the type 45 tumours. These observations imply that more than one tumour type should be studied when investigating the pharmacokinetics of new drugs. The ethanolamide tumour selectivity was thus tested on another animal-tumour model, namely the Balb c mice with a lung adenocarcinoma.

Tumour selectivity of PEA was exhibited in the *ex vivo* study of Balb c mice carrying the lung adenocarcinoma (Fig. 4.30). The tumour to muscle ratio (T/M) of 6 observed can be considered to be quite acceptable because transplanted tumours in the Balb c mice model often exhibit low selectivity with T/M ratios of about 2 (Henderson and Bellnier, 1989). In other tumour-animal models the selectivity can be higher. For example, EDA which is similar to PEA, has a T/M of 14.4 in Af mice with a sarcoma tumour (Gurinovich *et al.*, 1992). The T/M values in animal models reported in Table 1.2 are generally between 4 and 8, with a few exceptionally high values such as BPD-MA at 19.2 (Richter, 1994).

Skin photoreaction can be a problem during PDT if the drug concentration in the skin is high during phototherapy (Tralau *et al.*, 1989; Roberts *et al.*, 1989; and Henderson *et al.*, 1991). The photosensitization reaction will not be limited to the tumour if the skin, which overlies the tumour contains substantial amounts of the PDT drug. Thus a large tumour to skin (T/S) ratio is required in order to minimize unwanted normal skin

photodamage. Although PEA exhibited high concentrations in the skin at 1 h, by 3 h when the tumour drug concentration peaked, the skin drug concentration had dropped to half that of the tumour, giving a T/S of 2. In Table 1.2 the literature values given for T/S ratios vary from 1 to 6 for different potential PDT agents. Another chlorin derivative, HPPH, has a T/S ratio of 6 (Bellnier, 1994). Therefore the T/S of 2 for PEA is in the typical range of most current PDT agents.

In certain cases, the best treatment time may not be when the drug concentration peaks in the tumour. If the drug concentration in the skin is still high when the peak drug concentration in the tumour occurs, then there is still a risk of a skin photoreaction during treatment. Under such conditions, it may be preferable to photoactivate the tumour at a time when a lower total drug concentration is present in the tumour and skin, but when the T/S ratio is high. The time when the peak drug concentration is observed in the tumour is usually longer than that for the skin, for example 3 h for PEA in the lung adenocarcinoma tumour of Balb c mice and 1 h for the skin. While only a detailed human pharmacokinetic study would definitely decide what the optimal treatment time in human tumours, the animal model used in this study indicates that 3 h post injection would be a good time for PDT treatment when using PEA.

5.3.4 Photosensitization activity of the ethanolamides

Demonstration of photosensitization activity by direct measurement of photophysical parameters, such as Φ_{Δ} has only been performed in *in vitro* systems (McGarvey and Truscott, 1990). For potential PDT photosensitizers a biologically relevant system would be preferred. As discussed in section 2.1.4, photohemolysis can be used to estimate photosensitization activity in biological systems.

The photosensitization activity of the ethanolamides can be estimated by photohemolytic studies. The procedure used is sometimes referred to as delayed photohemolysis since the light induced damage occurs during a dark period after the light exposure (Pooler, 1984; Pooler and Girotti, 1986). The delayed photohemolysis method provides a rapid and simple assay to study the photosensitization ability of drugs towards

cell membranes. In tissues, the damage from photosensitization is often apparent several hours after the light treatment has ended, much the same as in delayed photohemolysis. The drug concentrations used in the photohemolysis study are of a similar order of magnitude to those typically found in tissues after administration of PDT drugs, namely values of $\mu g\ g^{-1}$. Both ethanolamides (HPPEEA and PEA) exhibited high photohemolytic activity as compared to their parent molecules and to pHP (Table 4.8). The photohemolytic activity of the ethanolamide and its parent molecule might be expected to be approximately the same since the porphin ring, which is responsible for the photon capture, is similar in both. A possible explanation for the higher activity of the ethanolamides may be the amphiphilic structure of these molecules (Bonnett and Berenbaum, 1989). Ben-Hur *et al.* (1993b) have shown that amphiphilic phthalocyanines had an order of magnitude higher photohemolytic activity than other phthalocyanines. The ethanolamide moiety provides a polar region on the PEA molecule, which is joined to the apolar porphin ring (see Fig. 4.12). Amphiphilic molecules may better penetrate red blood cell membranes and thus lead to higher cellular concentration due to their similarity to the amphiphilic phospholipids of membranes (Ben-Hur *et al.*, 1993b). More photohemolytic damage would thus occur since the amphiphilic sensitizer would be in proximity to the membranes. It is proposed that the amphiphilic nature of the ethanolamides may account for their higher photohemolytic activity.

In summary, PEA was synthesized in gram size quantities with a purity of 95%. A new class of compounds, the porphin ethanolamides, demonstrate chemotherapeutic activity, but with activity lower than conventional chemotherapeutic agents, as expected. The twofold higher chemotherapeutic activity of HPPEEA compared to PEA supports the hypothesis that the ethanolamides, as do the nitrogen mustards, have a mono- or di-functional reactivity based on the number of ethanolamide moieties present. PEA demonstrated significant localization in the lung adenocarcinoma of Balb c mice, but neither PEA or HPPEEA localizes in Lewis lung carcinoma. It is suggested that Lewis lung carcinoma may be a poor tumour model to study these compounds. PEA and HPPEEA demonstrated higher photohemolytic activity than their respective parent molecules and pHP. The high photohemolytic activity of the ethanolamides may be due to the amphiphilic nature of these compounds.

Chapter 6 Conclusions

A synthetic method was developed that was capable of producing large quantities of an ethanolamide derivative of chlorophyll *a*, pheophorbide *a* ethanolamide. This new compound shows high light absorption in the far red, with a molar extinction coefficient of 2.64×10^4 M^{-1} cm^{-1} at 665 nm. The photosensitization activity of PEA, as determined by photohemolysis, is high. The tumour tissue selectivity is relatively high (T/M = 6.0) in Balb c mice at 3 h with the lung adenocarcinoma; however PEA did not show selectivity toward Lewis lung carcinoma in $B6D2F_1$ or SKH-HR1 mice, indicating that this model is unsuitable for the assessment of this compound.

PEA has low toxicity (>166 mg kg^{-1} daily for 3 days) which suggests a high therapeutic index. It is not known why this ethanolamide has such low toxicity toward normal tissues, but such low toxicity may indicate that PEA is bound in a non-toxic form in normal tissues.

Photohemolytic studies indicate that PEA has higher than expected photosensitization activity. It is suggested that the amphiphilic nature of this new compound may permit it to be more closely associated with cell membranes, resulting in increased membrane damage via photosensitization.

Pharmacokinetic studies in both *in vivo* and *ex vivo* indicated rapid clearance of PEA (approximately 24 h). The amount of PEA in the skin was low (T/S = 2.0) when the peak levels were measured in the tumour of the Balb c mice. The lower skin concentration of PEA would tend to reduce ambient light induced skin photoreactions after PDT treatment, a favourable feature.

For PEA to be a potential PDT agent, it must demonstrate both photosensitization activity and selective tumour localization. Its photosensitization ability, indicated by the photohemolytic activity, and its selective localization in the Balb c adenocarcinoma, support the potential of PEA as a PDT agent. Based on this study using 10 mg kg^{-1} of PEA, the best time for PDT treatment in mice would be at 3 h post injection.

Animal model studies indicate that PEA is able to prevent the formation of secondary tumours in Lewis lung treated animals, indicating that the new drugs can stop metastasis. The MTT cytotoxicity studies indicated that PEA has chemotherapeutic activity, which is lower than the chemotherapeutic agent adriamycin. The animal

chemotherapeutic studies suggest some weak chemotherapeutic activity.

The ethanolamide compounds have a chemotherapeutic activity but at a lower level than the nitrogen mustards. PEA is representative of the ethanolamide derivatives that are a promising new class of dual action PDT agents that demonstrate both chemotherapeutic and photosensitization activity.

Bibliography

Abraham, R.J., & A.E. Rowan Nuclear magnetic resonance spectroscopy of chlorophyll. In H. Scheer (Ed.). Chlorophylls Boca Raton: CRC Press, 1990, pp. 797-834.

Adam, F., B. Röder, H. Stiel & H. Wabnitz Methods of optical spectroscopy - a useful tool for the investigation of the mechanism of photodynamic processes. Teubner Texte zun Physik. 1987, 13, 221-232.

Aveline, B., T. Hasan & R.W. Redman Photophysical and photosensitizing properties of benzoporphyrin derivative monoacid ring a (BPD-MA). Photochemistry and Photobiology. 1994, 59, 328-335.

Beems, E.M., T.M.A.R. Dubbelman, J. Lugtenburg, J.A. Van Best, M.F.M.A. Smeets & J.P.J. Boegheim Photosensitizing properties of bacteriochlorophyllin *a* and bacteriochlorin *a*, two derivatives of bacteriochlorophyll *a*. Photochemistry and Photobiology. 1987, 46, 639-643.

Bjellerup, M. Photohemolysis techniques In R.H. Douglas, J. Moan & F. Dall'Acqua (Eds.), Light in biology and medicine. (Vol. 1), New York: Plenum Press, 1988, pp. 255-259.

Bellamy, L.J. The infrared spectra of complex molecules. (Chapman and Hall, London 1975).

Bellnier, D.A., B.W. Henderson, R.K. Pandey, W.R. Potter & T.J. Dougherty Murine pharmacokinetics and antitumor efficacy of the photodynamic sensitizer 2-(1-hexyloxyethyl)-2-devinyl pyropheophorbide-a. Journal of Photochemistry and Photobiology, B: Biology. 1993, 20, 55-61.

Ben-Hur, E., I. Rosenthal & Y. Granot (Graziani) Inhibition of phthalocyanine-sensitized photohemolysis of human erthrocytes by quercetin. Photochemistry and photobiology. 1993a, 57, 984-988.

Ben-Hur, E., Z. Malik, T.M.A.R. Dubbelman, P. Margaron, H. Ali & J.E. van Lier Phthalocyanine-induced photohemolysis: Structure-activity relationship and the effect of fluoride. Photochemistry and photobiology. 1993b, 58, 351-355.

Biolo, R. University of Padova, Italy. 1995, Personal Communication.

Biolo, R., G. Jori, J.C. Kennedy, P. Nadeau, R. Pottier, E. Reddi & G. Weagle A comparison of fluorescence methods used in the pharmacokinetic studies of Zn(II)phthalocyanine in mice. Photochemistry and Photobiology. 1991, 53, 113-118.

Biolo, R., G. Jori, M. Soncin, R. Pratesi, U. Vanni, B. Rihter, M.E. Kenney & M.A.M. Rodgers Photodynamic therapy of B16 pigmented melanoma with liposome-delivered Si(IV)-naphthalocyanine. Photochemistry and Photobiology. 1994, 59, 362-365.

Bonnett, R., & M. Berenbaum Porphyrins as photosensitizers. In G. Bock & S. Harnett (Eds.), Photosensitizing compounds: their chemistry, biology and clinical use Chichester: John Wiley & Sons, 1989, pp. 40-53.

Bown, S.G., C.J. Tralau, P.D. Coleridge-Smith, D. Akdemir & T.J. Wieman Photodynamic therapy with porphyrin and phthalocyanine photosensitization: Quantitative studies in normal rat liver British Journal of Cancer. 1986, 54, 43-52.

Brown, S.R. Absorption coefficients of chlorophyll derivatives. Journal of Fisheries Research Board of Canada. 1968, 25, 523-540.

Brereton, R.G., A. Rahmani, Y.L. Liang & O.M. Kvalheim Investigation of the allomerization reaction of chlorophyll *a*: use of diode array HPLC, mass spectrometry and chemometric factor analysis for the detection of early products. Photochemistry and Photobiology. 1994, 59, 99-110.

Brockmann H. & N. Risch Preparative chromatography. In H. Scheer (Ed.), Chlorophylls Boca Raton: CRC Press, 1991, pp. 103-114.

Brown, S.R., & T.G. Truscott New light on cancer therapy. Chemistry in Britain. 1993, Nov, 955-958.

Brune, D.C., R.E. Blankenship & G.R. Seely Fluorescence quantum yields and lifetimes for bacteriochlorophyll *c*. Photochemistry and Photobiology. 1988, 47, 759-763.

Calabresi, P., & B.A. Chabner Chemotherapy of neoplastic diseases. In A.G. Gilman, T.W. Rall, A.S. Nies & P. Taylor (Eds.), The pharmacological basis of therapeutics 1990, pp. 1202-1219.

Calsou, P., & B. Salles Role of DNA repair in the mechanisms of cell resistance to alkylating agents and cisplatin. Cancer Chemotherapy Pharmacology. 1993, 32, 85-

89.

Chan, W., J. Marshall, G. Lam & I. Hart Tissue uptake, distribution and potency of the photoactivatable dye chloroaluminum sulfonated phthalocyanine in mice bearing transplantable tumours. Cancer Research. 1988, 48, 3040-3044.

Chapados, C. Aggregation of Chlorophyll *a* species absorbing near 700 nm-1. The infrared carbonyl bands. Photochemistry and Photobiology. 1988, 47, 115-132.

Chen, J-Y., W. Chen & H-X. Cai Studies on pharmacokinetics of sulfonated aluminum phthalocyanine in a transplantable mouse tumour by *in vivo* fluorescence. Journal of Photochemistry and Photobiology B: Biology. 1993, 18, 233-237.

Cole, S.P.C. Rapid chemosensitivity testing of human lung tumor cells using the MTT assay. Cancer Chemotherapy Pharmacology. 1986, 17, 259-263.

Corbett, T.H., B.J. Roberts, W.R. Leopold, J.C. Peckham, L.J. Wilkolff, D.P. Griswold, Jr. & F.M. Schabel, Jr. Induction and Chemotherapeutic Response of Two Transplantable Ductal Adenocarcinomas of the Pancreas in C57BL/6 Mice. Cancer Research. 1984, 44, 717-726.

Delettre, E., D. Brault, P. Bruneval, E. Vever-Bizer, M. Dellinger, O. Delgado, J.P. Camilleri, J.C. Gaux & P. Peronneau. *In vitro* uptake of dicarboxylic porphyrins by human atheroma. Kinetic and analytical studies. Photochemistry and Photobiology. 1991, 54, 239-246.

Detty, M.R., & P.B. Merkel Chalcogenapyrylium dyes as potential photochemotherapeutic agents. Solution studies of heavy atom effects on triplet yields, quantum efficiencies of singlet oxygen generation, rates of reaction with singlet oxygen, and emission quantum yields. Journal of the American Chemistry Society. 1990, 112, 3845-3855.

Diamond, I., S.G. Granelli, A.F. McDonagh, S. Nielsen, C.B. Wilson & R. Jaenicke Photodynamic therapy of malignant tumours. The Lancet. 1972, Dec, 1175-1177.

Diwu, Z. & J.W. Lown Photosensitization with anticancer agents 15. Perylenequinonoid pigments as potential photodynamic therapeutic agents: formation of semiquinone radicals and reactive oxygen species on illumination. Journal of Photochemistry and Photobiology, B: Biology. 1993, 18, 131-143.

Dougherty, T.J., & W.R. Potter Of what value is a highly absorbing photosensitizer in

PDT? Journal of Photochemistry and Photobiology, B: Biology. 1990, 8, 223-225.

Dougherty, T.J. Photodynamic therapy. Photochemistry and Photobiology. 1993, 58, 895-900.

Epstein, J.H. Photomedicine. In K.E. Smith (Ed.), The science of photobiology New York: Plenum Press, 1989, pp. 155-192.

Fiedor, L., A.A. Gorman, I. Hamblett, V. Rosenbach-Belkin, Y. Salomon, A. Scherz & I. Tregub A pulsed laser and pulse radiolysis study of amphiphilic chlorophyll derivatives with PDT activity toward malignant melanoma. Photochemistry and Photobiology. 1993, 58, 506-511.

Folch, J., M. Lees & G.H. Sloane Stanley A simple method for the isolation and purification of total lipids from animal tissues. Journal of Biological Chemistry. 1957, 226, 497-509.

Freitas, I. Tumor hypoxia and associated drawbacks to photodynamic therapy. In G. Jori, & C. Perria (Eds.), Photodynamic therapy of tumors and other diseases. Libreria Progetto Editore Padova, 1985, pp. 413-416.

Freitas, I. Overcoming tumor hypoxia. In G. Jori, & C. Perria (Eds.), Photodynamic therapy of tumors and other diseases. Libreria Progetto Editore Padova, 1985, pp. 417-420.

Gèze, M., P. Morlière, J.C. Mazière, K.M. Smith & R. Santus Lysosomes, a key target of hydrophobic photosensitizers proposed for photochemotherapeutic applications. Journal of Photochemistry and Photobiology, B: Biology. 1993, 20, 23-35.

Ghiggino, K.P., L.E. Bennett & R.W. Henderson Photochemical properties of porphyrin c: an agent for use in tumor phototherapy. Photochemistry and Photobiology. 1988, 47, 65-72.

Gilman, A.G., T.W. Rall, A.S. Nies & P. Taylor (Eds.), Goodman and Gilman's The pharmacological basis of therapeutics (8th ed.). New York: Pergamon Press, 1990.

Girard, D. Préparation et étude spectroscopique de porphyrines d'intérêt photothérapeutique. PhD. thèse, l'Université Laval, Québec, 1992.

Gomer, C.J., & A. Ferrario Tissue distribution and photosensitizing properties of mono-L-aspartyl chlorin e6 in a mouse tumor model. Cancer Research. 1990, 50, 3985-

3990.

Gross, E., B. Ehrenberg & F.M. Johnson Singlet oxygen generation by porphyrins and the kinetics of 9,10-dimethylanthracene photosensitization in liposomes. Photochemistry and Photobiology. 1993, 57, 808-813.

Grossweiner, L.I. Interactions of light with biological tissue. In G. Moreno, R.H. Pottier & T.G. Truscott (Eds.), Photosensitisation: molecular, cellular and medical aspects. Berlin: Sringer-Verlag, 1987, pp. 101-123.

Grossweiner, L.I. The science of phototherapy Boca Raton: CRC Press, 1994.

Gurinovich, G.P., T.E. Zorina, S.B. Melnov, N.I. Melnova, I.F. Gurinovich, L.A. Grubina, M.V. Sarzhevskaya & S.N. Cherenkevich Photodynamic activity of chlorin e_6 and chlorin e_6 ethylenediamide *in vitro* and *in vivo*. Journal of Photochemistry and Photobiology, B: Biology. 1992, 13, 51-57.

Hadjur, C., M.J. Richard, M.O. Parat, A. Favier & P. Jardon Photodynamically induced cytotoxicity of hypericin dye on human fibroblast cell line MRC5. Journal of Photochemistry and Photobiology, B: Biology. 1995, 27, 139-146.

Hamblin, M.R. On the mechanism of tumour-localising effect in photodynamic therapy. Journal of Photochemistry and Photobiology, B: Biology. 1994, 23, 3-8.

Hebeda, K.M., J.G. Wolbers, H.J.C.M. Sterenborg, W. Kamphorst, M.J.C. van Gemert & H.A.M. van Alphen Fluorescence localization in tumour and normal brain after intratumoral injection of haematoporphyrin derivative into rat brain tumour. Journal of Photochemistry and Photobiology, B: Biology. 1995, 27, 85-92.

Henderson, B.W., & D.A. Bellnier Tissue localization photosensitizers and the mechanism of photodynamic tissue destruction. In G. Bock & S. Harnett (Eds.), Photosensitizing compounds: their chemistry, biology and clinical use Chichester: John Wiley & Sons, 1989, pp. 112-130.

Henderson, B.W., Discussion. In G. Bock & S. Harnett (Eds.), Photosensitizing compounds: their chemistry, biology and clinical use Chichester: John Wiley & Sons, 1989, p. 27.

Henderson, B.W., A.G. Sumlin, B.L. Owczarczak & T.J. Dougherty Bacteriochlorophyll-*a* as photosensitizer for photodynamic treatment of transplantable murine tumors.

Journal of Photochemistry and Photobiology, B: Biology. 1991, 10, 303-314.

Henderson, B.W., & T.J. Dougherty How does photodynamic therapy work? Photochemistry and Photobiology. 1992, 55, 145-157.

Hoff, A.J., & J. Amesz Visible absorption spectroscopy of chlorophylls. In H. Scheer (Ed.), Chlorophylls. Boca Raton: CRC Press, 1991, pp. 723-738.

Hynninen, P.G., M.R. Wasielewski & J.J. Katz Chlorophylls. VI. epimerization and enolization of chlorophyll *a* and its magnesium-free derivatives. Acta Chemica Scandinavica B. 1979, 33, 637-648.

Jain, R.K. Mass and heat transfer in tumors. In A.S. Mujumdar & R.A. Mashelkar (Eds.), Advances in transport processes (Vol. 3). New York: John Wiley & Sons, 1984, pp. 228-324.

Jori, G., M. Beltramini, E. Reddi, B. Salvato, A. Pagnan, L. Ziron, L. Tomio & T. Tsanov Evidence for a major role of plasma lipoproteins as hematoporphyrin carriers *in vivo*. Cancer Letters. 1984, 24, 291-297.

Jori, G. Far-red-absorbing photosensitizers: their use in the photodynamic therapy of tumours. Journal of Photochemistry and Photobiology, A: Chemistry. 1992, 62, 371-378.

Katz, J.J. Infrared and nuclear magnetic resonance spectroscopy of chlorophyll. In L.P. Vernon & G.R. Seely (Eds.). The Chlorophylls Academic Press, 1966, pp. 185-251.

Katz, J.J., & T.R. Janson Chlorophyll-chlorophyll interactions from ^{1}H and ^{13}C nuclear magnetic resonance spectroscopy. Annals of the New York academy of sciences. 1973, 206, 579-601.

Katz, J.J., L.L. Shipman, T.M. Cotton & T.R. Janson Chlorophyll aggregation: coordination interactions in chlorophyll monomers, dimers, and oligomers. In D. Dolphin (Ed.), The porphyrins (Vol. 5). New York: Academic Press, 1978, pp. 402-458.

Kawabe, H., Y. Tamachi, K. Aizawa, T. Okunaka, T. Ohtani, H. Kato & Y. Hayata Photodynamic effects of quaternary ammonium salt derivatives of protoporphyrin derivatives on normal and tumor-bearing mice. Lasers in the Life Sciences. 1991, 4, 115-123.

Kenndy, J.C., & R.H. Pottier Endogenous protoporphyrin IX, a clinically useful photosensitizer for photodynamic therapy. Journal of Photochemistry and Photobiology, B: Biology. 1992, 14, 275-292.

Kessel, D., & M-L Cheng On the preparation and properties of dihematoporphyrin ether, the tumor-localizing component of HPD. Photochemistry and Photobiology. 1985, 41, 277-282.

Kessel, D., & K. Smith Photosensitization with derivatives of chlorophyll. Photochemistry and Photobiology. 1989, 49, 157-160.

Kessel, D., & A. Morgan Photosensitization with etiobenzochlorins and octaethylbenzochlorins. Photochemistry and Photobiology. 1993a, 58, 521-526.

Kessel, D., K.M. Smith, R.K. Pandey, F.-Y. Shiau & B. Henderson Photosensitization with bacteriochlorins. Photochemistry and Photobiology. 1993b, 58, 200-203.

Kohn, K.W. Molecular mechanisms of cross-linking by alkylating agents and platinum complexes. In A.C. Sartorelli, J.S. Lazo & J.R. Bertino (Eds.), Molecular actions and targets for cancer chemotherapeutic agents. New York: Academic Press, 1981, pp. 3-16.

Korbelik, M., & G. Krosl Cellular levels of photosensitisers in tumours: the role of proximity to the blood supply. British Journal of Cancer. 1994, 70, 604-610.

Kostenich, G.A., I.N. Zhuravkin, A.V. Furmanchuk &, E.A. Zhavrid Sensitivity of different rat tumour strains to photodynamic treatment with chlorin e_6. Journal of Photochemistry and Photobiology, B: Biology. 1993, 17, 187-194.

Kostenich, G.A., I.N. Zhuravkin & E.A. Zhavrid Experimental grounds for using chlorin e_6 in the photodynamic therapy of malignant tumors. Journal of Photochemistry and Photobiology, B: Biology. 1994, 22, 211-217.

Kostron, H., M.R. Swartz, D.A. Bellnier, C-W Lin & R.L. Martuza Co-60 and direct intraneoplastic injection of HPD enhances the effect of phototherapy. In G. Jori, & C. Perria (Eds.), Photodynamic therapy of tumors and other diseases. Libreria Progetto Editore Padova, 1985, pp. 247-250.

Krasnovsky, A.A. Jr., K.V. Neverov, S. & Y.U. Egorov Photophysical studies of pheophorbide *a* and pheophytin *a*. phosphorescence and photosensitized singlet

oxygen luminescence. Journal of Photochemistry and Photobiology, B: Biology. 1990, 5, 245-254.

Krasnovsky, A.A. Jr., P. Cheng, R.E. Blankenship, T.A. Moore & D. Gust The photophysics of monomeric bacteriochlorophylls *c* and *d* and their derivatives: properties of the triplet state and singlet oxygen photogeneration and quenching. Photochemistry and Photobiology. 1993, 57, 324-330.

Lipson, R.L., E.J. Baldes & A.M. Olsen The use of a derivative of hematoporphyrin in tumor detection. Journal of the National Cancer Institute. 1961, 26, 1-11.

Lutz, M., & W. Mäntele Vibrational spectroscopy of chlorophylls In H. Scheer (Ed.). Chlorophylls. Boca Raton: CRC Press, 1991, pp. 855-902.

Mantoura, R.F.C., & C.A. Llewellyn The rapid determination of algal chlorophyll and carotenoid pigments and their breakdown products in natural waters by reverse-phase high-performance liquid chromatography. Analytica Chimica Acta. 1983, 151, 297-314.

Marcus, S.L. Photodynamic therapy of human cancer. Proceedings of the IEEE. 1992, 80, 869-889.

Mayhew, E., L. Vaughan, A. Panus, M. Murray & B.W. Henderson Lipid-associated methylpheophorbide-a (hexyl-ether) as a photodynamic agent in tumor-bearing mice. Photochemistry and Photobiology. 1993, 58, 845-851.

McGarvey, D.J., & T.G. Truscott The triplet stare and singlet oxygen generation. In D. Kessel (Ed.), Photodynamic therapy of neoplastic disease (Vol. 2). Boca Raton: CRC Press, 1990, pp. 179-189.

Moan, J., Q. Peng, J.F. Evensen, K. Gerg, A. Western & C. Rimington Photosensitizing efficiencies, tumor- and cellular uptake of different photosensitizing drugs relevant for photodynamic therapy of cancer. Photochemistry and Photobiology. 1987, 46, 713-721.

Moan, J., & K. Berg Photochemotherapy of cancer: experimental research. Photochemistry and Photobiology. 1992, 55, 931-948.

Montforts, F.P., B. Gerlach & F. Höper Discovery and synthesis of less common natural hydroporphyrins. American Chemical

Moser, J.G., A. Rück, H-J Schwarzmaier & C. Westphal-Frösch Photodynamic cancer therapy: fluorescence localization and light absorption spectra of chlorophyll-derived photosensitizers inside cancer cells. Optical Engineering. 1992, 31, 1441-1446.

Obochi, M.O.K., R.W. Boyle & J.E. van Lier Biological activities of phthalocyanines. XIII. The effects of human serum components on the *in vitro* uptake and photodynamic activity of zinc phthalocyanine. Photochemistry and Photobiology. 1993, 57, 634-640.

Okada, K., K. Uehara & Y. Ozaki Fourier-transform infrared spectroscopic study of the structure of chlorophyll *a* and chlorophyll *b* in highly dilute water-saturated carbon tetrachloride solutions. Photochemistry and Photobiology. 1993, 57, 958-963.

Ozols, R.F., & L.J. Goldstein In Drug resistance. (Vol. 3). Boston: Kluwer Academic, 1994.

Pandey, R.K., D.A. Bellnier, K.M. Smith & T.J. Dougherty Chlorin and porphyrin derivatives as potential photosensitizers in photodynamic therapy. Photochemistry and Photobiology. 1991, 53, 65-72.

Parker, J.G. Optical monitoring of singlet oxygen during photodynamic treatment of tumors. IEEE circuits and devices magazine. 1987, Jan, 10-21.

Patterson M.S., S.J. Madsen & B.C. Wilson Experimental tests of the feasibility of singlet oxygen luminescence monitoring *in vivo* during photodynamic therapy. Journal of Photochemistry and Photobiology, B: Biology. 1990, 5, 69-84.

Patterson, M.S., B.C. Wilson & D.R. Wyman The propagation of optical radiation in tissue. I.: Models of radiation transport and their application. Lasers in Medical Science. 1991a, 6, 156-168.

Patterson, M.S., B.C. Wilson & D.R. Wyman The propagation of optical radiation in tissue. II.: Optical properties of tissues and resulting fluence distributions. Lasers in Medical Science. 1991b, 6, 379-390.

Peng Q., J. Moan, L-S. Cheng, J.M. Nesland & C. Rimington Potential photosensitizer for photochemotherapy of cancer: Uptake and localization of disulfonated aluminum phthalocyanine ($AlPCS_2$) in mice bearing a human malignant tumor. Lasers in the Life Sciences. 1993, 5, 175-184.

Pennington, F.C., H.H. Strain, W.A. Svec & J.J. Katz Preparation and properties of pyrochlorophyll *a*, methyl pyrochlorophyllide *a*, pyropheophytin *a*, and methyl pyropheophorbide *a* derived from chlorophyll by decarbomethoxylation. Journal of the American Chemical Society. 1964, 86, 1418-1426.

Pennington, F.C., S.D. Boyd, H. Horton, S.W. Taylor, D.G. Wulf, J.J. Katz & H.H. Strain Reaction of chlorophylls a and b with amines. Isocyclic ring rupture and formation of substituted chlorin-6-amides. Journal of the American Chemical Society. 1967, 89, 3871-3875.

Persad, S., I.A. Menon & H.F. Haberman Comparison of the effects of UV-visible irradiation of melanins and melanin-hematoporphyrin complexes from human black and red hair. Photochemistry and Photobiology. 1983, 37, 63-68.

Pooler, J.P. The potency of sensitized photohemolysis depends on the composition of the reaction vessel. Photochemistry and Photobiology 1983, 38, 407-409.

Pooler, J.P., & A.W. Girotti Photohemolysis of human erythrocytes labeled in band 3 with eosin-isothiocyanate. Photochemistry and Photobiology 1986, 44, 495-499.

Pottier, R., & T.G. Truscott The photochemistry of haematoporphyrin and related systems. International Journal of Radiation Biology. 1986, 50, 421-452.

Rahmani, A., C.B. Eckardt, R.G. Brereton & J.R. Maxwell The use of liquid chromatography-mass spectrometry to monitor the allomerization reactions of chlorophyll *a* and pheophytin *a*: identification of the allomers of pheophytin *a*. Photochemistry and Photobiology. 1993, 57, 1048-1052.

Rassmussen-Taxdal, D.S., G.E. Ward & F.H.I. Figge Fluorescence of human lymphatic and cancer tissue following high doses of intravenous hematoporphyrin. Cancer. 1955, 8, 78-81.

Reddi, E., G. Lo Castro, R. Biolo & G. Jori Pharmacokinetic studies with zinc(II)-Phthalocyanine in tumour-bearing mice. British Journal of Cancer. 1987, 56, 597-600.

Reddi, E., C. Zhou, R. Biolo, E. Menegaldo & G. Jori Liposome- or LDL-administered Zn (II)-phthalocyanine as a photodynamic agent for tumours. I. Pharmacokinetic properties and phototherapeutic efficiency. British Journal of Cancer. 1990, 61, 407-

411.

Reed, M.W.R., A.P. Mullins, G.L. Anderson, F.N. Miller & F.J. Wieman The effect of photodynamic therapy on tumor oxygenation. Surgery. 1989, 106, 94-99.

Ricchelli, F., S. Gobbo, G. Jori, G. Moreno, F. Vinzens & C. Salet Photosensitization of mitochondria by liposome-bound porphyrins. Photochemistry and Photobiology. 1993, 58, 53-58.

Richter, A.M., E. Waterfield, A.K. Jain, A.J. Canaan, B.A. Allison & J.G. Levy Liposomal delivery of a photosensitizer, benzoporphyrin derivative monoacid ring a (BPD), to tumor tissue in a mouse tumor model. Photochemistry and Photobiology. 1993, 57, 1000-1006.

Roberts, W.G., K.M. Smith, J.L. McCullough & M.W. Berns Skin photosensitivity and photodestruction of several potential photodynamic sensitizers. Photochemistry and Photobiology. 1989, 49, 431-438.

Roeder, B., & H. Wabnitz Time-resolved fluorescence spectroscopy of hematoporphyrin, mesoporphyrin, pheophorbide *a* and chlorin e_6 in ethanol and aqueous solution. Journal of Photochemistry and Photobiology, B: Biology. 1987, 1, 103-113.

Roitman, L., B. Ehrenberg & N. Kobayashi Spectral properties and absolute determination of singlet oxygen production yield by naphthaloporphyrins. Journal of Photochemistry and Photobiology, A: Chemistry. 1994, 77, 23-28.

Rosenberger, V., & R. Margalit Thermodynamics of the binding of hematoporphyrin ester, a hematoporphyrin derivative-like photosensitizer, and its components to human serum albumin, human high-density lipoprotein and human low-density lipoprotein. Photochemistry and Photobiology. 1993, 58, 627-630.

Roy, S. High-performance liquid chromatographic analysis of chloropigments. Journal of Chromatography. 1987, 391, 19-34.

Scheer, H., & J.J. Katz Peripheral metal complexex: chlorophyll "isomers" with magnesium bound to the ring E β-keto ester system. American Chemical Society. 1978, 100, 561-571.

Schiwon, K., H.-D. Brauer, B. Gerlach, C.M. Müller & F.-P. Montforts Potential photosensitizers for photodynamic therapy IV. Photophysical and photochemical

properties of azaporphyrin and azachlorin derivatives. Journal of Photochemistry and Photobiology, B: Biology. 1994, 23, 239-243.

Schuitmaker, J.J., H.L.L.M. Van Leengoed, N. Van Der Veen, T.M.A.R. Dubbelman & W.M. Star Laser-induced *in vivo* fluorescense of bacteriochlorin *a*: preliminary results. Lasers in Medical Science. 1993, 8, 39-42.

Shioi, Y. Analytical chromatography of chlorophylls. In H. Scheer (Ed.), Chlorophylls. Boca Raton: CRC Press, 1991, pp. 59-88.

Shopova, M., D. Wöhrle, N. Stichkova, A.D. Milev, V.N. Mantareva, S. Müller, K. Kassabov & K. Georgiev Hydrophobic Zn(II)-naphthalocyanines as photdynamic therapy agents for lewis lung carcinoma. Journal of Photochemistry and Photobiology, B: Biology. 1994, 23, 35-42.

Slater, T.F., B. Sawyer & U. Sträuli Studies on Succinate-Tetrazolium Reductase Systems III. Points of Coupling of Four Different Tetrazolium Salts. Biochimica et biophysica acta. 1963, 77, 383-393.

Smith, K.M., & J.F. Unsworth The nuclear magnetic resonance spectra of porphyrins-IX. Carbon-13 NMR spectra of some chlorins and other chlorophyll degradation products. Tetrahedron, 1975, 31, 367-375.

Spikes, J.D. New trends in photobiology: chlorins as photosensitizers in biology and medicine. Journal of Photochemistry and Photobiology, B: Biology. 1990, 6, 259-274.

Spikes, J.D., & J.C. Bommer Photosensitizing properties of mono-L-aspartyl chlorin e_6 (NPe6): a candidate sensitizer for the photodynamic therapy of tumors. Journal of Photochemistry and Photobiology, B: Biology. 1993, 17, 135-143.

Sobrero, A., C. Aschele, R. Rosso, A. Nicolin & J.R. Bertino Rapid development of resistance to antifolates *in vitro*: possible clinical implication. Journal of the National Cancer Institute. 1991, 83, 24-28.

Sroka, R., W. Beyer, M. Krug, A. Noack, E. Unsöld & C. Ell Laser light application and light monitoring for photodynamic therapy in hollow organs. Lasers in Medical Science. 1993, 8, 63-68.

Stamp, J.M., & J.L. Williams Photodynamic therapy in the bladder: can the light dose

be easily quantified? Lasers in Medical Science. 1991, 6, 147-154.

Strain, H.H., & W.A. Svec Extraction, separation, estimation, and isolation of the chlorophylls In L.P. Vernon & G.R. Seely (Eds.), The chlorophylls. New York: Academic Press, 1966, pp. 21-53.

Svec, W.A. The isolation, preparation, characterization, and estimation of the chlorophylls and the bacteriochlorophylls. In D. Dolphin (Ed.), The porphyrins (Vol. 5). New York: Academic Press, 1978, pp. 342-399.

Svec, W.A. The distribution and extraction of the chlorophylls. In H. Scheer (Ed.), Chlorophylls. Boca Raton: CRC Press, 1991, pp. 89-102.

Tannock, I.F., & D. Rotin Acid pH in tumors and its potential for therapeutic exploitation. Cancer Research, 1989, 49, 4373-4384.

Tibbetts, L.M., M.Y. Chu, J.C. Hager, D. L. Dexter & P. Calabresi Chemotherapy of cell line derived human colon carcinoma in mice immunosuppressed with antithymocyte serum Cancer. 1977, 40, 2651-2659.

Tralau, C.J., H. Barr, D.R. Sandeman, T. Barton, M.R. Lewin & S.G. Bown Aluminum sulfonated phthalocyanine distribution in rodent tumors of the colon, brain, pancreas. Photochemistry and Photobiology. 1987, 46, 777-781.

Tralau, C.J., A.R. Young, N.P.J. Walker, D.I. Vernon, A.J. MacRobert, S.B. Brown & S.G. Bown Mouse skin photosensitivity with dihaematoporphyrin ether (DHE) and aluminium sulphonated phthalocyanine (AlSPc): a comparative study. Photochemistry and Photobiology. 1989, 49, 305-312.

Tralau, C.J., H. Barr, A.J. MacRobert & S.G. Bown Relative merits of porphyrin and phthalocyanine sensitization for photodynamic therapy. In D. Kessel (Ed.), Photodynamic therapy of neoplastic disease (Vol. 1), Boca Raton: CRC Press, 1990, pp. 263-278.

Van Lier, J.E. New sensitizers for photodynamic therapy of cancer. In R.H. Douglas, J. Moan & F. Dall'Acqua (Eds.), Light in biology and medicine. (Vol. 1), New York: Plenum Press, 1988, pp. 133-142.

Van Lier, J.E., & J.D. Spikes The chemistry, photophysics and photosensitizing properties of phthalocyanines. In G. Bock & S. Harnett (Eds.), Photosensitizing

compounds: their chemistry, biology and clinical use Chichester: John Wiley & Sons, 1989, pp. 17-25.

Vernon, D.I. J.A. Holroyd, S.M. Stribbling & S.B. Brown The quantitative determination of Photofrin and polyhaematoporphyrin in plasma: pitfalls and inaccuracies. Journal of Photochemistry and Photobiology B: Biology. 1995, 27, 209-217.

Von Tappeiner, H., & A. Jesionek Therapeutische versuche mit fluoreszierenden stoffen, Muench. Med. Wochenschr., 1903, 50, 2042.

Wan, S., R.R. Anderson & J.A. Parrish Analytical modeling for the optical properties of the skin with *in vitro* and *in vivo* applications. Photochemistry and Photobiology. 1981, 34, 493-499.

Wilman, D.E.V., & T.A. Connors Molecular structure and antitumour activity of alkylating agents. In S. Neidle & M.J. Waring (Eds.), Molecular aspects of anti-cancer drug action. Weinheim: Verlag Chemie, 1983, pp. 233-282.

Wilson, B.C. Photodynamic therapy: light delivery and dosage for second generation photosensitizers. In G. Bock & S. Harnett (Eds.), Photosensitizing compounds:their chemistry, biology and clinical use Chichester: John Wiley & Sons, 1989, pp. 60-77.

Windholz, M., S. Budavari, R.F. Blumetti & E.S. Otterbein The merck index: An encyclopedia of chemicals, drugs, and biologicals tenth edition Rahway, N.J., USA: Merck and Co., Inc., 1983.

Wöhrle, D., M. Shopova, S. Müller, A.D. Milev, V.N. Mantareva & K.K. Krastev Liposome-delivered Zn(II)-2,3-naphthalocyanines as potential sensitizers for PDT: synthesis, photochemical, pharmacokinetic and phototherapeutic studies. Journal of Photochemistry and Photobiology B: Biology. 1993, 21, 155-165.

Woodburn, K., C.K. Chang, S. Lee, B. Henderson & D. Kessel Biodistribution and PDT efficacy of a ketochlorin photosensitizer as a function of the delivery vehicle. Photochemistry and Photobiology. 1994, 56, 154-159.

Zuk, M.M., BD. Rihter, ME. Kenney, M.A.J. Rodgers & M. Kreimer-Birnbaum Pharmacokinetic and tissue distribution studies of the photosensitizer *bis*(di-isobutyl octadecylsiloxy) silicon 2,3-naphthalocyanine (*iso*bosinc) in normal and tumor-bearing rats. Photochemistry and Photobiology. 1994, 59, 66-72